

Aus dem Institut für Biochemie, Campus Mitte der Medizinischen Fakultät Charité –
Universitätsmedizin Berlin

DISSERTATION

**Studying synergistic interactions of compounds targeting genome instability
and metabolism in different cancer cell lines for a combinatory therapy
approach.**

Zur Erlangung des akademischen Grades
Doctor medicinae (Dr. med.)

vorgelegt der Medizinischen Fakultät
Charité – Universitätsmedizin Berlin

von

Jonas Parczyk
aus Frankfurt am Main

Datum der Promotion: 26.06.2022

Content

1. List of abbreviations / Abkürzungsverzeichnis.....	3
2. Abstract.....	4
3. Zusammenfassung.....	5
4. Introduction.....	7
4.1 Objectives.....	8
5. Methods	10
5.1 Cell culture	10
5.2 Compounds.....	10
5.3 MTT and SRB assay	10
5.4 Screening method (Minimalistic Drug Interaction Screening (MDIS)).....	11
5.5 Confirmation of synergism	11
5.6 Western Blot analysis.....	12
5.7 Seahorse analysis.....	13
5.8 Statistical analysis.....	15
6. Results	16
6.1 Genome reorganization in different cancer types: Detection of cancer specific breakpoint regions (Publication 1)	16
6.2 Synergisms of genome and metabolism stabilizing antitumor therapy (GMSAT) in human breast and colon cancer cell lines: A novel approach to screen for synergism (Publication 2)	16
6.3 Dichloroacetate and PX-478 exhibit strong synergistic effects in a various number of cancer cell lines (Publication 3).....	17
7. Discussion	20
7.1 Minimalistic Drug Interaction Screening – an efficient screening tool	20
7.2 DCA and PX-478 exhibits strong synergistic potential for antitumoral therapy.....	20
7.3 Conclusion.....	21
8. References	22
9. Eidesstattliche Versicherung	27
10. Anteilserklärung an den erfolgten Publikationen / Declaration of own contribution to the publications.....	28
11. Druckexemplare der ausgewählten Publikation / Publications	29
11.1 Publication 1	29
11.2 Publication 2	38
11.3 Publication 3	53
12. Lebenslauf / Curriculum vitae.....	68
13. Publikationsliste / List of Publications	69
14. Danksagung / Acknowledgements	70

1. List of abbreviations / Abkürzungsverzeichnis

2-DG	2-deoxy-D-glucose
AMP	Adenosine monophosphate
AMPK	AMP-activated protein kinase
BSA	Bovine Serum Albumin
CSP	Conjectured Synergistic Potency
DCA	Dichloroacetate
DMEM	Dulbecco's Modified Eagle Medium
DMSO	Dimethyl sulfoxide
DNA	Deoxyribonucleic acid
ECAR	Extracellular acidification rate
EDTA	Ethylenediaminetetraacetic acid
EGTA	Ethylene glycol-bis(β -aminoethyl ether)-N,N,N',N'-tetraacetic acid
FACS	Fluorescence-activated Cell Sorter
FCCP	Carbonyl cyanide-4-(trifluoromethoxy)phenylhydrazone
GMSAT	Genome and Metabolism Stabilizing Antitumor Therapy
HTS	High throughput screening
HPLC	High Pressure Liquid Chromatography
MDIS	Minimalistic Drug Interaction Screening
MTT	3-(4,5-Dimethylthiazol-2-yl)-2,5-diphenyltetrazoliumbromid
OCR	Oxygen consumption rate
PARP	Poly (ADP-ribose) polymerase
PBS	Phosphate-Buffered Saline
PDCA	Pancreatic adenocarcinoma
PMSF	Phenylmethylsulfonylfluorid
ROS	Reactive oxygen species
SDS-PAGE	Sodium Dodecyl Sulfate Polyacrylamide Gel Electrophoresis
SNP	Single Nucleotide Polymorphism
SRB	Sulforhodamine B
TBS	Tris-buffered saline

2. Abstract

Introduction/Objective: Despite a lot of progress in cancer research throughout the last decades, cancer is still a leading cause of death in Germany. Tumorigenesis is a multi-step process which is accompanied by substantial changes in genome organization. The tumoral microevolution leads to therapy resistance and progression of disease. One key approach for anticancer therapy is drug combination. Drug combination can help to reduce doses and thereby decrease side effects. Furthermore, the likelihood of drug resistance is reduced. This work is dedicated towards detecting a promising drug combination among 14 selected compounds targeting mainly genome and metabolism that exerts synergistic antitumoral effects and thereby recommends itself for further preclinical and clinical studies.

Methods: 111 previously published SNP arrays from three different cancer types (pancreatic, breast and skin) and from non-malignant control samples as well as 917 arrays from cancer cell lines were analyzed for breakpoint regions. MTT and SRB assays were conducted for dose response curves, screening experiments and subsequent quantification of synergistic interaction in the breast cancer cell line MCF-7. The most promising combination was evaluated in seven other cell lines derived from hepatocellular carcinoma, glioblastoma, colon, lung and cervical cancer tissues. Western Blot, FACS and HPLC analyzes were performed to further investigate the effect of this combination on cell cycle, apoptosis and formation of reactive oxygen species. Real-time metabolic measurements (Seahorse XF Analyzer) were conducted to analyze Dichloroacetate mediated metabolic alterations.

Results: Some breakpoint regions were not randomly involved in genome reorganization since we detected fifteen of them in at least 20% of all tumor samples. The screening method (Minimalistic Drug Interaction Screening, MDIS) proved to be an efficient and reliable tool for the detection of synergistic drug interactions. A total of six drug combinations were identified. The newly detected synergism of DCA and PX-478 is observed in all eight cancer cell lines. Furthermore, this combination led synergistically to an increase of ROS, an inhibition of proliferation and the induction of apoptosis.

Conclusion: The Minimalistic Drug Interaction Screening proved to be cost- and time-efficient and delivered reliable results. The newly found combination of DCA and PX-478 shows synergistic activity in eight out of eight cancer cell lines, whereas the non-cancerous cell line HEK-293 was only minimally affected. *In vivo* experiments are necessary to evaluate if the combination can be recommended for clinical trials.

3. Zusammenfassung

Hintergrund/Ziele: Trotz zunehmender wissenschaftlicher Erkenntnisse in der Tumorthapie stellen Krebserkrankungen immer noch eine der Haupttodesursachen in Deutschland dar. Tumorentstehung ist ein komplexer mehrstufiger Prozess, welcher von substantiellen Veränderungen in der Genomstruktur begleitet wird. Die tumoröse Mikroevolution ist eine der Hauptursachen für die Entwicklung von Therapieresistenz und Progredienz dieser Erkrankung. Ein Schlüssel zur erfolgreichen Tumorbehandlung kann eine frühzeitige Kombinationstherapie darstellen. Die Kombination von Medikamenten kann Nebenwirkungen sowie die Wahrscheinlichkeit einer Therapieresistenz reduzieren. Ziel dieser Arbeit ist es, aus 14 ausgewählten Substanzen, die in Zellmetabolismus, Genomaktivität, Proliferation und Zellüberleben eingreifen, eine synergistische Kombination zu identifizieren, die vielversprechende antitumoröse Wirkung besitzt.

Methoden: SNP-Array Daten von 111 Tumorproben (Pankreas, Brust, Haut) und nicht-maligne Kontrollproben sowie von 917 Krebszelllinien wurden auf Bruchpunktregionen hin analysiert. Für die Erstellung von Dosis-Wirkungsbeziehungen, die Screening-Experimente und die darauffolgende Quantifizierung synergistischer Interaktionen wurden die Zellproliferationsraten mit MTT-Analysen und die zelluläre Proteinmasse mit SRB-Analysen bestimmt. Die vielversprechendste Kombination wurde in insgesamt acht Tumorzelllinien verschiedener Abstammung (Glioblastom, Kolon-, Lungen-, Zervixkarzinom und hepatozelluläres Karzinom) untersucht. Western Blot, FACS und HPLC Analysen wurden durchgeführt um die vielversprechendste Kombination in Bezug auf Zellzyklus, Apoptoseinduktion und die Bildung reaktiver Sauerstoffspezies weiter zu untersuchen. Metabolische Echtzeit-Untersuchungen wurden mit Dichloroacetat in MCF-7 Zellen mittels *Seahorse XF Analyzer* durchgeführt.

Ergebnisse: Eine umfassende Reorganisation des Genoms konnte für Tumore beschrieben werden. Interessanterweise konnten wir fünfzehn Bruchpunktregionen detektieren, die in mindestens 20 % aller Tumore zu finden waren. Eine Bruchpunktregion befand sich sogar in 43 % aller Tumore bzw. in 35 % aller (917) untersuchten Zelllinien. Die entwickelte Screening Methode (Minimalistic Drug Interaction Screening, MDIS) erwies sich als verlässlich und praktikabel. Für sechs Wirkstoffkombinationen konnten eine synergistische Aktivität bestimmt und quantifiziert werden. Die neu beschriebene Kombination von DCA und PX-478 zeigte eine synergistische Wirkung in allen acht untersuchten Zelllinien. Es wurde gezeigt, dass mit dieser synergistischen Wirkung eine vermehrte Entstehung reaktiver Sauerstoffspezies, eine Induktion der Apoptose, sowie ein Zellzyklusarrest einhergehen

Fazit: Die beschriebene Screening Methode hat sich für die Detektion von synergistischen Substanzkombinationen als effizient und verlässlich erwiesen. Die Kombination aus DCA und PX-478 zeigt vielversprechende Ergebnisse in allen untersuchten Tumorzelllinien und hat im Vergleich nur minimale Wirkungen auf die von embryotischen Nierenzellen abstammende Kontrollzelllinie HEK-293. *In vivo* Experimente sind notwendig, um eine Empfehlung für klinische Studien weiter zu bestärken.

4. Introduction

Research on formation and therapy of tumors belongs to the major fields of investigation in medical research. Despite substantial scientific progress throughout the last decades, cancer was still responsible for approximately one fourth of deaths in Germany in 2019 (4).

Tumorigenesis is a multi-step process which involves substantial changes in genome organization. The development of these changes is not only a random process, but rather comprises specific DNA regions that are prone to the reorganization process (5–9). A better understanding of genome reorganization that results in malignant tumor growth may contribute to the identification of further targets for therapeutic intervention.

After an initial response to cancer treatment, many patients undergo disease recurrence due to treatment resistance leading to a poor prognosis (10). One reason for this effect might be the microevolution tumor cells undergo under the selection pressure of a cytostatic therapy. Important driving forces of the microevolution are the genomic instability, the cancer metabolism and a deregulated cell cycle which leads to increased cell proliferation and an enhanced mutational rate (11–14). Microevolution of cancer cells often leads to drug resistance and tumor recurrence (15). A way to stop microevolution can be an important key for cancer therapy (16).

Drug combination might be an effective strategy to keep cancer in remission by targeting the driving forces of the tumoral microevolution. A combination of drugs that target different aspects of the disease and, in the best case, act synergistically may have the potential to keep the tumor in a progression free state (17,18). Today, synergy studies are often conducted within pharmaceutical companies (19). As industrial funding and the focus on commercial interests increase, research is mostly focused on newly bioengineered and patentable drugs of the respective company rather than generic compounds (20,21).

Synergistic drug combinations can lead to increased response rates, reduced risk of drug resistance and may allow lower drug doses with less pronounced side effects (18,22,23). Often, clinical trials are discarded, once a single compound shows to be ineffective or to mediate severe side-effects in a phase 1 clinical study. However, combination of the two compounds may lead to lower doses, less pronounced side effects and thereby a well tolerable and effective therapy regimen (17,18).

4.1 Objectives

The goal of the work presented was

- a. to design a screening method for the identification of synergisms among selected anti-cancer compounds in the breast cancer derived tumor cell line MCF-7,
- b. to further investigate the most promising combination in several additional cell lines derived from different tumor entities and
- c. to investigate the underlying mode of action behind this synergism.

The following steps are necessary to reach these objectives:

1. Identification of compounds.

As important driving forces of the tumor cell microevolution are the genomic instability, the cancer metabolism and a deregulated cell cycle (11–14), a MEDLINE® research was conducted to identify compounds targeting the tumor suppressor gene p53 function, metabolism, growth and survival. Further criteria included were that compounds should be orally available, cost effective and patent-free. The identified compounds are listed in Table 1.

2. Availability of an applicable screening method.

In the beginning, we analyzed combinations of compounds which seemed likely to act synergistical due to their respective mode of action. In preliminary experiments the combination of, for example, Nutlin-3 and PRIMA-1-Met lead to a modest success in terms of throughput and data quality. Hence, a development of a suitable screening method that is compatible with basic laboratory equipment (Viability assays, ELISA reader, cell culture laboratory) and a limited budget was necessary. In the following this method will be referred as Minimalistic Drug Interaction Screening (MDIS).

3. Verification of the identified synergisms.

We decided to use the method of Chou and Talalay. It takes the mass action law and thereby the dynamics of a dose response curve into account. Hence it is crucial to analyze combinations over the whole dose response curve with at least 4 concentrations (24,25)

4. Analysis of the most promising drug combination in several additional cell lines derived from different tumor types.

5. Analysis of the underlying mechanisms of synergism with focus on induction of apoptosis, ROS production and cell cycle alterations.

Table 1:

Compound	Mode of action
Nutlin-3	Inhibits the interaction between MDM2 and p53 leading to p53 protein stabilization (26).
Prima 1-Met	Improves the interaction of the DNA-binding domain of mutated p53 with the DNA in a broad variety of mutations except C176F (27).
Dichloroacetate	Inhibits the pyruvate dehydrogenase kinase leading to a more active pyruvate dehydrogenase (28). At the molecular level, DCA positively regulates p53 activity as well (29). DCA is approved for therapy of hereditary lactate acidosis (30).
Ym155	Leads to reduced expression of BIRC5 (survivin) and therefore to the induction of apoptosis (31,32).
SJ172550	MDMX may directly regulate p53 transcription. MDMX is genetically amplified in approximately 20% of breast-, lung- and colon-carcinoma (33).
Pictilisib	Pictilisib is an oral, potent, selective pan-inhibitor of class I phosphatidylinositol-3-kinase(34).
NHI-2	NHI2 is an inhibitor of the lactate dehydrogenase A and leads to less production of lactate in tumor cells (35).
PX-478	Stops transcription of HIF-1 α by an increase of eIF2a phosphorylation (reduction of HIF-1 α -mRNA). An inhibition of the translation of HIF-1 α and the deubiquitylation has also been shown. PX-478 has effects on metabolism, proliferation and apoptosis (36,37).
6-Shogaol (ginger derived)	Modulates the notch signaling pathway and induces autophagy in breast cancer cells while interacting with other pathways e.g. AKT/mTOR (38).
3-Bromopyruvate	Inhibits hexokinase 2 which is important for tumor metabolism in many different tumor types(39,40).
Metformin (approved for therapy of diabetes mellitus type 2)	Inhibits mitochondrial complex 1 \rightarrow AMP increases \rightarrow AMPK is being activated \rightarrow inhibits pyruvate dehydrogenase, activates β -oxidation and is a signal to lower the anabolic rate (41).
CB-839	Inhibits glutaminase and thus deprives the tumor of another way of energy production and anabolic function (42).
Inositol-C2-PAF	A lipid which interferes in the phosphorylation of AKT and PI3K-AKT-pathway. Inositol-C2-PAF has also other partially unknown mechanisms(43)
Cisplatin (approved)	Is a platinum based alkylating-like drug leading to DNA-crosslinks .

Table 1: List of all 14 compounds used for the MDIS and the respective mode of action.

5. Methods

In this section I focus on all the methods that were executed individually by myself. Methods like FACS analysis which I also supervised and assisted, are not included.

5.1 Cell culture

The breast cancer cell line MCF-7 was a kind gift from Göran Landberg (Sahlgrenska Cancer Center, University of Gothenburg, Gothenburg, Sweden). The hepatocellular cancer cell line HEPG2, the adenocarcinoma lung cancer cell line A549 as well as the embryonic kidney derived cell line HEK-293, were purchased from the American Type Culture Collection (ATCC). The glioblastoma cell line U251 was a kind gift from Kai Murk (Charité Berlin, Germany). A549, HEK-293, HEPG2, HeLa, MCF-7 and U251 cells were cultured in DMEM and H441 in DMEM/F12. All media contained penicillin/streptomycin (100 U ml⁻¹), L-glutamine (DMEM: 584 mg l⁻¹, DMEM/F12: 365.1 mg l⁻¹) and 10% heat-inactivated fetal calf serum (PAN Biotech, Germany). The humidified incubator was set at 37 °C with 5% CO₂. Cells were harvested using 0.05% trypsin/0.02% ethylenediaminetetraacetic acid (EDTA) in PBS.

5.2 Compounds

The 14 compounds used were purchased from: Prima-1met, Nutlin-3, SJ 172550, YM155 (Selleck Chemicals, Houston, TX, USA), 6-Shogaol (Hölzel Diagnostika Handels GmbH, Cologne, Germany), Pictilisib (Absource Diagnostics GmbH, Munich, Germany), Ino-C2-PAF (1-O-octadecyl-2-O-(2-(myo-inositolyl)-ethyl)-sn-glycero-3-(r/s)-phosphatidylcholine) (29), PX-478 (Hölzel Diagnostika Handels GmbH, Cologne, Germany), DCA, Metformin-hydrochloride (Sigma-Aldrich, Munich, Germany), CB-839 (Selleck Chemicals, Houston, TX, USA), 3-Bromopyruvate (Santa Cruz Biotechnology, Dallas, Texas, USA), NHI-2 (Bio-Techne GmbH, Wiesbaden-Nordenstadt, Germany) and Cisplatin (Cayman Chemical Ann Arbor, MI, USA).

3-Bromopyruvate, Cisplatin, Dichloroacetate, Metformin, PRIMA-1-met, PX-478, YM155 and Ino-C2-PAF were dissolved in distilled water. Dimethyl sulfoxide (DMSO) was used to solubilize 6-Shogaol, CB-839, NHI-2, Nutlin-3, Pictilisib and SJ-17255. Finally, DMSO concentration was kept under 0.6 µl per well (0.6 %).

5.3 MTT and SRB assay

A total of 0.75 x 10⁴ A549, 1 x 10⁴ HEK-293, 0.3 x 10⁴ HeLa, 0.6 x 10⁴ HEPG2, 1 x 10⁴ H441, 0.5 x 10⁴ MCF-7 and 0.3 x 10⁴ U251 cells per well were seeded in flat bottom 96-well plates. After 24 hours, when the cells were approximately 50% confluent, DCA, PX-478 or the combination was added. After 48 hours of further incubation, either a 3-(4,5-dimethylthiazol-2-yl)-2,5-diphenyltetrazolium bromide (MTT) assay (Bio-Techne GmbH, Germany) or a sulforhodamine B (SRB) assay was performed. The MTT assay was performed according to

the manufacturer's instructions. For the SRB assay, cells were fixed with 10% trichloroacetic acid (w/v) and stained with 0.06% SRB in 1% acetic acid for 30 minutes. Cells were then repeatedly washed with 1% acetic acid (v/v) and dissolved in 10 mM Tris (pH 10.5). The protein mass was measured by determining the optical density at a wavelength of 492 nm in a microplate reader. All experiments were performed independently three times with at least 2 technical triplicates (mostly with 3).

Dose response curves were generated using GraphPad Prism 7.05 statistical analysis software. The half-maximal effective concentration (EC_{50}) of each compound was determined via nonlinear regression.

5.4 Screening method (Minimalistic Drug Interaction Screening (MDIS))

0.5×10^4 MCF-7 cells per well were seeded in flat bottom 96-well plates. After 24 hours, when the cells were approximately 50% confluent, MCF-7 cells were treated with 14 single and their 91 pairwise combinations at dosages of approximately EC_{25} . After 48 hours of further incubation, a MTT assay was performed. All experiments were performed at least with three biological and two technical replicates. Thus about 909 data points (303 per biological replicate) were produced. The conjectured synergistical potency (CSP) of a combination was quantified by adding up the effect of the single compounds and subtracting the result from the combination's effect. E.g.: Single dose A: 20% cell viability-reduction, single dose B: 10% cell viability-reduction and the combination of A and B exhibit cell viability-reduction of 37%. Thus, the combination of A and B reduces the cell viability 7% more than it is expected from simply adding up the effects of the single compounds (CSP= 7). Analyzes were performed with Graph pad prism and Microsoft Excel. CSP-values between 10 and 15 are referred to as "*possible*", values between 15 and 25 as "*likely*" and values greater than 25 as "*very likely*" synergism, respectively.

5.5 Confirmation of synergism

Synergism was evaluated for four to seven concentrations (mostly with 6), as suggested by Chou and Talalay (24).

Cells were treated with the combination respective combination at a constant EC_{50} : EC_{50} ratio as well as with the single compounds alone. Significant differences between each single compound and the combination were assessed by an unpaired t-test. Only concentrations with p-values of at most 0.05 for both single compounds compared to the combination were considered to exhibit significant differences.

Combination indices (CIs) were calculated using CompuSyn software (44). The CI is a quantitative value indicating the synergism of a drug combination at specific concentrations. A value of less than 0.9 indicates synergism (the lower the CI, the stronger the synergism).

Values from 0.9 to 1 indicate a nearly additive effect, and a CI value of greater than 1.1 indicates antagonism (45,46). CI values were calculated as follows:

$$CI = \frac{(D)_1}{(Dx)_1} + \frac{(D)_2}{(Dx)_2}.$$

In the numerators, $(D)_1$ and $(D)_2$ are the concentrations of drug 1 and drug 2, respectively, in the drug combination that have a certain effect on cell viability (x %). In the denominators, $(Dx)_1$ and $(Dx)_2$ are the concentrations of each drug alone (drug 1 or drug 2, respectively) that are necessary to obtain the same effect (x %) as the drug combination (both drug 1 and drug 2). The concentrations $(Dx)_1$ and $(Dx)_2$ were calculated by CompuSyn with reference to the cell viability data for the respective compounds. To enhance analytical robustness, most concentrations of the compounds were doubled. Therefore, potential calculation errors were minimized, as suggested by Zhao et al. (47). To generate the median-effect plots, the following equation was used:

$$D_x = D_m \left[\frac{fa}{1 - fa} \right]^{\frac{1}{m}},$$

where D_m is the median effective dose, m is the slope of the median-effect curve, and fa is the fraction affected. Since calculation of a CI value is appropriate only when neither single compound has an effect close to 100%, the respective CI values are not shown in the Results section (47).

5.6 Western Blot analysis

For Western blotting, cells were seeded in 6 cm diameter Petri dishes, grown to approximately 80% confluence and treated with the noted compounds. 24 hours later, the cells were washed with PBS and lysed with lysis buffer (50 mM β -glycerophosphate pH 7.6, 1.5 mM EGTA, 1.0 mM EDTA, 1% (v/v) Triton X-100, 0.2% (v/v) protease inhibitor cocktail, 0.4% (v/v) PMSF, 100 mM sodium vanadate, 500 mM NaF) on ice for 60 minutes. The lysed cells were centrifuged for 15 minutes at 4°C and 11,000 \times g, and the supernatants were denatured by heat. The samples were separated under reducing conditions by 10% SDS-PAGE and transferred to nitrocellulose membranes (Thermo Fisher, Rockford, USA). The membranes were subsequently blocked overnight and were then incubated with the corresponding primary antibodies in blocking buffer (5% nonfat dry milk/TBS/0.1% Tween 20 for the anti-PARP antibody and 5% BSA/TBS/0.1% Tween 20 for all other antibodies) overnight at 4° C. The primary antibodies and the corresponding working concentrations are listed in Table 2. After

incubation with appropriate peroxidase-conjugated secondary antibodies, proteins were detected using SuperSignal West Pico Chemiluminescent Substrate (Pierce, Thermo Fisher Scientific, Bonn, Germany). Signals were visualized using a VersaDoc™ 4000 MP imaging system together with the software QuantityOne® 4.6.5 (BioRad Laboratories, Munich, Germany) and quantified using ImageJ 1.52a software (National Institute of Health, USA; version 1.8.0_112).

Table 2: List of antibodies

Antigen	Commercial source	Source	Dilution
β-actin	Cell Signaling (Danvers, USA)	Mouse	1:4000
PARP/cleaved PARP (9542)	Cell Signaling (Danvers, USA)	Rabbit	1:1000
Retinoblastoma p795 (9301)	Cell Signaling (Danvers, USA)	Rabbit	1:1000
Cyclin D1 (DCS-6)	Thermo Scientific (Waltham, USA)	Mouse	1:200

5.7 Seahorse analysis

Table 2: List of all used primary antibodies as well as the corresponding working solution.

MCF-7 cells were seeded in an XF 96-well culture microplate (Agilent, Santa Clara, USA) at 3×10^4 cells per well in 180 µl of prewarmed assay medium. Three biological replicates and 3-4 technical replicates were performed. The specific agents used for the different experiments in the seahorse were provided by Hao Wu. After 24 hours, a mitochondrial respiration assay or glycolytic rate assay was performed with a Seahorse XFe96 Analyzer (Agilent Technologies).

The sensor cartridge was hydrated with 200µl Seahorse XF Calibrant per well in a non-CO₂ incubator at 37° for at least 4 hours. Seahorse XF DMEM was either prepared for the mitochondrial stress test or the glycolysis stress test (see below).

The respective medium was pre-warmed to 37° and the pH was adjusted to 7.4 with 0.1 N NaOH or 0.1 N HCL, respectively. Then cells were washed 2 times with the prepared Seahorse XF DMEM medium and finally 180µl per well was added. Cells were incubated for 45 minutes in a non-CO₂ incubator at 37°. The Seahorse port A was loaded with DCA (final concentration: 31.5 mM).

Port B-D were loaded as described for the different stress tests below. The experimental setup was designed using the WAVE 2.6.0 software. After preparations were finished, Seahorse XF 96 was started. Before each measurement, the assay medium was gently mixed to restore

normal oxygen tension and pH in the microenvironment surrounding the cells. Baseline ECAR (extracellular acidification rate) and OCR (oxygen consumption rate) were measured 4 times at an interval of 5 minutes. After injection of Port A, measurements were performed every 20 minutes another 6 times. Then the mitochondrial stress test or the glycolysis stress test was performed using port B, C and D as illustrated in Figure 1 (48,49). After approximately 220 minutes, when the Seahorse analysis was finished, cells were immediately fixed and an SRB-Assay was performed to conduct normalization. Graphs were produced using GraphPad Prism statistical analysis software 7.05. Glycolytic capacity and maximal respiration were calculated using an automated excel macro included in the software WAVE 2.6.0.

Glycolytic capacity and maximal respiration were calculated as follows:

- maximal respiration (OCR) = (maximum rate measured after injection of carbonyl cyanide-4-(trifluoromethoxy)phenylhydrazone [FCCP]) – (non-mitochondrial respiration rate)
- non-mitochondrial respiration (OCR) = minimum rate measured after injection of rotenone & antimycin A)
- Glycolytic capacity (ECAR) = (maximum rate measured after injection of oligomycin) – (non-glycolytic acidification rate)
- non-glycolytic acidification (ECAR) = minimum rate measured after injection of 2-deoxy-D-glucose (2DG).

Mitochondrial stress test (Figure 1): For this experiment Seahorse XF DMEM medium was used with 2mM glutamine, 1mM pyruvate and 10mM glucose. Port B was loaded with Oligomycin (final concentration 2 μ M) an inhibitor of the mitochondrial membrane adenosine triphosphate synthase (Complex V), port C was filled with FCCP (1 μ M) (Carbonyl cyanide-4-(trifluoromethoxy)phenylhydrazone) an uncoupling agent transporting protons across the mitochondrial membrane and port D was loaded with Rotenone (5 μ M) an inhibitor of mitochondrial electron transport in Complex 1 and Antimycin A (5 μ M) an inhibitor of the mitochondrial electron transport chain from cytochrome b to cytochrome C1. After each port-injection OCR and ECAR was measured 3 times (approximately every 3 minutes). This allows us to measure metabolism after specific modulations.

Glycolysis stress test (Figure 1): For this experiment Seahorse XF DMEM medium was used with 1 mM glutamine leaving pyruvate and glucose out. The port-injection protocol is similar to the mitochondrial stress test with different compounds being used. Port B was loaded with glucose (final concentration 10mM), port C was loaded with Oligomycin (1 μ M) and port D was

filled with 2-DG (50mM)(2-deoxy-D-glucose) a glucose analog which is not metabolized leading to inhibition of glycolysis.

Figure 1: Mitochondrial stress test (left) and Glycolysis stress test (right)

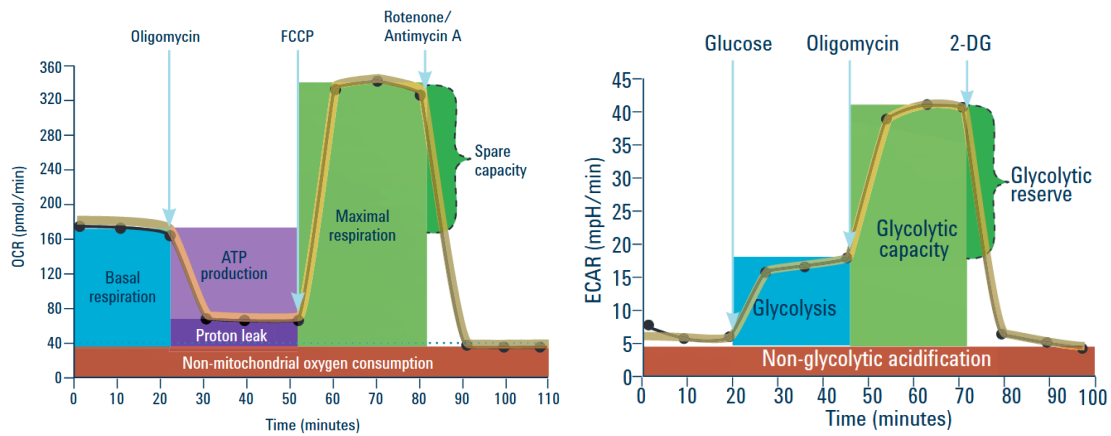


Figure 1: Exemplarily, the routine of the mitochondrial stress test (left) and the glycolysis stress test (right) is presented. Effects of each agent on the OCR or ECAR and the possible interpretation of the effect can be seen, respectively. The figures are taken from the respective flyers from Agilent (48, 49).

5.8 Statistical analysis

Statistical analysis was performed using unpaired T-tests in GraphPad Prism 7.05 statistical analysis software. Differences with a p-value of at most 0.05 were considered significant: significant differences compared to the control are marked with an asterisk (*), while significant differences between the combination and both the control and each single compound are marked with two asterisks (**). All experiments were performed with at least 2 technical and 3 biological replicates.

6. Results

6.1 Genome reorganization in different cancer types: Detection of cancer specific breakpoint regions (Publication 1)

We have analyzed previously published SNP (Single Nucleotide Polymorphism) array data from three different cancer types (pancreatic adenocarcinoma, breast cancer and metastatic melanoma) and from non-malignant control samples (1). Altogether, data from 111 tumor samples, 20 non-malignant control tissues and 917 tumor cell lines were used. We calculated breakpoint regions as well as segmental copy number variations. Some of these regions were involved in genome reorganization above average since we detected fifteen of them in at least 20% of all tumor samples and one region on chromosome 9 where 43% of tumors have a breakpoint. Furthermore, the top-15 breakpoint regions show an association to already known fragile sites. The relevance of these common breakpoint regions was further confirmed by analyzing SNP arrays from 917 cancer cell lines. Additionally, we could show that pancreatic adenocarcinomas (PDCA) cell lines exhibit considerably different breakpoint regions than solid PDCA.

These results indicate that genome reorganization is common in tumorigenesis and results in a great heterogeneity of established tumors. For therapy of such heterogeneous tumors, a combination of different treatment regimens could be a valuable approach which motivated us to further focus our studies on the synergism of anti-tumor agents with a different mode of action in various tumor derived cell lines (2,3).

6.2 Synergisms of genome and metabolism stabilizing antitumor therapy (GMSAT) in human breast and colon cancer cell lines: A novel approach to screen for synergism (Publication 2)

To identify synergisms among 14 selected compounds (see Table 1), we developed a three-step concept (2).

First, dose-response curves were conducted. Second, a screening experiment (Minimal Drug Interaction Screening – MDIS) in which all 91 possible pairwise combinations were investigated was performed. Third, the most promising combinations were verified by the method of Chou and Talalay.

In this study, all 14 compounds did exhibit antitumor effects on each of the three cell lines. MDIS resulted in 19 potential synergisms detected in HT-29 (20.9% of all combinations) and 27 in MCF-7 (29.7% of all combinations) (2).

In subsequent experiments including measurements of whole dose response curves seven of the top combinations were further analyzed, and for five combinations a significant synergy

could be confirmed. (DCA + NHI-2, Nutlin-3 + PX-478, Prima-1met + YM155, DCA + Metformin and Prima-1met + NHI-2). The combination Nutlin-3 (inhibition of MDM2) and PX-478 (inhibition of HIF-1 α) could be confirmed as synergistic for all three cell lines analyzed (MCF7, HT-29 and MDA-MB-231). The same accounts for the combination of Dichloroacetate (PDH activation) and NHI-2 (LDH-A inhibition).

Dichloroacetate (DCA), a pyruvate dehydrogenase kinase inhibitor and the HIF-1 α inhibitor PX-478, both compounds targeting cancer metabolism pathways showed to have a “very likely” synergism when combined in the MDIS. This combination turned out to have the highest *conjectured synergistic potency* (CSP) detected among all combinations as it added 60.8% to the sum of the antitumoral effects of the single compounds in HT-29 cells. In MCF-7 cells this combination showed to have a possible synergism (CSP-value between 10 and 15).

The resulting dose response curves of the combination of DCA and PX-478 in HT-29 and MCF-7 cells (3) motivated us to investigate this combination in greater detail. We decided to further analyze this combination in multiple cell lines of different cancer types and to analyze the biochemical effects of this combination in a separate work.

6.3 Dichloroacetate and PX-478 exhibit strong synergistic effects in a various number of cancer cell lines (Publication 3)

The two cancer metabolism targeting compounds DCA and PX-478 were analyzed for their synergistic interaction in eight cell lines originating from different cancer types. In addition, the underlying biochemical mechanisms were investigated (3). The dose-dependent antiproliferative effects of the single drugs and their combination were assessed using SRB assays. The combination of DCA and PX-478 exhibited synergistic effects in all eight investigated cancer cell lines including colorectal, lung, breast, cervical, liver and brain cancer and showed only minimal effects on the embryonic kidney derived cell line HEK-293.

FACS, Western blot and HPLC based experiments were performed to determine changes in reactive oxygen species levels, induction of apoptosis and cell cycle parameters. Additionally, real-time metabolic analyzes (Seahorse XF Analyzer) were performed with DCA-treated MCF-7 cells.

The combination of DCA and PX-478 leads to increased ROS levels and the induction of apoptosis in HT-29, MCF-7 and HeLa cell lines. As one exemplary part of our data, the results of Western blot analysis are shown in Figure 2. In both cell lines combination of DCA and PX-478 resulted in a significant increase of cleaved PARP, a marker for enhanced apoptosis activity in cells. In the same cellular extracts, the amounts of Cyclin D1 and of the

phosphorylated retinoblastoma protein 1 (pRB1), which are associated with a high cell proliferation rate, were significantly reduced.

Real-time measurement of metabolism using the Seahorse XF Analyzer showed that DCA induces metabolic shift from aerobic glycolysis to oxidative phosphorylation.

Figure 2: Western blot analysis (3)

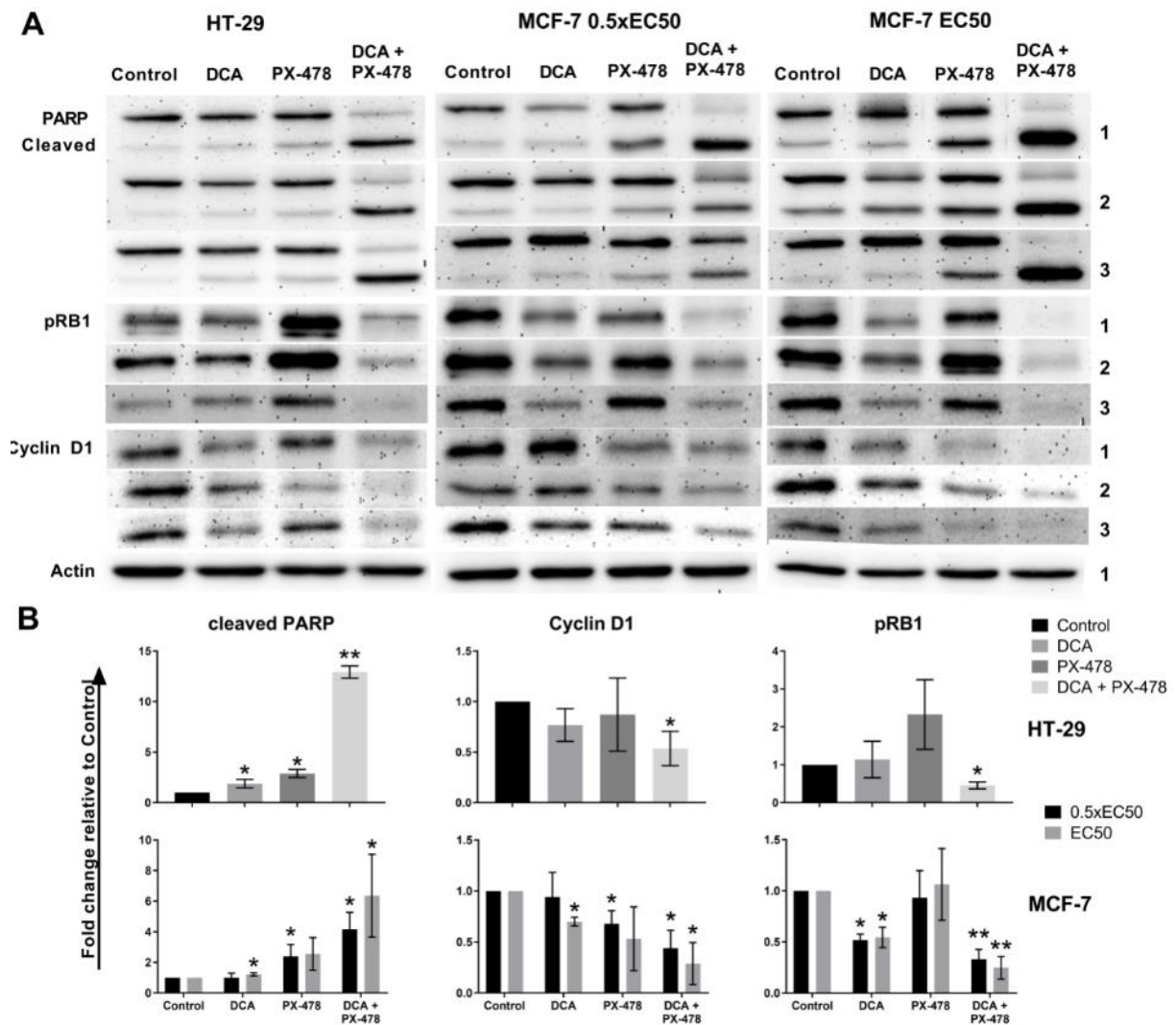


Figure 2: The combination of DCA and PX-478 leads to increased levels of cleaved PARP and reduced levels of Cyclin D1 and pRB1 in HT-29 and MCF-7 cells. Cells were incubated to a confluence of approximately 80% and treated with DCA and PX-478 at the following concentrations: HT-29—DCA, EC₅₀ and PX-478, 0.5 x EC₅₀; MCF-7—either DCA and PX-478, 0.5 x EC₅₀ or EC₅₀. 24 hours later, the cells were harvested, and Western blot analyses were performed. A: Three independent Western blots are shown for each antibody except for β-actin (only one representative blot is shown here). The blots presented here are cropped; please see additional files for full-length blots. B: The results are presented as the fold change relative to the control. Significant differences are marked with an asterisk (*). The level of cleaved PARP was significantly increased in HT-29 cells treated with the combination (p = 0.00002) compared to HT-29 cells treated with the single compounds. For MCF-7 cells, a clear trend was visible for both concentrations (p = 0.086 or p = 0.087, respectively). Significant differences compared to the control are marked with an asterisk (*); significant differences between the combination of DCA and PX-478 and each single compound are marked with two asterisks (**). The combination of DCA and PX-478 significantly reduced cyclin D1 and pRB1 levels in both cell lines and at both concentrations in MCF-7 cells.

7. Discussion

7.1 Minimalistic Drug Interaction Screening – an efficient screening tool

The screening method (MDIS) proved to be a cost- and time-efficient approach to analyze drug-drug combinations in tissue culture model systems. MDIS allows to systematically screen for and reliably describe synergies between a high number of compounds with high efficiency and sufficient data quality. Compared to high-throughput robot-assisted approaches as described by Borisy et al., MDIS requires generation of ca. 20 fold less data points (50). Applying this method for 14 compounds, we identified five synergistic combinations of genome and metabolism stabilizing compounds. Nutlin-3 + PX-478 as well as DCA + NHI-2 proved to be synergistic in all cell lines (MCF-7, MDA-MB-231 and HT-29) (2). Four out of four tested combinations identified as “*likely*” or “*very likely*” synergism with MDIS could be verified by the method of Chou and Talalay. Only two out of four tested drug combinations identified to have a “*possible*” synergism proved to have a significant synergism. Hence, MDIS is an efficient tool that is reliable in its projections when looking at “*likely*” or “*very likely*” synergisms.

7.2 DCA and PX-478 exhibits strong synergistic potential for antitumoral therapy

One of the most promising drug combinations identified by MDIS was DCA + PX-478. The synergism was verified in eight out of eight tumor cell lines. In addition, the combination therapy shows only minimal effects on the embryonic kidney cell line HEK-293.

Further investigation of the mechanisms behind this synergistic interaction showed that it led to increased ROS production as well as the induction of apoptosis and cell cycle arrest. In addition, we could verify the DCA mediated shift from aerobic glycolysis to oxidative phosphorylation via real time measurement (Seahorse FX Analyzer) partly reversing the Warburg effect.

In other studies PX-478 has been shown to induce ROS generation, apoptosis and cell cycle arrest (51,52). DCA is already approved for therapy of hereditary lactic acidosis (30,53) and a lot of research has been conducted with heterogenic results. Some groups have found DCA to induces ROS generation and apoptosis (54–57) while others state that DCA did not significantly increase ROS but acts as a ROS sensitizer, which is more consistent with our data (3,58,59).

In our hands, DCA strongly increased maximal respiration and decreased glycolytic capacity in MCF-7 cells, while it has been described that both maximal respiration and glycolytic capacity were decreased in pancreatic carcinoma as well as head and neck squamous cancer cells (3,60,61). However, Ma et al. found increased maximal respiration in non-small cell lung cancer cells treated with DCA (62). Hence, literature as well as our data suggest that DCA

mediates heterogenic metabolic modulation depending on the metabolic status of a cancer cell. The promising synergism between the two compounds presented here, in context with the evidence generated by various research groups about the effects of DCA and PX-478, deserves further attention. In conclusion, more work needs to be conducted to gain a deeper understanding of this promising combination of DCA and PX-478.

Cell lines are prone to genotypic and phenotypic drift during their continuous culture (63). In line with this, we could show with our genome reorganization study that pancreatic adenocarcinomas (PDCA) cell lines differ considerably from solid PDCAs (1). In conclusion data from *in vitro* trials are of limited predictivity for the *in vivo* situation. Hence, for future studies, we do recommend conducting *in vivo* experiments rather than continuing with further *in vitro* analyzes.

7.3 Conclusion

We recommend the Minimalistic Drug Interaction Screening (MDIS) to screen for promising synergism in a time- and cost-efficient way.

In our application of the MDIS we detected a promising synergism for the combination of DCA and PX-478 that we could confirm in eight cell lines and by mechanistic studies. For future studies, we recommend commencing with *in vivo* experiments. If promising results continue in the *in vivo* stage, the combination should be further evaluated in clinical trials. In addition, the use of this combination with conventional chemotherapy or radiotherapy may be taken into account for further translational approaches.

8. References

1. Standfuß C, Parczyk J, Ruhnau J, Klein A. Genome reorganization in different cancer types: detection of cancer specific breakpoint regions. *Mol Cytogenet.* 2019;12(1):1-8.
2. Ruhnau J, Parczyk J, Danker K, Eickholt B, Klein A. Synergisms of genome and metabolism stabilizing antitumor therapy (GMSAT) in human breast and colon cancer cell lines: A novel approach to screen for synergism. *BMC Cancer.* 2020 Jul 2;20(1).
3. Parczyk J, Ruhnau J, Pelz C, Schilling M, Wu H, Piaskowski NN, Eickholt B, Kühn H, Danker K, Klein A. Dichloroacetate and PX-478 exhibit strong synergistic effects in a various number of cancer cell lines. *BMC Cancer.* 2021;21(1).
4. Krebs war 2019 für ein Viertel aller Todesfälle in Deutschland verantwortlich. 2021. Available from: https://www.destatis.de/DE/Presse/Pressemitteilungen/2021/02/PD21_N010_231.html Accessed April 25 2021
5. Vogelstein B, Kinzler KW. The multistep nature of cancer. *Trends Genet.* 1993;9(4):138–41.
6. Foulds L. The experimental study of tumor progression: a review. *Cancer Res.* 1954;14(5):327–39.
7. Pevzner P, Tesler G. Human and mouse genomic sequences reveal extensive breakpoint reuse in mammalian evolution. *Proc Natl Acad Sci.* 2003;100(13):7672–7.
8. Magenis RE, Hecht F, Lovrien EW. Heritable fragile site on chromosome 16: probable localization of haptoglobin locus in man. *Science.* 1970;170(3953):85–7.
9. Hecht F, Sutherland GR. Fragile sites and cancer breakpoints. *Cancer Genet Cytogenet.* 1984;12(2):179–81.
10. Swanton C, Nicke B, Marani M, Kelly G, Downward J. Initiation of high frequency multi-drug resistance following kinase targeting by siRNAs. *Cell Cycle.* 2007;6(16):2001–4.
11. Andor N, Maley CC, Ji HP. Genomic Instability in Cancer: Teetering on the Limit of Tolerance. *Cancer Res.* 2017;77(9):2179–85.
12. Vander Heiden MG, DeBerardinis RJ. Understanding the Intersections between Metabolism and Cancer Biology. *Cell.* 2017;168(4):657–69.
13. Roy D, Sheng GY, Herve S, Carvalho E, Mahanty A, Yuan S, Sun L. Interplay between cancer cell cycle and metabolism: Challenges, targets and therapeutic opportunities. *Biomed Pharmacother.* 2017;89:288–96.
14. Evan GI, Vousden KH. Proliferation, cell cycle and apoptosis in cancer. *Nature.* 2001;411(6835):342–8.
15. Chisholm RH, Lorenzi T, Clairambault J. Cell population heterogeneity and evolution towards drug resistance in cancer: Biological and mathematical assessment, theoretical treatment optimisation. *Biochim Biophys Acta - Gen Subj.* 2016;1860(11):2627–45.
16. Hanahan D, Weinberg RA. Hallmarks of cancer: The next generation. *Cell.* 2011;144(5):646–74.
17. Zimmermann GR, Lehár J, Keith CT. Multi-target therapeutics: when the whole is greater than the sum of the parts. *Drug Discov Today.* 2007;12(1–2):34–42.

18. Al-Lazikani B, Banerji U, Workman P. Combinatorial drug therapy for cancer in the post-genomic era. *Nat Biotechnol.* 2012;30(7):679–92.
19. Schweim JK, Schweim HG. Status quo and future developments of combinations of medicinal products. *Synergy.* 2014;1(1):70–5.
20. Research America. U.S. Investments in Medical and Health Research and Development. 2016. Available from: https://www.researchamerica.org/sites/default/files/2016US_Invest_R%26D_report.pdf Accessed April 25 2021
21. Moses H, Matheson DHM, Cairns-Smith S, George BP, Palisch C, Dorsey ER. The Anatomy of Medical Research. *JAMA.* 2015;313(2):174.
22. Zimmermann GR, Lehár J, Keith CT. Multi-target therapeutics: when the whole is greater than the sum of the parts. *Drug Discov Today.* 2007;12(1–2):34–42.
23. Schweim JK, Schweim HG. Status quo and future developments of combinations of medicinal products. *Synergy.* 2014;1(1):70–5.
24. Chou TC, Talalay P. Quantitative analysis of dose-effect relationships: the combined effects of multiple drugs or enzyme inhibitors. *Adv Enzyme Regul.* 1984;22:27–55.
25. Chou T. Preclinical versus clinical drug combination studies. *Leuk Lymphoma.* 2008;49(11):2059–80.
26. Essmann F, Schulze-Osthoff K. Translational approaches targeting the p53 pathway for anti-cancer therapy. *Br J Pharmacol.* 2012;165(2):328–44.
27. Lambert JMR, Gorzov P, Veprintsev DB, Söderquist M, Segerbäck D, Bergman J, Fersht AR, Hainaut P, Wiman KG, Bykov VJN. PRIMA-1 Reactivates Mutant p53 by Covalent Binding to the Core Domain. *Cancer Cell.* 2009;15(5):376–88.
28. Stacpoole PW. The pharmacology of dichloroacetate. *Metabolism.* 1989;38(11):1124–44.
29. Agnoletto C, Melloni E, Casciano F, Rigolin GM, Rimondi E, Celeghini C, Brunelli L, Cuneo A, Secchiero P, Zauli G. Sodium dichloroacetate exhibits anti-leukemic activity in B-chronic lymphocytic leukemia (B-CLL) and synergizes with the p53 activator Nutlin-3. *Oncotarget.* 2014;5(12):4347–60.
30. Abdelmalak M, Lew A, Ramezani R, Shroads AL, Coats BS, Langae T, Shankar MN, Neiberger RE, Subramony SH, Stacpoole PW. Long-term safety of dichloroacetate in congenital lactic acidosis. *Mol Genet Metab.* 2013;109(2):139–43.
31. Ambrosini G, Adida C, Altieri DC. A novel anti-apoptosis gene, survivin, expressed in cancer and lymphoma. *Nat Med.* 1997;3(8):917–21.
32. Nakahara T, Takeuchi M, Kinoyama I, Minematsu T, Shirasuna K, Matsuhisa A, Kita A, Tominaga F, Yamanaka K, Kudoh M, Sasamata M. YM155 , a Novel Small-Molecule Survivin Suppressant , Induces Regression of Established Human Hormone-Refractory Prostate Tumor Xenografts. *Cancer Res.* 2007;67(17):8014–21.
33. Reed D, Shen Y, Shelat AA, Arnold LA, Ferreira AM, Zhu F, Mills N, Smithson DC, Regni CA, Bashford D, Cicero SA, Schulman BA, Jochemsen AG, Guy RK, Dyer MA. Identification and Characterization of the First Small Molecule Inhibitor of MDMX. *J Biol Chem.* 2010;285(14):10786–96.
34. Folkes AJ, Ahmadi K, Alderton WK, Alix S, Baker SJ, Box G, Chuckowree IS, Clarke PA, Depledge P, Eccles SA, Friedman LS, Hayes A, Hancox TC, Kugendradas A, Lensun L, Moore P, Olivero AG, Pang J, Patel S, Pergl-Wilson GH, Raynaud FI,

- Robson A, Saghir N, Salphati, L, Sohal S, Ultsch MH, Valenti M, Wallweber HJA, Wan NC, Wiesmann C, Workman P, Zhyvoloup A, Zvelebil MJ, Shuttleworth J. The identification of 2-(1H-indazol-4-yl)-6-(4-methanesulfonyl-piperazin-1-ylmethyl)-4-morpholin-4-yl-t hieno[3,2-d]pyrimidine (GDC-0941) as a potent, selective, orally bioavailable inhibitor of class I PI3 kinase for the treatment of cancer. *J Med Chem.* 2008;51(18):5522–32.
35. Allison SJ, Knight JRP, Granchi C, Rani R, Minutolo F, Milner J, Phillips RM. Identification of LDH-A as a therapeutic target for cancer cell killing via (i) p53/NAD(H)-dependent and (ii) p53-independent pathways. *Oncogenesis.* 2014;3(5):e102.
 36. Koh MY, Spivak-Kroizman T, Venturini S, Welsh S, Williams RR, Kirkpatrick DL, Powis G. Molecular mechanisms for the activity of PX-478, an antitumor inhibitor of the hypoxia-inducible factor-1alpha. *Mol Cancer Ther.* 2008;7(1):90–100.
 37. Lee K, Kim HM. A novel approach to cancer therapy using PX-478 as a HIF-1 α inhibitor. *Arch Pharm Res.* 2011;34(10):1583–5.
 38. Hung J-Y, Hsu Y-L, Li C-T, Ko Y-C, Ni W-C, Huang M-S, Kuo P-L. 6-Shogaol, an Active Constituent of Dietary Ginger, Induces Autophagy by Inhibiting the AKT / mTOR Pathway in Human Non-Small Cell Lung Cancer A549 Cells. *J Agric Food Chem.* 2009;57(20):9809–16.
 39. Lis P, Dylağ M, Niedźwiecka K, Ko JH, Pedersen PL, Goffeau A, Ułaszewski S. The HK2 Dependent "Warburg Effect" and Mitochondrial Oxidative Phosphorylation in Cancer: Targets for Effective Therapy with 3-Bromopyruvate. *Molecules.* 2016;21(12):1730.
 40. Chiasserini D, Davidescu M, Luigi P, Susta F, Macchioni L, Petricciuolo M, Castigli E, Roberti R, Binaglia L, Corazzi L. 3-Bromopyruvate treatment induces alterations of metabolic and stress-related pathways in glioblastoma cells. *J Proteomics.* 2017;152:329–38.
 41. Wheaton WW, Weinberg SE, Hamanaka RB, Soberanes S, Sullivan LB, Anso E, Glasauer A, Dufour E, Mutlu GM, Budigner GRS, Chandel NS. Metformin inhibits mitochondrial complex I of cancer cells to reduce tumorigenesis. *Elife.* 2014; 3:e02242.
 42. Zimmermann SC, Wolf EF, Luu A, Thomas AG, Stathis M, Poore B, Nguyen C, Le A, Rojas C, Slusher BS, Tsukamoto T. Allosteric Glutaminase Inhibitors Based on a 1,4-Di(5-amino-1,3,4-thiadiazol-2-yl)butane Scaffold. *ACS Med Chem Lett.* 2016;7(5):520–4.
 43. Pelz C, Häckel S, Semini G, Schrötter S, Bintig W, Stricker S, Mrawietz G, Klein A, Lucka L, Shmanai V, Eickholt B, Hildmann A, Danker K. Inositol-C2-PAF acts as a biological response modifier and antagonizes cancer-relevant processes in mammary carcinoma cells. *Cell Oncol.* 2018;41(5):505-16.
 44. Chou TC, Martin N. *CompuSyn for Drug Combinations: PC Software and User's Guide: A Computer Program for Quantitation of Synergism and Antagonism in Drug Combinations, and the Determination of IC₅₀ und ED₅₀ and LD₅₀ Values.* ComboSyn, Paramus (NJ). 2005.
 45. Chou T-C. Preclinical versus clinical drug combination studies. *Leuk Lymphoma.* 2008;49(11):2059–80.
 46. Chou T-C. Theoretical basis, experimental design, and computerized simulation of synergism and antagonism in drug combination studies. *Pharmacol Rev.* 2006 Sep;58(3):621–81.

47. Zhao L, Wientjes MG, Au JL-S. Evaluation of combination chemotherapy: integration of nonlinear regression, curve shift, isobologram, and combination index analyses. *Clin Cancer Res*. 2004;10(23):7994–8004.
48. AGILENT SEAHORSEXF CELL MITO STRESS TEST KIT. 2020. Available from: <https://www.agilent.com/cs/library/flyers/public/5991-7118EN.pdf>. Accessed April 25 2021
49. AGILENT SEAHORSEXF GLYCOLYSIS STRESS TEST KIT. 2016. Available from: <https://www.agilent.com/cs/library/flyers/public/5991-7120EN.pdf>. Accessed April 25 2021
50. Borisy AA, Elliott PJ, Hurst NW, Lee MS, Lehar J, Price ER, Serbedzija G, Zimmermann GR, Foley MA, Stockwell BR, Keith CT. Systematic discovery of multicomponent therapeutics. *Proc Natl Acad Sci U S A*. 2003;100(13):7977–82.
51. Palayoor ST, Mitchell JB, Cerna D, Degraff W, John-Aryankalayil M, Coleman CN. PX-478, an inhibitor of hypoxia-inducible factor-1alpha, enhances radiosensitivity of prostate carcinoma cells. *Int J cancer*. 2008;123(10):2430–7.
52. Lang M, Wang X, Wang H, Dong J, Lan C, Hao J, Huang C, Li X, Yu M, Yang Y, Yang S, Ren H. Arsenic trioxide plus PX-478 achieves effective treatment in pancreatic ductal adenocarcinoma. *Cancer Lett*. 2016;378(2):87–96.
53. Shroads AL, Langae T, Coats BS, Kurtz TL, Bullock JR, Weithorn D, Gong Y, Wagner DA, Ostrov DA, Johnson JA, Stacpoole PW. Human polymorphisms in the glutathione transferase zeta 1/maleylacetoacetate isomerase gene influence the toxicokinetics of dichloroacetate. *J Clin Pharmacol*. 2012;52(6):837–49.
54. Saed GM, Fletcher NM, Jiang ZL, Abu-Soud HM, Diamond MP. Dichloroacetate induces apoptosis of epithelial ovarian cancer cells through a mechanism involving modulation of oxidative stress. *Reprod Sci*. 2011;18(12):1253–61.
55. Sutendra G, Dromparis P, Kinnaird A, Stenson TH, Haromy A, Parker JMR, Mcmurtry MS, Michelakis ED. Mitochondrial activation by inhibition of PDKII suppresses HIF1a signaling and angiogenesis in cancer. *Oncogene*. 2013;32(13):1638–50.
56. Ward NP, Poff AM, Koutnik AP, D'Agostino DP. Complex I inhibition augments dichloroacetate cytotoxicity through enhancing oxidative stress in VM-M3 glioblastoma cells. *PLoS One*. 2017;12(6): e0180061.
57. Tataranni T, Piccoli C. Dichloroacetate (DCA) and Cancer: An Overview towards Clinical Applications. *Oxid Med Cell Longev*. 2019;2019:8201079.
58. Alkarakooly Z, Al-Anbaky QA, Kannan K, Ali N. Metabolic reprogramming by Dichloroacetic acid potentiates photodynamic therapy of human breast adenocarcinoma MCF-7 cells. *PLoS One*. 2018;13(10): e0206182.
59. Lu H, Lu Y, Xie Y, Qiu S, Li X, Fan Z. Rational combination with PDK1 inhibition overcomes cetuximab resistance in head and neck squamous cell carcinoma. *JCI Insight*. 2019;4(19): e131106.
60. Tataranni T, Agriesti F, Pacelli C, Ruggieri V, Laurenzana I, Mazzoccoli C, Della Sala G, Panebianco C, Paziienza V, Capitanio N, Piccoli C. Dichloroacetate Affects Mitochondrial Function and Stemness-Associated Properties in Pancreatic Cancer Cell Lines. *Cells*. 2019;8(5):478.
61. Lucido CT, Miskimins WK, Vermeer PD. Propranolol promotes glucose dependence and synergizes with dichloroacetate for anti-cancer activity in HNSCC. *Cancers (Basel)*. 2018;10(12):476.

62. Ma W, Zhao X, Wang K, Liu J, Huang G. Dichloroacetic acid (DCA) synergizes with the SIRT2 inhibitor Sirtinol and AGK2 to enhance anti-tumor efficacy in non-small cell lung cancer. *Cancer Biol Ther.* 2018;19(9):835–46.
63. Burdall SE, Hanby AM, Lansdown MRJ, Speirs V. Breast cancer cell lines: Friend or foe? *Breast Cancer Res.* 2003;5(2):89–95.

9. Eidesstattliche Versicherung

„Ich, **Jonas Parczyk**, versichere an Eides statt durch meine eigenhändige Unterschrift, dass ich die vorgelegte Dissertation mit dem Thema:

Deutsch:

„Untersuchung von synergistischen Interaktionen zwischen Substanzen mit Fokus auf Genominstabilität und Metabolismus in verschiedenen Tumorzelllinien zur Entwicklung einer Kombinationstherapie.“

English:

„Studying synergistic interactions of compounds targeting genome instability and metabolism in different cancer cell lines for a combinatory therapy approach.“

selbstständig und ohne nicht offengelegte Hilfe Dritter verfasst und keine anderen als die angegebenen Quellen und Hilfsmittel genutzt habe.

Alle Stellen, die wörtlich oder dem Sinne nach auf Publikationen oder Vorträgen anderer Autoren/innen beruhen, sind als solche in korrekter Zitierung kenntlich gemacht. Die Abschnitte zu Methodik (insbesondere praktische Arbeiten, Laborbestimmungen, statistische Aufarbeitung) und Resultaten (insbesondere Abbildungen, Graphiken und Tabellen) werden von mir verantwortet.

[Für den Fall, dass Sie die Forschung für Ihre Promotion ganz oder teilweise in Gruppenarbeit durchgeführt haben:] Ich versichere ferner, dass ich die in Zusammenarbeit mit anderen Personen generierten Daten, Datenauswertungen und Schlussfolgerungen korrekt gekennzeichnet und meinen eigenen Beitrag sowie die Beiträge anderer Personen korrekt kenntlich gemacht habe (siehe Anteilserklärung). Texte oder Textteile, die gemeinsam mit anderen erstellt oder verwendet wurden, habe ich korrekt kenntlich gemacht.

Meine Anteile an etwaigen Publikationen zu dieser Dissertation entsprechen denen, die in der untenstehenden gemeinsamen Erklärung mit dem/der Erstbetreuer/in, angegeben sind. Für sämtliche im Rahmen der Dissertation entstandenen Publikationen wurden die Richtlinien des ICMJE (International Committee of Medical Journal Editors; www.icmje.org) zur Autorenschaft eingehalten. Ich erkläre ferner, dass ich mich zur Einhaltung der Satzung der Charité – Universitätsmedizin Berlin zur Sicherung Guter Wissenschaftlicher Praxis verpflichte.

Weiterhin versichere ich, dass ich diese Dissertation weder in gleicher noch in ähnlicher Form bereits an einer anderen Fakultät eingereicht habe.

Die Bedeutung dieser eidesstattlichen Versicherung und die strafrechtlichen Folgen einer unwahren eidesstattlichen Versicherung (§§156, 161 des Strafgesetzbuches) sind mir bekannt und bewusst.“

Datum 27.04.2021

Unterschrift

10. Anteilserklärung an den erfolgten Publikationen / Declaration of own contribution to the publications

Jonas Parczyk contributed the following to the below listed publications

Genome reorganization in different cancer types: detection of cancer specific breakpoint regions

Christoph Standfuß, Jonas Parczyk, Jérôme Ruhnau and Andreas Klein
Molecular Cytogenetics 2019

Contribution in detail: data analyses concerning colocalization of genes and fragile sites, figure editing and creation, writing parts of the results-section, writing and editing of the manuscript

Synergisms of genome and metabolism stabilizing antitumor therapy (GMSAT) in human breast and colon cancer cell lines: a novel approach to screen for synergism

Jérôme Ruhnau*, Jonas Parczyk*, Kerstin Danker, Britta Eickholt, and Andreas Klein
BMC Cancer 2020

Contribution in detail: Planning and conception of the project, literature research, critical reading of the manuscript, all experiments (MTT-, SRB-, MDIS) with MCF-7 cells (table 1, 2, figure 3, 4, 5,6), data analysis

Dichloroacetate and PX-478 Exhibit Strong Synergistic Effects in a Various Number of Cancer Cell Lines

Jonas Parczyk*, Jérôme Ruhnau*, Carsten Pelz, Max Schilling, Hao Wu, Nicole Nadine Piaskowski, Britta Eickholt, Hartmut Kühn, Kerstin Danker, Andreas Klein

*shared primary authorship

BMC Cancer 2021

Contribution in detail: Planning and conception of the project, literature research, writing of the manuscript, all experiments (SRB-, Westernblots, Seahorse XF Analyzer) with MCF-7, A549, HepG2, U251 and HEK-293 cells (table 1, 2; figure 1, 2, 5, 7), data analysis, supervision of Max Schilling performing FACS analyses concerning induction of apoptosis

Unterschrift, Datum und Stempel des/der erstbetreuenden Hochschullehrers/in

Unterschrift des Doktoranden/der Doktorandin

11. Druckexemplare der ausgewählten Publikation / Publications

11.1 Publication 1

Genome reorganization in different cancer types: detection of cancer specific breakpoint regions

Christoph Standfuß, Jonas Parczyk, Jérôme Ruhnau and Andreas Klein

Mol Cytogenet 12, 25 (2019). Molecular Cytogenetics volume 12, Article number: 25 (2019)

doi:10.1186/s13039-019-0435-3


Impact factor: 1.233 - 2-year Impact Factor 1.408 - 5-year Impact Factor

RESEARCH

Open Access

Genome reorganization in different cancer types: detection of cancer specific breakpoint regions



Christoph Standfuß^{1,2}, Jonas Parczyk¹, Jerome Ruhnau¹ and Andreas Klein^{1*} 

Abstract

Background: Tumorigenesis is a multi-step process which is accompanied by substantial changes in genome organization. The development of these changes is not only a random process, but rather comprise specific DNA regions that are prone to the reorganization process.

Results: We have analyzed previously published SNP arrays from three different cancer types (pancreatic adenocarcinoma, breast cancer and metastatic melanoma) and from non-malignant control samples. We calculated segmental copy number variations as well as breakpoint regions. Some of these regions were not randomly involved in genome reorganization since we detected fifteen of them in at least 20% of all tumor samples and one region on chromosome 9 where 43% of tumors have a breakpoint. Further, the top-15 breakpoint regions show an association to known fragile sites. The relevance of these common breakpoint regions was further confirmed by analyzing SNP arrays from 917 cancer cell lines.

Conclusion: Our analyses suggest that genome reorganization is common in tumorigenesis and that some breakpoint regions can be found across all cancer types, while others exclusively occur in specific entities.

Keywords: Pancreatic ductal adenocarcinoma, Breast cancer, Melanoma, Copy number variation, Cancer genomics, Breakpoint and genome reorganization

Background

Tumorigenesis is a stepwise process, which involves multiple genetic, epigenetic and genomic events to transform a normal cell into a tumor cell [1–6]. Genomic changes like copy number variations (CNVs) or segmental copy number variations (segCNVs) increase throughout tumorigenesis [7–9] and are caused by various mechanisms, like fork stalling during replication or non-allelic homologous recombination [10–12].

These changes can affect the chromatin structure and therefore the spatial localization of specific genes, the DNA sequence like single nucleotide mutations, amplifications, deletions or translocations as well as changes of karyotypes like aneuploidies [1, 13–16].

It is also speculated that DNA regions exist which are prone for reorganization. Pevzner and Tesler stated in their seminal work “that mammalian genomes are mosaics of fragile regions with high propensity for rearrangements and solid regions with low propensity for rearrangements [17].”

Their thesis stands in contrast to the established theory of the random breakage model. The latter is based on the following two assumptions: Chromosomal segments are conserved among different species and chromosomal rearrangements are randomly distributed within the genome [18]. Indeed, it is well established that chromosomal segments exist in different species where orthologous genes are located in the same arrangement. On the other hand, it is now also established that specific DNA regions throughout the genome are prone to breakage and reorganization [17, 19–21]. Ruiz-Herrera et al stated that “certain chromosomal regions in the human genome have been repeatedly used in the evolutionary process. As a consequence, the

* Correspondence: andreas.klein@charite.de

¹Institute of Biochemistry, Charité – Universitätsmedizin Berlin, Corporate Member of Freie Universität Berlin, Humboldt-Universität zu Berlin, and Berlin Institute of Health, Charitéplatz 1, 10117 Berlin, Germany

Full list of author information is available at the end of the article



© The Author(s). 2019 **Open Access** This article is distributed under the terms of the Creative Commons Attribution 4.0 International License (<http://creativecommons.org/licenses/by/4.0/>), which permits unrestricted use, distribution, and reproduction in any medium, provided you give appropriate credit to the original author(s) and the source, provide a link to the Creative Commons license, and indicate if changes were made. The Creative Commons Public Domain Dedication waiver (<http://creativecommons.org/publicdomain/zero/1.0/>) applies to the data made available in this article, unless otherwise stated.

genome is a composite of fragile regions prone to reorganization...” Well known regions exhibiting chromosomal instability are fragile sites, which were firstly described by Magenis et al 1970 [22, 23]. “Fragile sites are specific loci that form gaps, constrictions, and breaks on chromosomes exposed to partial replication stress and are rearranged in tumors [24].” Fragile sites can be divided in rare and common fragile sites (CFSs). Rare fragile sites are only expressed in a few individuals. They are associated with the expansion of micro- or minisatellite repeats and inheritable diseases like fragile X syndrome. CFSs are regular parts of chromosomes and therefore found in all humans. CFSs are hotspots for metaphase chromosomal gaps and breaks and chromosomal rearrangements. CFS instability is an early step in tumorigenesis and could be responsible for genome reorganization in cancer [23, 25–29].

In 2012, Standfuß et al observed the stepwise increase in genome reorganization in a simian virus 40 (SV40) transformed mouse breast cancer model. The number of genomic changes increased from non-malignant, to hyperplastic and to tumor samples of mammary glands. Moreover, distinct breakpoint regions, where genome reorganization events take place, could be detected. They argued that unique and common breakpoint regions exist in breast cancer. However, due to the small sample size, the final proof was missing [9].

In this study, we analyzed DNA SNP arrays from 20 healthy controls and 111 cancer samples as well as 917 cancer cell lines. We found unique and common breakpoint regions in different cancer entities and more strikingly, we found a breakpoint region which was common in more than one third of all tumors and cancer cell lines tested.

Thus, we addressed the questions, whether genome reorganization is a random process, and whether specific DNA regions are prone to this reorganization procedure.

Material and methods

SNP array data

We reanalyzed 131 single-nucleotide polymorphism (SNP) microarrays, produced using the Genome-Wide Human SNP Array 6.0 platform (https://tools.thermo-fisher.com/content/sfs/brochures/genomewide_snp6_datasheet.pdf). The 111 tumor samples comprise 25 pancreatic adenocarcinomas (PDAC) from Donahue et al [30] [GSE32688], 22 PDAC derived cell lines from Barretina et al [31] [GSE36139], 16 metastatic melanomas from Marzese et al [32] [GSE44019] and 48 breast cancer samples from [GSE26232]. The 20 non-malignant control experiments (NMCE) comprise 15 samples derived from B cells isolated from peripheral blood of healthy donors from Xie et al [33] [GSE49045] and 5 samples derived from peripheral blood cells of breast

cancer patients [GSE48377]. The 15 blood samples from healthy donors were further termed as “reference” and the five peripheral blood cells from breast cancer patients were termed as “control”.

Further, we analyzed 917 cancer cell line samples from the Cancer Cell Line Encyclopedia (CCLE) [31] [GSE36139]. All samples are publicly available.

Copy-number variation

Raw SNP microarray data was processed using the Affymetrix Power Tools 1.15.0 (now OncoPrint™ Power Tools, Thermo Fisher Scientific) and the BRLMM-P algorithm to extract the normalized SNP signal intensities. To compare the total signal intensity distributions of all samples, intensities of both alleles for each SNP were added up. CNVs for each SNP was computed as log₂-ratios of each tumor sample and the reference dataset comprising 15 blood samples from healthy donors. The reference for each SNP was calculated as the average signal intensity of the 15 reference samples.

SegCNVs for each sample were computed with the DNACopy package (1.36.0) of Bioconductor (2.13) [34] with the following parameters: alpha = 0.001, undo.splits = “sdundo”, undo.SD = 0.5, min.width = 4. The DNACopy package implements the circular binary segmentation algorithm introduced by Olshen et al [35]. The number of segCNVs were counted for each experiment and set in relation to the number of base pairs for each chromosome. We excluded Chromosome Y (860 SNPs) and MT (411 SNPs) from our analyses. The heat map was generated using ggplot2 package of R. Hg19, provided by the University of California, Santa Cruz (UCSC), was used for human genome assembly.

Common breakpoints

The genome was divided into 30,951 bins of 100 kb size or less, if the bin represents a chromosomal end region. The occurrence of each breakpoint was counted in all 1048 analyzed samples to find regions of predisposed alterations. To enhance stringency, a breakpoint between two segCNVs was defined as follows: 1) the log₂-ratio difference between both segments has to be greater than 0.5. 2) at least one segment has to include a minimum of 10 and the other of 4 SNPs.

Odds ratio

To decide whether a breakpoint event (BP) is more frequent in cancer samples than in the NMCE, we calculated the odds ratios.

$$\text{oddsNMCE} = (\text{number of NMCE with BP}) / (\text{total number of NMCE} - \text{number of NMCE with BP}).$$

$$\text{oddsTumor} = (\text{number of tumors with BP}) / (\text{total number of tumors} - \text{number of tumors with BP}).$$

$$\text{oddsRatio} = (\text{oddsTumors}) / (\text{oddsNMCE})$$

Since some of the breakpoints were not found in the NMCE but had a high count in the tumor group odds ratio, calculations were not trivial. In accordance with the Cochrane Handbook for Systematic Reviews of Interventions we added 0.5 in those cases:

$$\text{oddsNMCE} = (\text{number of NMCE with BP} + 0.5) / (\text{total number of NMCE} + 0.5 - \text{number of NMCE with BP} + 0.5).$$

$$\text{oddsTumor} = (\text{number of tumors with BP} + 0.5) / (\text{total number of tumors} + 0.5 - \text{number of tumors with BP} + 0.5).$$

$$\text{oddsRatio} = (\text{oddsTumors}) / (\text{oddsNMCE})$$

Fragile sites

We used the chromosomal location of the 230 fragile sites published by Mrasek et al [36] and analyzed their occurrence within our breakpoint regions. Therefore, the cytogenetic location was translated into the chromosomal location with the help of the “Ensemble Genome Browser version GRCh37.p13.”

Results

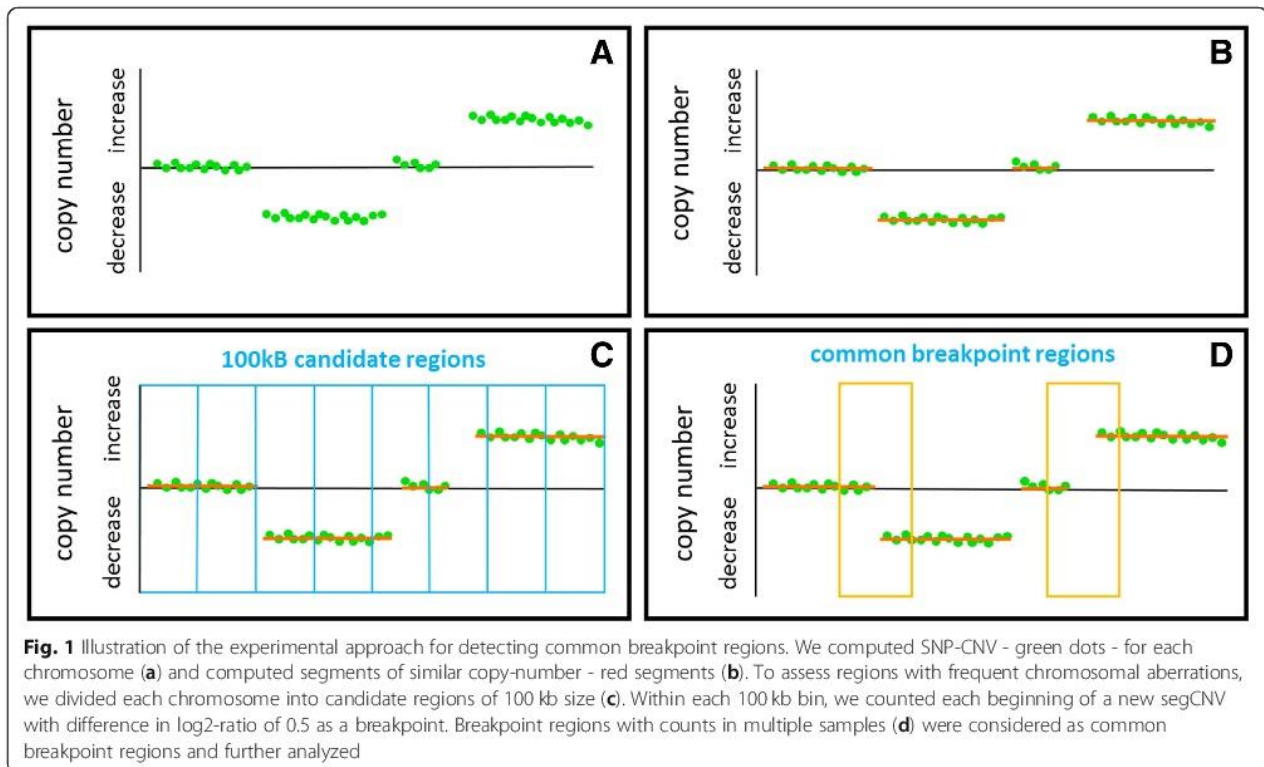
SNP CNVs in different tumor entities

To study the changes in genome reorganization during tumorigenesis, we analyzed previously published SNP arrays from 111 cancer samples: 25 pancreatic ductal adenocarcinoma, 22 PDAC derived cell lines, 16 metastatic melanoma and 48 breast cancer samples. As

NMCE, we used DNA from peripheral blood samples from healthy donors and from breast cancer patients.

We added up the signal intensities for SNP alleles and further determined continuous SNP CNV regions for all chromosomes using the circular binary segmentation algorithm introduced by Olshen and colleagues [35]. In order to define DNA regions with a high probability of genomic reorganization and which were common in multiple cancer samples, we divided the genome into 30,951 bins of 100 kb size and defined a breakpoint region as follows: at least two DNA segments have to differ in their average copy number values of more than a log₂-ratio of 0.5 and one segment has to consist of 10 SNPs instead of the minimum of four SNPs. Thus, breakpoint regions were defined as DNA sites where segmental copy number level shifts occur. If a breakpoint is present in multiple tumor samples, we call it common breakpoint region. This approach is illustrated in Fig. 1.

In total, we found 19,687 regions (63.61%) where at least one experiment had a breakpoint. However, since most of the breakpoint regions were present in only one or two tumor samples, we focused on genomic regions in which at least 23 out of the 111 tumors (20%) had a breakpoint (Fig. 2, Table 1). The heat map shows the fifteen 100 kb sized breakpoint regions, which appear in at least 20% of all tumor samples. We highlighted breakpoints more frequent in PDAC tumor samples with



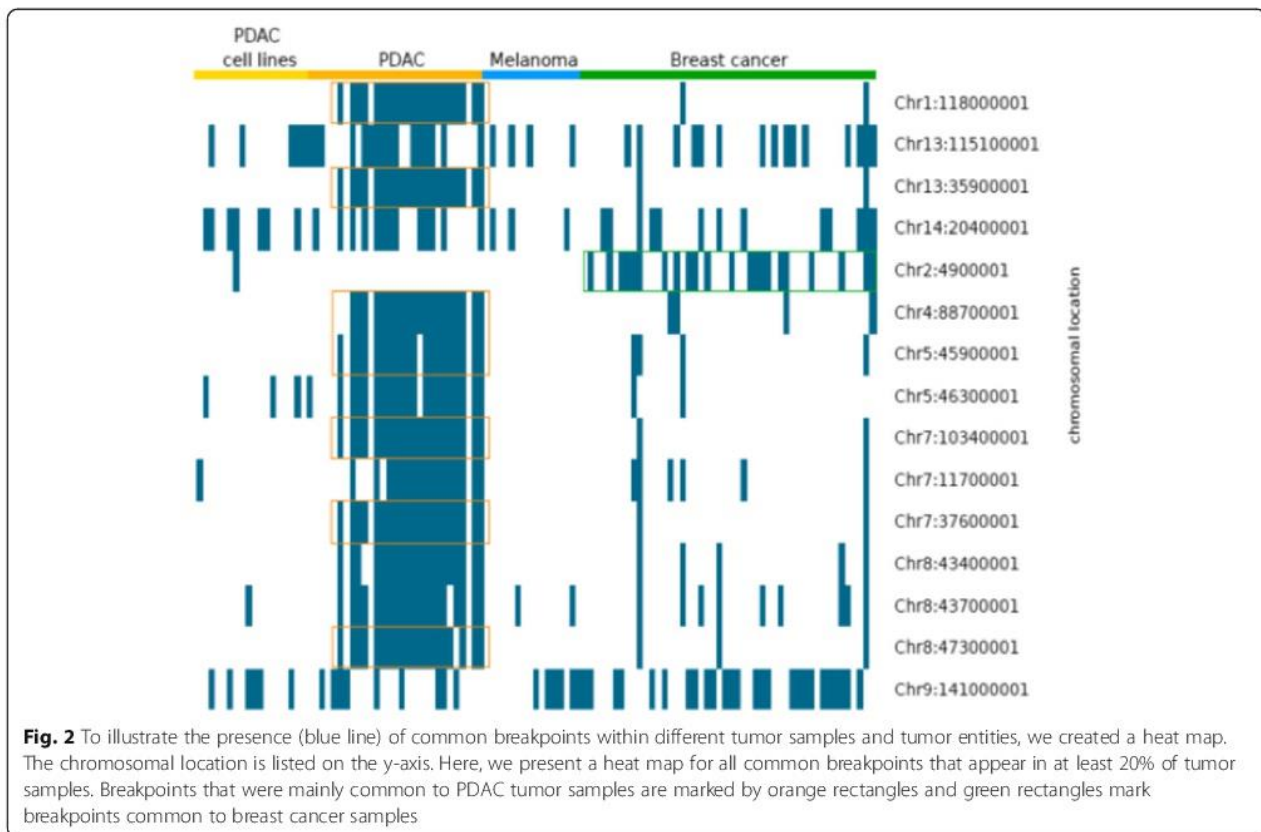


Table 1 Chromosomal location, occurrence of breakpoint events (BP), odds ratio, located genes and association to fragile sites of the top-15 breakpoint regions. Genes that are associated with cancer in literature are marked with an asterisk

Chr	Start	End	Cytoband	BP in NMCE (20)	BP in Tumors (111)	Odds Ratio	BP in CCLE (917)	Genes	Fragile Sites
1	118000001	118100001	1p12	0	23	10,68	4	<i>MAN1A2</i>	–
2	4900001	5000001	2p25.2	0	23	10,68	26	–	FRA2M
4	88700001	88800001	4q22.1	0	24	11,26	2	<i>IBSP*</i> , <i>MPEP*</i>	FRA4F
5	45900001	46000001	5p12	0	24	11,26	1	–	–
5	46300001	46400001	5p11	0	26	12,47	81	–	FRA5I
7	11700001	11800001	7p21.3	0	24	11,26	5	<i>THSD7A*</i>	FRA7L
7	37600001	37700001	7p14.1	0	23	10,68	0	<i>NECAP1P1</i>	–
7	103400001	103500001	7q22.1	1	23	4,97	1	<i>RELN*</i>	FRA7F
8	43400001	43500001	8p11.1	0	25	11,86	2	–	FRA8I
8	43700001	43800001	8p11.1	0	32	16,46	48	–	FRA8I
8	47300001	47400001	8q11.1	0	23	10,68	1	–	FRA8I
9	141000001	141100001	9q34.3	1	48	14,48	321	<i>CACNA1B*</i>	FRA9N
13	35900001	36000001	13q13.3	0	23	10,68	1	<i>NBEA*</i>	–
13	115100001	115106996	13q34	3	40	3,19	210	–	FRA13I
14	20400001	20500001	14q11.2	3	36	2,72	61	<i>OR4K1</i> , <i>OR4K5</i> , <i>OR4K14</i> , <i>OR4K15</i>	FRA14D

orange boxes, and regions more frequent in breast cancer samples with green boxes. This result indicates that some breakpoints are more frequent in only one tumor entity (like chromosomes 1, 2 and 13) whereas other regions are present in all tumor entities (like chromosomes 9 and 13). The breakpoints on Chromosomes 9 and 13 had 43 and 36% of all tumors in common. Since some breakpoints were also present in the NMCE, we verified the relevance of a breakpoint region by determining the odds ratio for being tumor specific.

Table 1 shows the odds ratio for the breakpoints illustrated in Fig. 2. In all of the top-15 breakpoint regions, we observed that on average, an odds ratio > 10 indicates a high prevalence for these breakpoints to occur in tumor samples. The two highest odds ratio values were calculated for the breakpoint of chromosome 9 present in 48 different tumor samples and one NMCE (odds ratio = 14.5) and the breakpoint on chromosome 8 (43,700,001) present only in 32 different tumor samples (odds ratio = 16.5). Twelve genes were located in eight of the top-15 breakpoint regions, and six of these genes are associated with cancer (*CACNA1B*, *IBSP*, *MEPE*, *NBEA*, *RELN* and *THSD7A*) (Table 1).

Cancer cell line encyclopedia (CCLE)

To further validate, the top-15 breakpoint regions, we included 917 cancer cell line samples in our analyses. We summarized in Table 2 the seven 100 kb sized breakpoint regions which appear in at least 20% of all CCLE samples. The breakpoint regions on Chromosomes 9 (141,000,001) and 13 (115,100,001) which were present in all tumor entities, also had the most breakpoints in the analyzed cancer cell lines. On Chromosome 9, 321 cancer cell lines (34%) and on Chromosome 13, 210 (22%) cancer cell lines had a breakpoint within the aforementioned regions. Five genes were located in four of the seven breakpoint regions and three of these genes (*CACNA1B*, *C8orf33* and *KIAA0513*) are associated with cancer (Table 2). Interestingly, only very few cancer cell lines (< 0.5%) had breakpoints in the seven breakpoint regions that were associated with PDAC: e.g. the region on chromosome 7

(37,600,001) had no breakpoint in cancer cell lines and the regions on chromosomes 5 (45,900,001), 7 (103,400,001), 8 (47,300,001) and 13 (35,900,001) had only one breakpoint in cancer cell lines (Table 1). The breast cancer associated breakpoint region on chromosome 2 is also only shared by 2.8% of cancer cell lines.

The presented results indicate that we created a set of common breakpoint regions with the help of PDAC, melanoma metastasis and breast cancer samples that were more highly associated with single cancer entities, whereas other breakpoint regions can be found in a variety of tumors.

Fragile site

Since fragile sites are well known regions exhibiting chromosome instability, we compared the chromosomal locations of the common breakpoint regions we found with data from chromosomal fragile sites [36]. Eleven thousand three hundred sixty out of the 19,687 breakpoint regions contained a fragile site (58%).

Since an odds ratio less than one indicates a higher likelihood of a breakpoint region to occur in NMCE, and an odds ratio above one indicates higher odds for occurring in tumor samples, we determined the percentage of a fragile site to occur in relation to the odds ratio. Out of the 19,687 breakpoint regions, 13,063 had an odds ratio of less than one and 6624 above one. A region with an odds ratio < 1 occurred in 57% (7471 out of 13,063) associated with fragile sites and a region with an odds ratio > 1 occurred in 59% (3889 out of 6624) associated with fragile sites. Thus, we could not determine a crucial difference in the association to fragile sites in the more tumor linked breakpoint regions.

However, 11 of the top-15 breakpoint regions (73%) were associated with fragile sites and 6 of the 7 CCLE related breakpoint region (86%), indicating a strong association of the top-ranked breakpoint regions to known fragile sites.

Targeted investigation

Further, we evaluated important regions known for genome reorganization from literature (e.g. loss-of

Table 2 Chromosomal location, occurrence of breakpoint events (BP), odds ratio, located genes and association to fragile sites of the top-ranked CCLE breakpoint regions. Genes that are associated with cancer in literature are marked with an asterisk. Interestingly, the breakpoint region in chromosome 2 is close to the cancer associated *SDC1* gene by about 558 bases

Chr	Start	End	Cytoband	BP in NMCE (20)	BP in Tumors (111)	Odds Ratio	BP in CCLE (917)	Gene	Fragile Sites
2	20300001	20400001	2p24.1	0	9	3,73	248	–	–
4	190900001	191000001	4q35.2	0	14	5,98	190	<i>FRG2</i>	FRA4L, FRA4M
7	159100001	159119220	7q36.3	0	22	10,11	230	–	FRA7I
8	146200001	146300001	8q24.3	0	21	9,56	238	<i>C8orf33*</i>	FRA8D
9	141000001	141100001	9q34.3	1	48	14,48	321	<i>CACNA1B*</i>	FRA9N
13	115100001	115106996	13q34	3	40	3,19	210	–	FRA13I
16	85000001	85100001	16q24.1	0	8	3,30	244	<i>KIAA0513*</i> , <i>ZDHHC7</i>	FRA16J

heterozygosity or homozygous deletion) and looked for the relevance of those regions in our dataset concerning the occurrence of breakpoints. Fragile site FRA16D (16q23.2) is within a region of frequent loss-of-heterozygosity in breast and prostate cancers. Interestingly, we found 64 breakpoints in 13 tumor samples (11.7%) for this fragile site, whereof 61 were found in nine breast cancer samples (18.75% of all breast cancer samples). Another frequently altered chromosomal region is located on chromosome 9 (21,900,001) where the *tumor suppressor p16* (official symbol *CDKN2A*) is present. In the corresponding bins, 104 cancer cell lines had a breakpoint (11.34%) and eight tumor samples (7.2%). Interestingly, this region is part of the fragile site FRA9A. In this CFS 56 tumor samples (50.5%) had at least one breakpoint.

The most commonly known unstable CFS region is FRA3B [37]. In this CFS, spanning over 43 bins, 148 breakpoints were detected in 26 cancer samples (23.4%). It is also noteworthy that 23 out of the 26 cancer samples had a breakpoint in the region of the gene *FHIT* lying inside of FRA3B. In line with this, 243 cancer cell lines have breakpoints in FRA3B and 223 of those have breakpoints in the 16 bins containing *FHIT*.

Discussion

In this study, we examined the theory that genome reorganization during tumorigenesis is not a random process but rather a directed process, involving defined DNA regions. Therefore, we have reanalyzed 1,048 DNA SNP arrays from different cancer entities and non-malignant samples. We found an increase of DNA breakpoint regions in tumor samples compared to NMCE. Interestingly, several breakpoint regions were common in several tumor specimen (up to 43%) where as other regions seemed to be more restricted to a specific tumor entity. Surprisingly, breakpoint regions between PDCA and PDCA derived cell lines differ considerably. On the one hand, Kalinina and colleagues established a pancreatic cancer cell line from a primary tumor. Kalinina and colleagues also observed a similar CNV pattern between tumor and cell line after passing the cell line 15–20 times, as well as a considerable number of similar large chromosomal alterations [38]. On the other hand, Burdall and colleagues stated that “Cell lines are prone to genotypic and phenotypic drift during their continual culture. This is particularly common in the more frequently used cell lines, especially those that have been deposited in cell banks for many years [39].” This might be applicable for the used cell lines in our approach, e.g. Capan 1 and 2 were established 1974 and 1975, respectively [40, 41].

It is well known that cancers develop from stem lines in a stepwise process and are characterized by

chromosomal aberrations and chromosomal instability [42, 43]. The Mitelman Database of Chromosome Aberrations and Gene Fusions in Cancer currently lists 69,134 human cancers with individual clonal karyotypes [44]. In 2012, Standfuß et al found a stepwise increase in genome reorganization in a mouse breast cancer model. The number of genomic changes increased from non-malignant, to hyperplastic and to tumor samples of mammary glands [9]. Further, an analysis of 2,737 tumor samples from 8 different tumor entities (including breast cancers) showed that tumor entity-specific breakpoints could be found for all examined tumor entities. The breakpoint regions were equally distributed over all entities [45]. Further, colocalization assessment identified 20,077 CNV-affecting genes and 169 of these being known tumor-related genes. In another study, Beroukhi et al looked for somatic CNVs in 3,131 cancer specimen and found 158 regions of focal somatic CNVs of which only 36 can be explained by the presence of known cancer target genes located within this region like *FHIT* and *p16* [8]. Meaburn and Misteli also identified several genes specifically repositioned during tumorigenesis. The alterations of the spatial positioning were unrelated to gene activity [15]. In our study, genes were located in eight of the top-15 and four of the top-7 CCLE breakpoint regions. Eight of these genes are linked to cancer, but none are well characterized oncogenes or tumor suppressor genes. Interestingly, only *C8orf33* and *NBEA* seemed to have tumor suppressor functions [46, 47]. The other six genes are associated with tumor progression. *IBSP*, *MEPE*, *RELN* and *THSD7A* are associated with migration, invasion, infiltration and angiogenesis [48–51]; *CACNA1B* and *KIAA0513* are associated with cell proliferation and apoptosis. *CACNA1B* overexpression is associated with an unfavorable prognosis in non-small cellular lung cancer [52] and altered expression of *KIAA0513*, due to an aberrant methylation pattern, correlated with non-survivors in Neuroblastoma [53].

As early as 1984, several scientists postulated an association between human fragile sites and cancer breakpoints [25, 26, 54]. CFSs in cancer were considered as regions of chromosomal instability and their associated genes are frequently deleted or rearranged in cancer cells [55]. Since we found a strong correlation of our top breakpoint regions with fragile sites, we were also interested to look for breakpoints in specific CFSs described in literature. Finnis and colleagues found out that the CFS FRA16D (16q23.2) is located within regions of frequent loss-of-heterozygosity in breast and prostate cancers [56]. Here we found a breakpoint almost specific for breast cancer, since 61 from 64 breakpoints stem from breast cancer samples. 1986 Smeets and colleagues described FRA3B as the most unstable CFS region within

chromosomal band 3p14.2 [37]. This chromosomal region is a hot-spot for deletions and other alterations in a variety of different cancers. *FHIT*, a large tumor suppressor gene spanning over approximately 35% of this fragile site, is also harbored in this region [57]. While 26 tumors and 243 cancer cell lines have a breakpoint in FR3B, the majority of these breakpoints, namely 23 and 223, lay in the *FHIT* gene. Thus, it is not surprising that estimates designate *FHIT* as the most frequently altered gene in cancer [58]. Inside the CFS, FRA9A the *p16* gene is located. Cox and Colleagues found in their “survey of homozygous deletions in human cancer genomes” that *p16* was the most frequent target of homozygous deletions (24.6%) [59]. Further, they argued that genetic rearrangement in this region might signify less negative selection compared to other regions because *p16* is located adjacent to one of the largest gene-poor regions of the human genome. When looking at the direct adjacent bins of *p16*, it stands out that the area of and around *p16* is the area of FRA9A where most of the breakpoints occur. This indicates that those breakpoints occurring in this CFS might play a role for tumor development, instead of being a random side effect of genomic instability.

However, genome rearrangements are not restricted to cancer cells. Rather, they are also present in adaptive processes, such as response to selective pressures from the environment and are associated with various diseases [60–62].

Conclusion

In this study, we found that genome reorganization is more enhanced in tumor samples compared to the non-malignant controls and that some genome regions exist that are prone to rearrangements. We identified regions which may play an important role in the tumorigenesis of specific tumor entities and others that occur commonly during tumorigenesis.

For further investigations, genomic profiles could be linked to clinical data in order to produce additional prognostic markers for clinical outcome.

Abbreviations

BP: breakpoint event; CCL: Cancer Cell Line Encyclopedia; CFS: common fragile site; CNV: copy number variation; NMCE: non-malignant control experiment; PDAC: pancreatic adenocarcinoma; segCNV: segmental copy number variation; SNP: single-nucleotide polymorphism

Acknowledgements

We gratefully acknowledge the support of Cara Reiter-Brennan for editing the English version and critical discussions of this manuscript. We acknowledge support from the German Research Foundation (DFG) and the Open Access Publication Fund of Charité – Universitätsmedizin Berlin.

Funding

N/A

Availability of data and materials

All analyzed samples are publicly available.

Authors' contributions

Conceptualization: CS and AK; Analyses and graphic design: CS, JP and JR; Project administration and supervision: AK; Writing and editing: CS, JP, JR and AK. All authors read and approved the manuscript.

Ethics approval and consent to participate

The authors have no ethical conflicts to disclose.

Consent for publication

Not applicable.

Competing interests

The authors declare that they have no competing interests.

Publisher's Note

Springer Nature remains neutral with regard to jurisdictional claims in published maps and institutional affiliations.

Author details

¹Institute of Biochemistry, Charité – Universitätsmedizin Berlin, Corporate Member of Freie Universität Berlin, Humboldt-Universität zu Berlin, and Berlin Institute of Health, Charitéplatz 1, 10117 Berlin, Germany. ²Institute of Biochemistry, Charité – Universitätsmedizin Berlin, corporate member of Freie Universität Berlin, Humboldt-Universität zu Berlin, and Berlin Institute of Health, MTU Aero Engines, 80995 Munich, Germany.

Received: 8 February 2019 Accepted: 15 May 2019

Published online: 20 June 2019

References

- Vogelstein B, Kinzler KW. The multistep nature of cancer. *Trends Genet.* 1993;9:138–41.
- Hanahan D, Weinberg RA. Hallmarks of cancer: the next generation. *Cell.* 2011;144:646–74.
- Loeb LA, Loeb KR, Anderson JP. Multiple mutations and cancer. *Proc Natl Acad Sci.* 2003;100:776–81.
- Osborne C. Oncogenes and tumor suppressor genes in breast Cancer: potential diagnostic and therapeutic applications. *Oncologist.* 2004;9:361–77.
- Klein A, Guhl E, Zollinger R, et al. Gene expression profiling: cell cycle deregulation and aneuploidy do not cause breast cancer formation in WAP-SVT/t transgenic animals. *J Mol Med.* 2005;83:362–76.
- Foulds L. The experimental study of tumor progression: a review. *Cancer Res.* 1954;14:327–39.
- Shlien A, Malkin D. Copy number variations and cancer. *Genome Med.* 2009;1:1–9.
- Beroukhim R, Mermel CH, Porter D, et al. The landscape of somatic copy-number alteration across human cancers. *Nature.* 2010;463:899–905.
- Standfuß C, Pospisil H, Klein A. SNP microarray analyses reveal copy number alterations and progressive genome reorganization during tumor development in SVT/t driven mice breast cancer. *BMC Cancer.* 2012;12:380.
- Redon R, Ishikawa S, Fitch KR, et al. Global variation in copy number in the human genome. *Nature.* 2006;444:444–54.
- Malhotra D, Sebat J. CNVs: harbingers of a rare variant revolution in psychiatric genetics. *Cell.* 2012;148:1223–41.
- Zhang F, Khajavi M, Connolly AM, et al. The DNA replication FoSTeS/MMBIR mechanism can generate genomic, genic and exonic complex rearrangements in humans. *Nat Genet.* 2009;41:849–53.
- Sen S. Aneuploidy and cancer. *Curr Opin Oncol.* 2000;12:82–8.
- Mitelman F, Johansson B, Mertens F. The impact of translocations and gene fusions on cancer causation. *Nat Rev Cancer.* 2007;7:233–45.
- Meaburn KJ, Misteli T. Locus-specific and activity-independent gene repositioning during early tumorigenesis. *J Cell Biol.* 2008;180:39–50.
- Klein A, Li N, Nicholson JM, et al. Transgenic oncogenes induce oncogene-independent cancers with individual karyotypes and phenotypes. *Cancer Genet Cytogenet.* 2010;200:79–99.
- Pevzner P, Tesler G. Human and mouse genomic sequences reveal extensive breakpoint reuse in mammalian evolution. *Proc Natl Acad Sci.* 2003;100:7672–7.
- Nadeau JH, Taylor BA. Lengths of chromosomal segments conserved since divergence of man and mouse. *Proc Natl Acad Sci.* 1984;81:814–8.
- Zhao S, Shetty J, Hou L, et al. Human, mouse, and rat genome large-scale rearrangements: stability versus speciation. *Genome Res.* 2004;14:1851–60.

20. Murphy WJ, Larkin DM, Everts-Van Der Wind A, et al. Evolution: Dynamics of mammalian chromosome evolution inferred from multispecies comparative maps. *Science*. 1997;275:309–313.
21. Ruiz-Herrera A, Castresana J, Robinson TJ. Is mammalian chromosomal evolution driven by regions of genome fragility? *Genome Biol*. 2006;7:R115.
22. Magenis RE, Hecht F, Lovrien EW. Heritable fragile site on chromosome 16: probable localization of haptoglobin locus in man. *Science*. 1970;170:85–7.
23. Durkin SG, Glover TW. Chromosome fragile sites. *Annu Rev Genet*. 2007;41:169–92.
24. Zlotorynski E, Rahat A, Skaug J, et al. Molecular basis for expression of common and rare fragile sites. *Mol Cell Biol*. 2003;23:7143–51.
25. Hecht F, Sutherland GR. Fragile sites and cancer breakpoints. *Cancer Genet Cytogenet*. 1984;12:179–81.
26. Yunis JJ, Soreng AL. Constitutive fragile sites and cancer. *Science*. 1984;226:1199–204.
27. Bartkova J, Hořejší Z, Koed K, et al. DNA damage response as a candidate anti-cancer barrier in early human tumorigenesis. *Nature*. 2005;434:864–70.
28. Tsantoulis PK, Kotsinas A, Sfikakis PP, et al. Oncogene-induced replication stress preferentially targets common fragile sites in preneoplastic lesions. A genome-wide study. *Oncogene*. 2008;27:3256–64.
29. Debatisse M, Le Tallec B, Letessier A, et al. Common fragile sites: mechanisms of instability revisited. *Trends Genet*. 2012;28:22–32.
30. Donahue TR, Tran LM, Hill R, et al. Integrative survival-based molecular profiling of human pancreatic Cancer. *Clin Cancer Res*. 2012;18:1352–63.
31. Barretina J, Caponigro G, Stransky N, et al. The Cancer cell line encyclopedia enables predictive modelling of anticancer drug sensitivity. *Nature*. 2012;483:603–307.
32. Marzese DM, Scolyer RA, Huynh JL, et al. Epigenome-wide DNA methylation landscape of melanoma progression to brain metastasis reveals aberrations on homeobox D cluster associated with prognosis. *Hum Mol Genet*. 2013;23:226–38.
33. Xie Z, Nagarajan V, Sturdevant DE, et al. Genome-wide SNP analysis of the Systemic Capillary Leak Syndrome (Clarkson disease). *Rare Dis (Austin, Tex)*. 1. Epub ahead of print 2013. DOI: <https://doi.org/10.4161/rdis.27445>.
34. Gentleman RC, Carey VJ, Bates DM, et al. Bioconductor: open software development for computational biology and bioinformatics. *Genome Biol*. 2004;5:R80.
35. Olshen AB, Venkatraman ES, Lucito R, et al. Circular binary segmentation for the analysis of array-based DNA copy number data. *Biostatistics*. 2004;5:557–72.
36. Mrasek K, Schoder C, Teichmann A-C, et al. Global screening and extended nomenclature for 230 aphidicolin-inducible fragile sites, including 61 yet unreported ones. *Int J Oncol*. 2010;36:929–40.
37. Smeets DF, Scheres JM, Hustinx TW. The most common fragile site in man is 3p14. *Hum Genet*. 1986;72:215–20.
38. Kalinina T, Güngör C, Thielges S, et al. Establishment and characterization of a new human pancreatic adenocarcinoma cell line with high metastatic potential to the lung. *BMC Cancer*; 10. Epub ahead of print 2010. DOI: <https://doi.org/10.1186/1471-2407-10-295>.
39. Burdall SE, Hanby AM, Lansdown MRJ, et al. Breast cancer cell lines: friend or foe? *Breast Cancer Res*. 2003;5:89–95.
40. Kyriazis AP, Kyriazis AA, Scarpelli DG, Fogh J, Rao MSLR. Human pancreatic adenocarcinoma line Capan-1 in tissue culture and the nude mouse: morphologic, biologic, and biochemical characteristics. *Am Assoc Pathol*. 1982;106:250–60.
41. Kyriazis AA, Kyriazis AP, Sternberg CN, Sloane NHLJ. Morphological, biological, biochemical, and karyotypic characteristics of human pancreatic ductal adenocarcinoma Capan-2 in tissue culture and the nude mouse. *Cancer Res*. 1986;58:10–5.
42. Thompson SL, Compton DA. Chromosomes and cancer cells. *Chromosome Res*. 2011;19:433–44.
43. Vargas-Rondón N, Villegas VE, Rondón-Lagos M. The role of chromosomal instability in cancer and therapeutic responses. *Cancers (Basel)*. 2018;10:1–21. <https://doi.org/10.3390/cancers10050121>. Accessed 5 MAY 2019.
44. Mrazek K, Schoder C, Teichmann A-C, et al. Global screening and extended nomenclature for 230 aphidicolin-inducible fragile sites, including 61 yet unreported ones. *Int J Oncol*. 2010;36:929–40.
45. Marczok S, Bortz B, Wang C, et al. Comprehensive analysis of genome rearrangements in eight human malignant tumor tissues. *PLoS One*. 2016;11:e0158995.
46. Shao P, Sun D, Wang L, et al. Deep sequencing and comprehensive expression analysis identifies several molecules potentially related to human poorly differentiated hepatocellular carcinoma. *FEBS Open Bio*. 2017;7:1696–706.
47. O'Neal J, Gao F, Hassan A, et al. Neurobeachin (NBEA) is a target of recurrent interstitial deletions at 13q13 in patients with MGUS and multiple myeloma. *Exp Hematol*. 2009;37:234–44.
48. Xu T, Qin R, Zhou J, et al. High Bone Sialoprotein (BSP) Expression Correlates with Increased Tumor Grade and Predicts a Poorer Prognosis of High-Grade Glioma Patients. *PLoS One*; 7. Epub ahead of print 2012. DOI: <https://doi.org/10.1371/journal.pone.0048415>.
49. Gao Z, Zhao Y, Geng Q, et al. Regulatory roles of miRNA-758 and matrix extracellular phosphoglycoprotein in cervical cancer. *Exp Ther Med*. 2017;14:2789–94.
50. Dou A, Wang Z, Zhang N, et al. Loss of reelin suppresses cell survival and mobility in non-Hodgkin lymphoma. *Oncol Rep*. 2017;37:3572–80.
51. Wiech T, Hoxha E, Schröder C, et al. THSD7A expression in human cancer. *Genes Chromosom Cancer*. 2016;56:314–27.
52. Zhou X, Wang W, Zhang S, et al. CACNA1B (ca_v2.2) overexpression and its association with Clinicopathologic characteristics and unfavorable prognosis in non-small cell lung Cancer. *Dis Markers*. 2017;2017:1–8.
53. Olsson M, Beck S, Kogner P, et al. Genome-wide methylation profiling identifies novel methylated genes in neuroblastoma tumors. *Epigenetics*. 2016;11:74–84.
54. Glover TW, Berger C, Coyle J, et al. DNA polymerase α inhibition by aphidicolin induces gaps and breaks at common fragile sites in human chromosomes. *Hum Genet*. 1984;67:136–42.
55. Glover TW, Wilson TE, Arit MF. Fragile sites in cancer: more than meets the eye. *Nat Rev Cancer*. 2017;17:489–501.
56. Finnis M, Dayan S, Hobson L, et al. Common chromosomal fragile site FRA16D mutation in cancer cells. *Hum Mol Genet*. 2005;14:1341–9.
57. Smith DJ, Zhu Y, McAvoy S, et al. Common fragile sites, extremely large genes, neural development and cancer. *Cancer Lett*. 2006;232:48–57.
58. Saldivar JC, Bene J, Hosseini SA, et al. Characterization of the role of Fhit in suppression of DNA damage. *Adv Biol Regul*. 2013;53:77–85.
59. Cox C, Bignell G, Greenman C, et al. A survey of homozygous deletions in human cancer genomes. *Proc Natl Acad Sci*. 2005;102:4542–7.
60. Dunham MJ, Badrane H, Ferea T, et al. Characteristic genome rearrangements in experimental evolution of *Saccharomyces cerevisiae*. *Proc Natl Acad Sci*. 2002;99:16144–9.
61. Tang Y-C, Amon A. Gene copy-number alterations: a cost-benefit analysis. *Cell*. 2013;152:394–405.
62. Meaburn KJ. Spatial genome organization and its emerging role as a potential diagnosis tool. *Front Genet*. 2016;7:1–18.

Ready to submit your research? Choose BMC and benefit from:

- fast, convenient online submission
- thorough peer review by experienced researchers in your field
- rapid publication on acceptance
- support for research data, including large and complex data types
- gold Open Access which fosters wider collaboration and increased citations
- maximum visibility for your research: over 100M website views per year

At BMC, research is always in progress.

Learn more biomedcentral.com/submissions



11.2 Publication 2

Synergisms of genome and metabolism stabilizing antitumor therapy (GMSAT) in human breast and colon cancer cell lines: a novel approach to screen for synergism

Jérôme Ruhnau*, Jonas Parczyk*, Kerstin Danker, Britta Eickholt, and Andreas Klein

*geteilte Erstautorenschaft

BMC Cancer. 2020; 20: 617. Published online 2020 Jul 2.

doi: 10.1186/s12885-020-07062-2

PMCID: PMC7331156

PMID:

32615946

Impact factor: 3.15 - 2-year Impact Factor 3.432 - 5-year Impact Factor

RESEARCH ARTICLE

Open Access



Synergisms of genome and metabolism stabilizing antitumor therapy (GMSAT) in human breast and colon cancer cell lines: a novel approach to screen for synergism

Jérôme Ruhnau^{*†}, Jonas Parczyk^{*†} , Kerstin Danker, Britta Eickholt and Andreas Klein

Abstract

Background: Despite an improvement of prognosis in breast and colon cancer, the outcome of the metastatic disease is still severe. Microevolution of cancer cells often leads to drug resistance and tumor-recurrence. To target the driving forces of the tumor microevolution, we focused on synergistic drug combinations of selected compounds. The aim is to prevent the tumor from evolving in order to stabilize disease remission. To identify synergisms in a high number of compounds, we propose here a three-step concept that is cost efficient, independent of high-throughput machines and reliable in its predictions.

Methods: We created dose response curves using MTT- and SRB-assays with 14 different compounds in MCF-7, HT-29 and MDA-MB-231 cells. In order to efficiently screen for synergies, we developed a screening tool in which 14 drugs were combined (91 combinations) in MCF-7 and HT-29 using EC₂₅ or less. The most promising combinations were verified by the method of Chou and Talalay.

Results: All 14 compounds exhibit antitumor effects on each of the three cell lines. The screening tool resulted in 19 potential synergisms detected in HT-29 (20.9%) and 27 in MCF-7 (29.7%). Seven of the top combinations were further verified over the whole dose response curve, and for five combinations a significant synergy could be confirmed. The combination Nutlin-3 (inhibition of MDM2) and PX-478 (inhibition of HIF-1 α) could be confirmed for all three cell lines. The same accounts for the combination of Dichloroacetate (PDH activation) and NHI-2 (LDH-A inhibition). Our screening method proved to be an efficient tool that is reliable in its projections.

Conclusions: The presented three-step concept proved to be cost- and time-efficient with respect to the resulting data. The newly found combinations show promising results in MCF-7, HT-29 and MDA-MB231 cancer cells.

Keywords: Synergism, drug combination, cancer therapy, Nutlin-3, PX-478, Dichloroacetate, NHI-2, MDA-MB-231, MCF-7, HT-29

* Correspondence: jerome.ruhnau@gmail.com; jonasparczyk@outlook.com

[†]Jérôme Ruhnau and Jonas Parczyk contributed equally to this work.

Charité – Universitätsmedizin Berlin, Corporate Member of Freie Universität Berlin, Humboldt-Universität zu Berlin, and Berlin Institute of Health, Institute of Biochemistry, Charitéplatz 1, 10117 Berlin, Germany



© The Author(s). 2020 **Open Access** This article is licensed under a Creative Commons Attribution 4.0 International License, which permits use, sharing, adaptation, distribution and reproduction in any medium or format, as long as you give appropriate credit to the original author(s) and the source, provide a link to the Creative Commons licence, and indicate if changes were made. The images or other third party material in this article are included in the article's Creative Commons licence, unless indicated otherwise in a credit line to the material. If material is not included in the article's Creative Commons licence and your intended use is not permitted by statutory regulation or exceeds the permitted use, you will need to obtain permission directly from the copyright holder. To view a copy of this licence, visit <http://creativecommons.org/licenses/by/4.0/>. The Creative Commons Public Domain Dedication waiver (<http://creativecommons.org/publicdomain/zero/1.0/>) applies to the data made available in this article, unless otherwise stated in a credit line to the data.

Background

Introduction

Although a lot of progress has been made in the research of potential anti-cancer agents over the last decade, secondary therapy failure and disease progression is still the major problem in most tumor entities especially in the metastatic state of solid tumors [1, 2]. The tumor microevolution gives constantly rise to new populations of cancer cells with diverse properties [3] making it difficult to target them. Therefore, we developed a combinatory therapeutic approach that targets the tumor microevolution and its driving forces.

Industrial funds become more important in research. As industrial funding [4] and the focus on commercial interests increase, research is favourably conducted on newly bioengineered and patentable drugs [5] rather than generic compounds. Therefore, we aimed to establish a cost-efficient screening strategy that is feasible for independent work groups. In order to screen a relatively high number of potential compounds for their synergistic potency, we present here a three-step approach including a minimalistic drug interaction screening (MDIS) that is cost-efficient and can easily be established with basic laboratory equipment independent of expensive high-throughput devices.

The tumor microevolution and its driving forces

Unfortunately, initial antitumor treatment frequently leaves residual disease from which the tumor regrows [6]. Microevolution of cancer cells often leads to drug resistance and tumor recurrence [7]. Important driving forces of the microevolution are the genomic instability [8], the tumor metabolism [9, 10] and a deregulated cell cycle [11] that converge in a high proliferation rate combined with a high occurrence of mutations. To treat such complex diseases, combinations of drugs that target different aspects of the disease and at best, act synergistically may be the method of choice. Another complex disease that can currently be kept in remission with a combinatory approach (combined antiretroviral therapy, “cART”) [12] is the infection with the human immunodeficiency virus (HIV). As HIV itself undergoes a microevolution due to the high mutagenesis by virus reverse transcriptase [13] it took decades to find an adequate multi-target treatment. And even with cART, the development of drug resistances especially for nucleotide reverse transcriptase inhibitors (NRTI) is still a major problem [14]. Due to the complexity of cancer, it can be anticipated that more sophisticated combinatory approaches are needed. An example for such a concept is CUSP9 where multiple drugs that are approved for non-cancer indications are combined as a treatment approach for recurrent glioblastoma [15–17]. The combination of compounds can lead to a broader effect on different tumor subtypes which may reduce

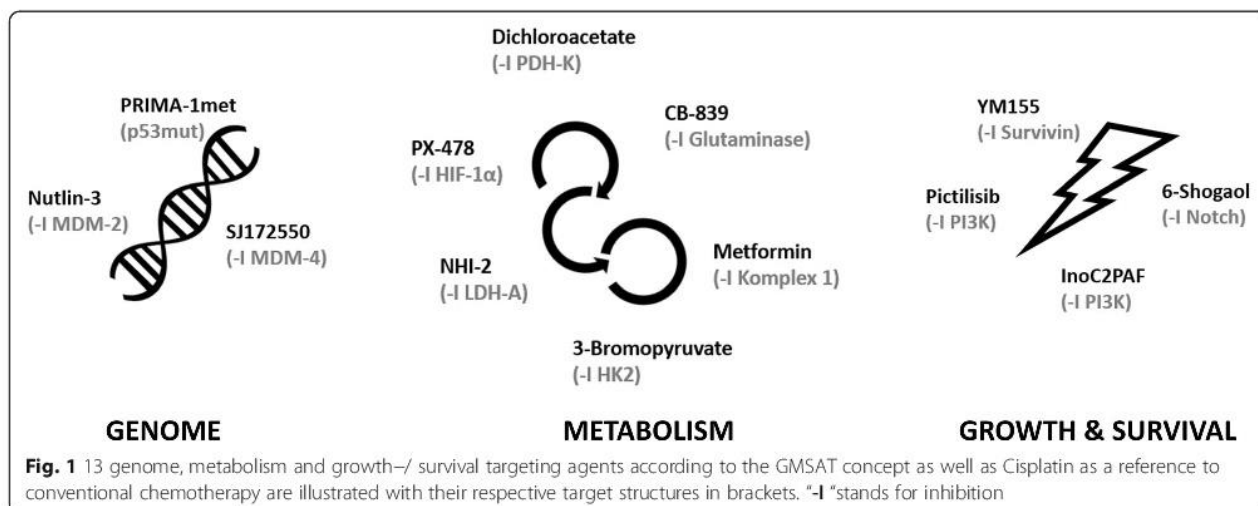
chances of relapses or keep the tumor in a progression free state [18].

Genome and metabolism stabilizing antitumor therapy (GMSAT)

The here presented combinatory approach aims to counteract the tumor microevolution by targeting the genome, tumor metabolism as well as growth and survival (Fig. 1). PRIMA-1met and Nutlin-3 are two compounds targeting p53 which is often referred to as the “guardian of the genome” [19]. PRIMA-1met binds and reactivates mutated p53 [20] whereas Nutlin-3 increases p53 levels by disrupting the p53-MDM2 interaction and thereby inhibiting its degradation [21]. Likewise, SJ172550 counteracts the p53-MDM4 interaction which also leads to elevated p53 levels [22]. Compounds that modulate metabolism include Dichloroacetate (DCA) which aims to reverse the Warburg effect via activation of pyruvate dehydrogenase (PDH) by inhibition of pyruvate dehydrogenase kinase, promoting the entry of pyruvate into tricarboxylic acid cycle [23]. Other important metabolism targeting compounds used for our study are the hypoxia-inducible factor 1 α (HIF-1 α) inhibitor PX-478 (Koh et al. 2008), Metformin, which inhibits complex 1 of the respiratory chain [24], the inhibitor of lactate dehydrogenase A (LDH-A) NHI-2 (Allison et al. 2014) and the hexokinase 2 (HK2) inhibitor 3-Bromopyruvate (Ko, Pedersen, and Geschwind 2001). Another important energy source in cancer is Glutamine metabolism [25] which is targeted by the Glutaminase inhibitor CB-839 [26]. Finally, compounds targeting growth and survival are the survivin inhibitor YM155 [27], the phosphatidylinositol 3-kinase (PI3K) inhibitor pictilisib/GDC-0941 [28], InoC2PAF [29, 30] and the ginger derivate 6-Shogaol targeting the AKT/mTOR pathway [31].

Screening for and evaluation of synergisms

In order to screen for potent synergisms, various successful methods have been tested and published recently [32, 33]. While some are relying on high throughput [34, 35] others are partially computerised to reduce the amount of actual experimental data points being investigated like the Feedback System Control [36–38]. There are also methods investigating synergism via mostly computerised analyses (Stochastic Searching Model, Statistical Model and Multi-Scale Agent-Based Model) [33, 39]. In literature, more than 10 different ways of defining synergism are described [40]. First referred to as the Loewe Additivity [41], quantification of synergistic drug interaction by the combination index (CI) is nowadays widely accepted. A precise method to estimate the specific dosages of fractional effects needed to calculate the CI, is the median effect method of Chou and Talalay that is derived from the mass action law [42, 43]. Quantification of synergisms via the CompuSyn software [44] based on multiple concentrations across the dose response curves is a well-established procedure [45].



Methods

Cell culture

MCF-7 breast cancer cells express p53 wild-type, are estrogen (ER) and progesterone receptor (PR) positive and express low levels of human epidermal growth factor receptor 2 (HER2) [46, 47]. MDA-MB-231 breast cancer cells that were originally isolated from a human breast cancer pleural effusion express a p53-mutation (R280K), are negative for ER and PR and express no amplification of HER2 [46, 48]. Both breast cancer cell lines were a kind gift of Göran Landberg (Sahlgrenska Cancer Center, University of Gothenburg, Gothenburg, Sweden) and were initially purchased from ATCC (Catalogue number: CRL-3435 and HTB-26). The primary colon cancer cell line HT-29 was isolated in 1964 by Fogh and Trempe. HT-29 cells carry a p53 mutation (R273H) and are deregulated for *c-MYC* [48]. HT-29 was a kind gift from Karsten Parczyk (Bayer AG) and initially purchased from ATCC (Catalogue number: HTB-38). All cell lines were routinely tested for mycoplasma contamination. For testing of mycoplasma contamination either PCR (GATC Biotech) or staining with Hoechst 33342 dye (Sigma-Aldrich, Steinheim, Germany) was conducted. HT-29 and MCF-7 cells were cultured in DMEM and the MDA-MB-231 in DMEM/F12 containing penicillin/streptomycin (100 U ml^{-1}), L-glutamine (DMEM: 584 mg l^{-1} , DMEM/F12: $365,1 \text{ mg l}^{-1}$) and 10% heat-inactivated fetal calf serum (FCS) at 37°C in a humidified incubator with 5% CO_2 . Cells were harvested using 0.05% trypsin/0.02% EDTA in PBS.

Compounds

Fourteen compounds were used: Prima-1met, Nutlin-3, SJ 172550, YM155 (Selleck Chemicals, Houston, TX, USA), 6-Shogaol (Hölzel Diagnostika Handels GmbH, Cologne, Germany), Pictilisib (Absource Diagnostics GmbH, Munich, Germany), Ino-C2-PAF (1-O-octadecyl-2-O-(2-

(myo-inositolyl)-ethyl)-sn-glycero-3-(r/s)-phosphatidylcholine) [29], PX-478 (Hölzel Diagnostika Handels GmbH, Cologne, Germany), DCA, Metformin-hydrochloride (Sigma-Aldrich, Munich, Germany), CB-839 (Selleck Chemicals, Houston, TX, USA), 3-Bromopyruvate (Santa Cruz Biotechnology, Dallas, Texas, USA), NHI-2 (Bio-Techne GmbH, Wiesbaden-Nordenstadt, Germany) and Cisplatin (Cayman Chemical Ann Arbor, MI, USA). 3-Bromopyruvate, Cisplatin, Dichloroacetate, Metformin, PRIMA-1-met, PX-478, YM155 and Ino-C2-PAF were solved in distilled water. Dimethyl sulfoxide (DMSO) was used to solubilize 6-Shogaol, CB-839, NHI-2, Nutlin-3, Pictilisib and SJ-17255. Finally, DMSO concentration was kept under $0.6 \mu\text{l}$ per well (0.6%).

All data collected in this study can be found in the additional file (Additional file 1). This includes all data produced for dose response curves and all combination experiments.

Cell viability assay and cell proliferation assay

0.5×10^4 MCF-7, 1.5×10^4 HT-29 and 1.5×10^4 MDA-MB-231 cells per well were seeded in flat bottom 96-well plates. After 24 h and reaching a cell-confluence of approximately 50%, the respective compound or combination was added. As a negative control, cells were cultured in the presence of 0.6% DMSO. However, we could not detect any differences in cell viability between 0.6% DMSO and no DMSO. After 48 h of further incubation, either MTT assay (3-(4,5-dimethylthiazol-2-yl)-2,5-diphenyltetrazolium bromide, a tetrazole assay, Bio-Techne GmbH, Germany) or SRB (Sulforhodamin B) assay were applied. The MTT assay was performed according to the manufacturer's instructions. For the SRB assay, cells were treated with 10% trichloroacetic acid (w/v) and stained with 0.06% SRB in 1% acetic acid for 30 min. Cells were then repeatedly washed using 1% acetic acid (v/v) followed by dissolution in 10 mM Tris

(pH10.5). Protein mass was monitored using a microplate reader at an optical density of 492 nm. All experiments were performed at least with two replicates in three independent experiments.

Dose response curves were obtained for 14 compounds using GraphPad Prism statistical analysis software 7.05. EC₅₀ of the respective compounds was determined via nonlinear regression.

Minimalistic drug interaction screening (MDIS)

MCF-7 and HT-29 cells were treated with 14 single and their 91 pairwise combinations at dosages of approximately EC₂₅. All experiments were performed at least with three biological and two technical replicates. Thus, for one cell lines we produced about 909 data points (303 per biological replicate). The conjectured synergistic potency (CSP) of a combination was quantified by adding up the effect of the single compounds and subtracting the result from the combination's effect. E.g.: Single dose A: 20% cell viability-reduction, single dose B: 10% cell viability-reduction and the combination of A and B exhibit cell viability-reduction of 37%. Thus, the combination of A and B reduces the cell viability 7% more than it is expected from simply adding up the effects of the single compounds (CSP = 7). Analyses were performed with Graph pad prism and Microsoft Excel.

Confirmation of synergism

Synergism predicted by MDIS was evaluated with three to seven concentrations as suggested by Chou and Talalay [49].

MCF-7 and HT-29 cells were treated with the respective combination of compounds at a constant EC₅₀:EC₅₀ ratio as well as the same concentrations of each drug individually. Significant differences between single compound viabilities and combination viability was assessed by unpaired t-test. Only concentrations with p-values ≤ 0.05 for both compounds were considered as significant and marked by an asteriks (*) in the figures.

The combination indices (CI) were calculated using the CompuSyn software [44]. The CI is a quantitative value for the synergism of a drug combination at specific concentrations. A value below 0.3 indicates a "strong", 0.3–0.7 a "robust" (originally referred to as "synergism" by Chou and Talalay), 0.7 to 0.85 a "moderate" and 0.85 to 0.9 a "slight" synergism. Values from 0.9 to 1.1 show an "additive" effect and a CI above 1.1 indicates "antagonism" [50, 51]. The CI was calculated as follows:

$$CI = \frac{(D)_1}{(Dx)_1} + \frac{(D)_2}{(Dx)_2}$$

In the numerators, (D)₁ and (D)₂, are the concentrations of drug 1 and drug 2 in the drug-combination which have a certain effect on cell viability (x %). In the

denominators, (Dx)₁ and (Dx)₂, stand for the concentration of each drug alone (drug 1 or drug 2) that is necessary to obtain the same effect (x %) as the drug-combination (drug 1 and drug 2). The concentrations (Dx)₁ and (Dx)₂ were calculated by CompySyn referring to individual cell-viability data of the concerning compounds. To enhance rigidity, (Dx)₁ and (Dx)₂ were predominantly generated via direct experimental data points. This way, potential calculation errors are ruled out as suggested by Zhao et al. [45]. To produce the median effect plots the following equation was used:

$$D_x = D_m \left[\frac{fa}{1-fa} \right]^{1/m}$$

D_m is the median effect dose, m counts for the slope of the median-effect plot and fa stands for fraction affected.

Results

Three-step concept to identify synergisms between selected compounds

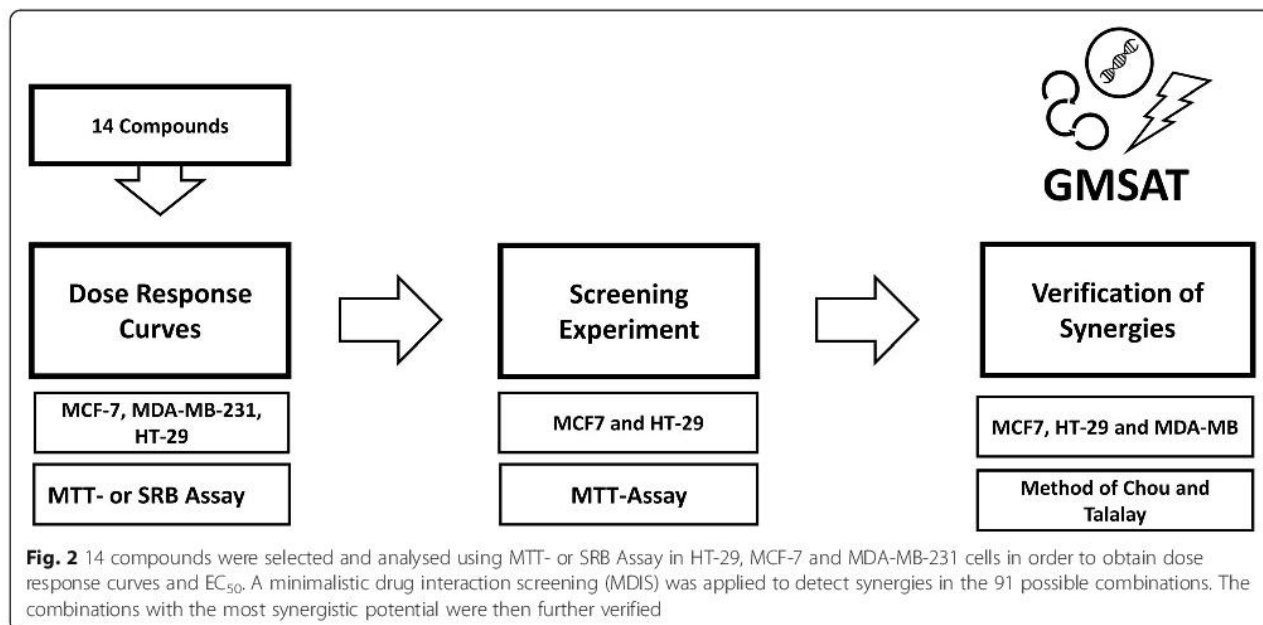
In this work, we applied the following three steps to identify synergisms between the compounds for our combinatory approach (Fig. 2).

1. Dose response curves aiming to detect the single drug effect in cancer cell lines and calculate fractional effects like EC₅₀ or EC₂₅.
2. The minimalistic drug interaction screening (MDIS) to identify potential synergies.
3. Verification by the method of Chou and Talalay to reliably prove the projected synergisms.

Following these steps, we identified 27 potential synergisms in MCF-7 (29.7%) and 19 in HT-29 (20.9%) of the 91 pairwise combinations. A selection of combinations was further analysed by the method of Chou and Talalay.

Dose response curves in MCF-7, MDA-MB-231 and HT-29 cells

Dose response experiments were conducted in order to identify the dose range for MDIS and evaluate the anti-tumor effects of the single compounds in different cell lines. Therefore, MCF-7, MDA-MB-231 and HT-29 cells were cultivated for 24 h before being treated with increasing concentrations of the 14 different compounds (Fig. 1). After an additional cultivation period of 48 h, cell viability or protein mass were quantified using the MTT or SRB assay. In Fig. 3, we exemplarily illustrated the dose response curves of Nutlin-3 and DCA for all three cell lines. Furthermore, we calculated the median effective concentration (EC₅₀) for all compounds with



the help of GraphPad Prism (Table 1). Data for all dose response curves can be found in the Additional file 1.

Overall, we observe that the triple negative breast cancer cell line MDA-MB-231 is the most resistant cell line requiring the highest dosages in 11 out of the 14 tested compounds. Although Prima-1met is intended to stabilize p53-mut, the strongest efficacy is shown in the p53 wild-type cell line MCF-7. YM155 is effective at very low concentrations at EC_{50} in a nM range in all three cell lines.

Minimalistic drug interaction screening (MDIS)

To identify synergistic actions of compound combinations, we developed a minimalistic drug interaction screening (MDIS). For this experiment, HT-29 and MCF-7 cells were treated with 14 different compounds in all 91 possible pairwise combinations. In this approach, dosages of approximately EC_{25} were used for all compounds. The conjectured synergistic potency (CSP) of a combination was quantified adding up the effect of the single compounds and subtracting the result from the combination's effect (c.f. Material and Methods). We applied this rather simple mathematical approach not to prove synergisms, but to narrow down the number of effective combinations. The overall average standard deviations in MDIS were 7.5% for MCF-7 and 10.6% for HT-29 respectively. CSP values above 10 were chosen as a cut off for a 'possible' (+) synergism, 15 for a "likely" (++) and 25 for a "very likely" (+++) synergism (Fig. 4). Pure numerical values can be found in Additional file 1.

For HT-29 cells, a total amount of 19 synergistic projections out of the 91 combinations (20.9%) were predicted. Eleven of the latter were "possible" (12.1%), seven "likely" (7.7%) and one a "very likely" synergism (1.1%).

For the p53 wild type breast cancer cell line MCF-7, a total of 27 combinations (29.7%) were identified, including 16 "possible" (17.6%), ten "likely" (11.0%) and one "very likely" (1.1%) synergism.

The highest CSP could be achieved in HT-29 for the combination of DCA + PX-478 which led to an average increase in inhibition of cell growth of 62.4% compared to the sum of the single dose effects determined for both drugs. Therefore, we performed deeper investigations with the combination of DCA + PX-478 in different cancer cell lines in a separate study. The second highest value was obtained for DCA + NHI-2 (43.4%) in MCF-7. Four combinations were projected to be synergistic in both cell lines: Nutlin-3 + YM155, DCA + Metformine, DCA + PX-478 and Nutlin-3 + PX-478.

DCA, PX-478, Nutlin-3 and NHI-2 exhibit highest potential for synergistic interactions in MDIS

There were substantial differences in the count of potential synergies and their strength for the 14 compounds. The total number of "+" attributed to a compound by MDIS illustrates the synergistic potential of a compound since it summarizes quantity and quality of predicted synergistic interactions. With a total of 19 "+" the two compounds DCA and PX-478 have the highest synergistic potential. While PX-478 has the highest count of possible synergisms [12], DCA compensates a lower count [10] with stronger predictions (one vs. two "very likely" synergisms).

Additionally, with a total of 11 projections each, Nutlin-3 with 16 "+" and NHI-2 with 15 "+" show high synergistic potential. The lowest count of synergistic interaction was identified for the two PI3K-pathway

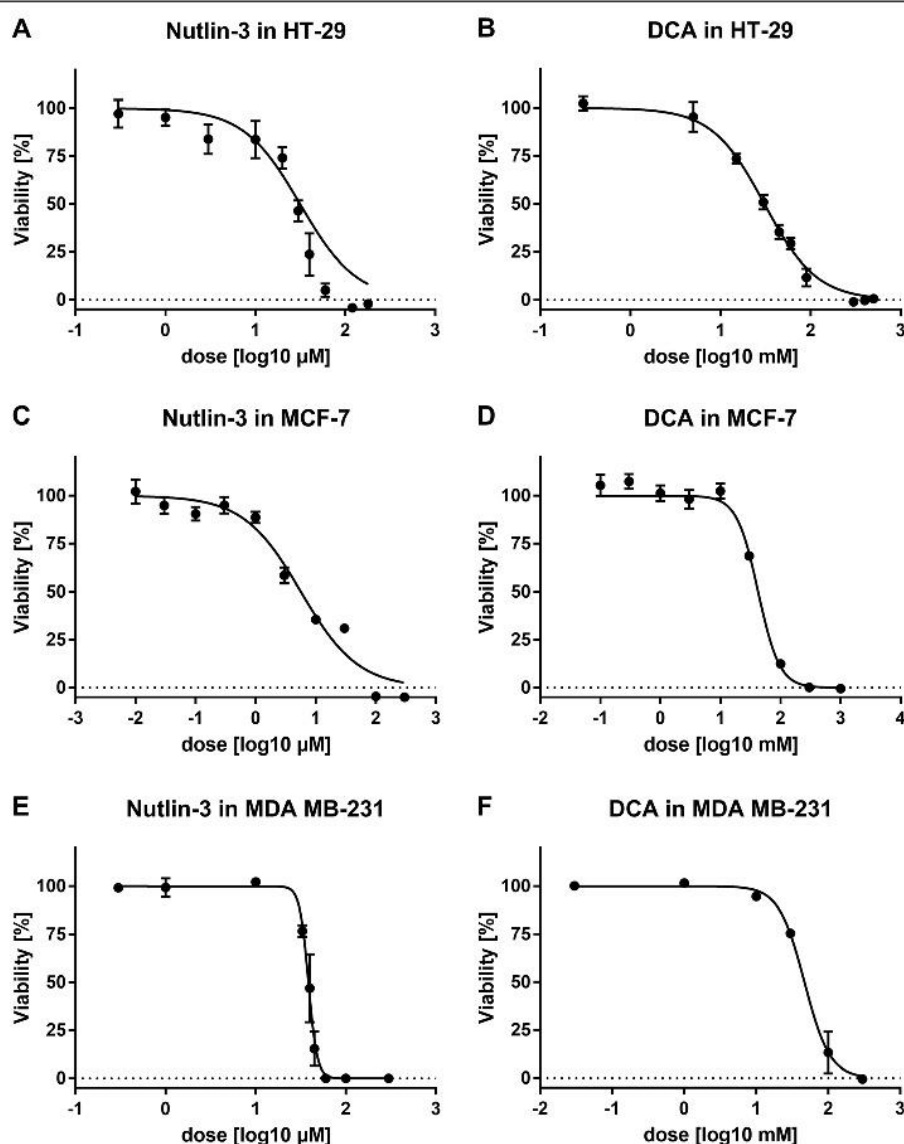


Fig. 3 dose response curves Cells were seeded into a 96 well plate at a density of 1.5 (HT-29, MDA-MB) and 0.5×10^4 /well (MCF-7), incubated 24 h to a confluence of 50%, then cells were treated with increasing concentrations of the 14 selected drugs for 48 h. Viability was assessed using the MTT-Assay and curves were obtained using the four-parameter variable slope function of Graphpad Prism. Exemplarily the resulting curves for Nutlin-3 and DCA are shown for the three cell lines

targeting drugs Pictilisib and InoC2PAF with 0 and 2 predictions, respectively. YM155 had seven projections in MCF-7 and only one in HT-29. For 6-Shogaol, the opposite was the case: Five predictions in HT-29 and none in MCF-7.

Analysis of the synergies by the method of Chou and Talalay

For further evaluation of these predicted synergisms according to the method of Chou and Talalay, we used the CompuSyn Software to calculate the combination

indices (CI). The CI is a quantitative value for the synergism of a drug combination at specific concentrations. A value below 0.9 indicates synergism and the lower a CI, the stronger a synergism: A value below 0.3 indicates a “strong”, 0.3 to 0.7 a “robust” 0.7 to 0.85 a “moderate” and 0.85 to 0.9 a “slight” synergism. Values from 0.9 to 1 show a nearly “additive” effect and a CI above 1.1 indicates “antagonism”. Furthermore, significance in the differences between a combination and the respective single compounds was evaluated by unpaired T-test. We evaluated seven combinations projected by MDIS

Table 1 EC₅₀ of the 14 compounds

Compound	Unit	HT-29 EC50	MCF-7 EC50	MDA-MB-231 EC50
Prima-1met	[μ M]	64.9	18.1	71.1
Nutlin-3	[μ M]	28.8	6.0	39.2
SJ172550	[μ M]	15.4	15.6	229.5
YM155	[nM]	50.9	2.54	23.6
6-Shogaol	[μ M]	29.7	148.9	503.5
Pictilisib	[μ M]	19.8	0.16	532.8
InoC2PAF	[μ M]	7.4	9.5	91.7
PX-478	[μ M]	77.4	15.92	164.3
DCA	[mM]	34.9	40.7	48.7
CB-839	[μ M]	3.3	6.0	13.3
3-BP	[μ M]	15.6	110.7	554.8
Metformin	[mM]	6.9	13.4	100
NHI-2	[μ M]	32.7	29.82	26.14
Cisplatin	[μ M]	549.8	84.35	484.5

Cells were seeded into a 96 well plate at a density of 1.5 (HT-29, MDA-MB) and 0.5×10^4 /well (MCF-7), incubated 24 h to a confluence of 50%, then incubated with increasing concentrations of the 14 selected drugs for 48 h. Then, viability was assessed using the MTT-Assay and EC₅₀ was calculated using Graphpad Prism

(Table 2). Five of the latter could be confirmed by the method of Chou and Talalay, while two combinations, PRIMA-1met + Nutlin-3 and Nutlin-3 + 3-Bromopyruvate did not reach significant p-values in detected synergisms (CI = 0.89 and 0.72 respectively). Since the combination of DCA + NHI-2 was promising in MCF-7 cells in both the screening trial (CSP = 43) and the method of Chou and Talalay (CI = 0.27), we further verified it in HT-29 (Table 2 and Fig. 6-C, D). Although it could not be detected by MDIS, we found the combination to be synergistic in HT-29 cells (CI = 0.50). Furthermore, we verified the most promising synergisms in MDA-MB-231 by calculating the CI-value using the dose response curves and equation of Loewe [41]. Thereby, we could confirm the top synergies DCA + NHI-2 (CI = 0.) and Nutlin-3 + PX-478 (CI = 0.62). Since we found a “likely” synergism between DCA + Nutlin-3 in p53 wild-type MCF-7 cells (Fig. 4), we checked the combination of p53mut binding PRIMA-1met + DCA in the p53-mutated MDA-MB-231 cells. Interestingly, a synergy exclusively found in MDA-MB-231 cells could be confirmed (CI = 0.78). After the evaluation of MDIS, we named synergies with CSP values between ten and 15 “possible”, 15 and 25 “likely” and greater than 25 “very likely” synergisms. Out of the seven verified synergies, we could prove all “likely” and “very likely” (4/4) but only two of the four possible synergisms. Thus, we detected eight (8.8%) and 11 (12.1%) “likely” and “very likely” synergisms in HT-29 and MCF-7 respectively.

Interpretation of the combination index

When analysing drug interactions, looking at certain concentrations alone may lead to a false interpretation of synergism [42, 45]. The example of the synergism between PRIMA-1met + YM155 illustrates the principle of the CI-value interpretation (Fig. 5). At first sight, the combination of Prima-1met + YM155 shown in Fig. 5-D seems to exhibit stronger synergistic effects compared to lower dosages presented in Fig. 5-B. Contrarily to that assumption, the opposite is the case: 5-B shows indeed a “robust” synergism (CI = 0.34) while the effects shown in Fig. 5-D are not even “additive” (CI = 1.19). The explanation for this counter-intuitive finding is that doubling the single doses of PRIMA-1met + YM155 in EC₅₀ results in a much stronger effect than the combination of both drugs at EC₅₀ (Fig. 5-D, E). Therefore, one can conclude that the shape of and position on the curve is important to accurately describe and interpret synergisms. The easiest method to interpret synergistic effects of these curves consists in doubling the fractions of EC₅₀. As a result, the CI calculations are mainly based on experimental data and can easily be interpreted by studying the curve progression. This method also helps minimizing errors that might occur with mathematical dose fitting [45].

The combinations of Nutlin-3 + PX-478 and DCA + NHI-2 act synergistically in MCF-7, MDA-MB and HT-29 cells

The combination Nutlin-3 (inhibition of MDM-2) + PX-478 (inhibition of HIF-1 α) was predicted to be synergistic by MDIS for HT-29 and MCF-7 cells. Via the method of Chou and Talalay, we analysed this synergism over the whole dose response curve. Exemplarily, we show in Fig. 6a and b the dose response curves for the combination Nutlin-3 + PX-478 and the single compounds. Best CI-values were 0.33 for MCF-7 (Fig. 6a) as well as 0.63 and 0.62 for HT-29 and MDA-MB-231, respectively (Table 2). In the reduction of protein mass (Fig. 6b) as well as the reduction of viability (Fig. 6a) it was mainly synergistic at 0.125x, 0.25x and 0.5x EC₅₀.

Further, we confirmed the synergism of DCA + NHI-2 (PDH activation and LDH-A inhibition) in all three cell lines (Fig. 6c and d for MCF-7 and Table 2 for HT-29 and MDA-MB-231). A “strong” synergism was identified for the cell line MCF-7 (CI = 0.27) whereas a “robust” synergism could be found in HT-29 (CI = 0.50) and MDA-MB-231 (CI = 0.62).

Discussion

We present here a three-step concept to systematically screen for and reliably describe synergies between a high number of compounds at a minimal cost and time budget. With that concept, we identified five synergistic combinations of genome and metabolism stabilizing compounds of which Nutlin-3 + PX-478 as well as DCA + NHI-2 were

		Prima-1met	Nutlin-3	SJ172550	YM155	6-Shogaol	Pictilisib	InoC2PAF	PX-478	DCA	CB-839	3-BP	Metformin	NHI-2	Cisplatin
Prima-1met (12+)	MCF-7		+		++								+	+	
	HT-29		+	+		+			++				+	+	
Nutlin-3 (16+)	MCF-7	+			++				++	++			+	+	++
	HT-29	+			++				+				+	+	++
SJ172550 (2+)	MCF-7														+
	HT-29														+
YM-155 (13+)	MCF-7	++	++						+	+	++	+		++	
	HT-29	++	++											++	
6-Shogaol (5+)	MCF-7								++	+					+
	HT-29								++	+					+
Pictilisib (0+)	MCF-7														
	HT-29														
InoC2PAF (2+)	MCF-7									++			+		
	HT-29									++			+		
PX-478 (19+)	MCF-7		++		+					+			+		+
	HT-29	++	+		++					+++	++		+	++	+
DCA (19+)	MCF-7		++		+			++	+				++	+++	
	HT-29		++		+			++	+++			++	++	+++	
CB-839 (5+)	MCF-7				++										+
	HT-29				++										+
3-BP (7+)	MCF-7		+		+								+	+	+
	HT-29		+		+								+	+	+
Metformin (13+)	MCF-7	+	+					+	+	++		+		+++	
	HT-29	+	+					+	+	++		+		+++	
NHI-2 (15+)	MCF-7	+	+		++					++	+	+	++		
	HT-29	+	+	+	++	+			++	++	+	+	++		
Cisplatin (3+)	MCF-7		++										+		
	HT-29		++						+				+		

Fig. 4 minimalistic drug interaction screening. HT-29 and MCF-7 cells were seeded into a 96 well plate at a density of 1.5 (HT-29) or 0.5 × 10⁴/well (MCF-7) and incubated 24 h to a confluence of 50%. Then, cells were incubated with 14 single compounds and the respective 91 combinations at a concentration about EC₂₅ for 48 h. Viability was assessed using the MTT-Assay and the CSP (conjectured synergistical potency) values were calculated. CSP of a combination was quantified by adding up the effect of the single compounds and subtracting the result from the combination's effect. All CSP values above ten are highlighted in green. Values between ten and 15 are marked by one plus (+), between 15 and 25 by two plus (++) , greater than 25 by three plus (+++) and referred to as "possible", "likely" and "very likely" synergism respectively. The number of total "+" is given in the first column below the name of the compounds and summarizes the number and strength of projected synergistic interactions

found in all three cell lines MCF-7, MDA-MB-231 (breast cancer) and HT-29 (colon cancer).

In contrast to the here presented approach, Borisy and colleagues designed a sophisticated high-throughput robot-assisted approach where 30 antifungal drugs and their 435 pairwise combinations were screened for potential synergistic interactions. For their screening experiment, six different concentrations with two technical replicates were used, resulting in a total of 31,320 data points [34]. For 14 compounds the same experimental design would result in 6552 compared to 303 data points with MDIS. While this approach provides a substantial amount of valuable information, it is material, cost and time intensive. Thus, optimization in material use and number of conducted experiments is needed to make drug interaction research feasible for a broader range of work groups.

Dose-ratio based screening

Yin and colleagues reviewed, how computational based approaches such as the Feedback System Control [37] or Stochastic Searching Model with an heuristic idea can help to minimize costs of mainly experimental approaches [32]. Both approaches incorporate different dose-ratios already in the screening process. This design respects the fact that compounds interacting synergistically at a specific dose ratio may be antagonistic at other ratios [35]. Consequently, a screening without different dose-ratios may fail to detect synergisms that have antagonistic, additive or just slightly synergistic effects in the tested dose-ratio. In the here presented minimalistic drug interaction screening, this phenomenon is reflected in the fact that DCA + NHI-2 has not been projected to be synergistic by MDIS in HT-29 but could be proved by the method of Chou and Talalay (CI = 0.50). The

Table 2 Verified synergies

Combination	Cell line	MDIS	C & T	MDA-MB
DCA	MCF-7	+++	0.27*	0.62*
+ NHI-2	HT-29	-	0.50*	
Nutlin-3	MCF-7	+++	0.33*	0.62*
+ PX-478	HT-29	+	0.63*	
PRIMA-1met	MCF-7	++	0.34*	n.d.
+ YM155				
DCA	MCF-7	++	0.51*	n.d.
+ Metformin				
PRIMA-1met	HT-29	+	0.24*	n.d.
+ NHI-2				
Nutlin-3	HT-29	+	0.89	n.d.
+ PRIMA-1met				
Nutlin-3	MCF-7	+	0.72	n.d.
+ 3-Bromopyruvate				

Table 2 shows the seven combinations that were selected for further verification by the method of Chou and Talalay. The third column shows the predictions by MDIS: + indicates a "possible" ++ a "likely", +++ a "very likely" synergism and - no synergism. The respective best CI-values calculated by the method of Chou and Talalay (C & T) are listed in the fourth column. They were marked with an * if unpaired T-test was significant for the respective concentration of the combination in comparison with the single compounds. A CI-value indicates the quality of a synergism at a specific concentration. A value below 0.3 indicates a "strong", 0.3 to 0.7 a "robust" and 0.7 to 0.85 a "moderate" synergism. In the case of MDA-MB cells, CI-values were calculated by the method of Loewe with the help of the earlier obtained dose response curves and Graphpad Prism. The resulting CI-values are listed in the fifth column. Combinations that were not analysed in MDA-MB-231 cells are marked with n.d. Out of the seven verified synergies, we could prove all "likely" and "very likely" (4/4) but only two of the four "possible" synergisms (two combinations had no significant CI-value below 0.9). Details concerning the combinations (the complete dose response curve and all the respective CI-values) can be found in Figs. 5 and 6 as well as in the Additional file 1.

opposite accounts for PRIMA-1met + YM155 which is synergistic in low doses (e.g. 0.125x EC₅₀) and antagonistic at 8x EC₅₀. Nevertheless, MDIS represents a substantial decrease in experimental scope: If for example three concentrations (e.g. EC₂₅, EC₅₀ and EC₇₅) and all possible dose-ratios are used instead of one, the number of combinations increases from one to nine. Additionally, MDIS resulted in a total of 19 potential synergisms in HT-29 and 27 in MCF-7, a number that requires immense efforts to further verify and describe. Even when selecting only "likely" (++) and "very likely" (+++) synergisms, nine (HT-29) and 11 (MCF-7) combinations remain (Fig. 4). The focus on mechanistically interesting and most solid combinations in different cell lines is necessary to select most promising candidates. A dose-ratio based screening method is likely to detect even weak synergisms at an optimized dose-ratio and in that way it multiplies the number of projections. Therefore, we recommend the here presented cost-efficient design for projects that aim to evaluate interesting compounds of newly anticipated antitumor concepts for their synergistic potency. We recommend verifying the synergy over the entire dose-response curve at a constant dose-ratio before the determination of the optimal dose-

ratios. Dose-ratio based screening might rather be appropriate for detailed analyses in order to optimize therapies of already implemented compounds [34].

Synergy interpretation

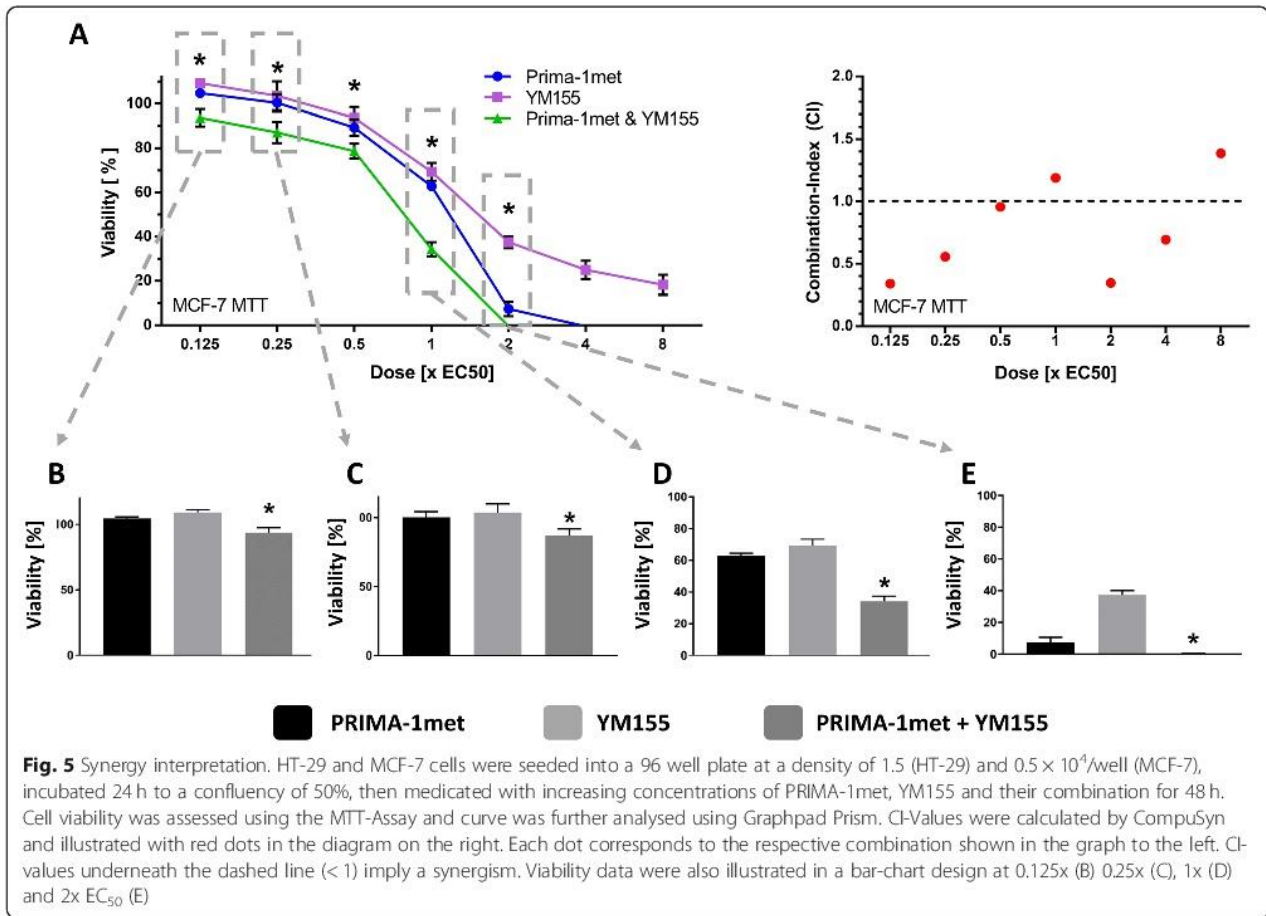
After performing the three phases of the here proposed concept, we consider "likely" and "very likely" synergisms predicted by MDIS as the most relevant and solid results. In HT-29, we detected eight (8.8%) and in MCF-7 11 (12.1%) "likely" and "very likely" synergisms. Out of this group, we could confirm four of four tested synergisms (Table 2). In the case of "possible" synergisms, only two of four tested combinations could be confirmed. Nutlin-3 + PRIMA-1met and Nutlin-3 + 3-Bromopyruvate did reach synergistic CI values at some concentrations (CI: 0.89 and 0.72 respectively), but without significance. Furthermore, the CI-values over the whole dose-response curve of these combinations were mainly additive or even antagonistic. Another "possible" synergisms detected by MDIS in MCF-7 is Metformin + Nutlin-3 which has already been described for mesothelioma cells by Shimazu et al. [52]. In general, "possible" synergisms might be worth examining as the "robust" synergistic effect between Nutlin-3 + PX-478 in HT-29 (CI = 0.63) illustrates (Table 2).

Out of the five detected and proven synergies, two top combinations were synergistic in all three cell lines. Nutlin-3 inhibits p53 degradation [21] while PX-478 modulates metabolism by inhibiting HIF-1 α and thereby aerobic glycolysis [53]. While a mechanistic overlap is described in literature, we were - to the best of our knowledge - the first to detect this synergism. Lee and colleagues reported in 2009 that Nutlin-3 inhibits HIF-1 α in a p53 dependent and vascular endothelial growth factor (VEGF) in a p53 independent manner [54]. These findings are supported by the fact that the Nutlin-3 + PX-478 showed the strongest synergism in the p53 wild-type cell line MCF-7 (CI = 0.33) compared to the p53 mutated cell lines HT-29 (CI = 0.63) and MDA-MB (CI = 0.62).

The second combination present in all three cell lines is DCA (PDH activation [55]) + NHI-2 (LDH-A inhibition [56]) which showed a "strong" synergism for the cancer cell line MCF-7 (CI = 0.27) and "robust" synergisms for HT-29 (CI = 0.50) and MDA-MB-231 (CI = 0.62). This combination has not been described in literature yet and is particularly interesting as both compounds target the "Warburg" effect [55], inhibiting the conversion of pyruvate to lactate and promoting its entrance into the tricarboxylic acid cycle. Out of the other four synergisms we were able to identify and prove, DCA + Metformin was already described thoroughly in literature [57].

Validation of conjectured synergies

For the verification of the synergisms projected by MDIS, the widely accepted median-effect principle of the mass



action law implemented in the method of Chou and Talalay was used [58]. To keep the transformation error low, we decided not to simplify our experiments by the overextended use of calculation and curve fitting for the determination of synergism [45]. In detail, we combined our compounds in a constant ratio of EC_{50} to EC_{50} , stepwise doubling the dosages. We favour this method as the data necessary to calculate the CI-values have a solid empirical base. When a combination commends itself for further investigation, we suggest the following analyses:

1. The dose-ratio is crucial in the description of synergisms but cost and time expensive. Therefore, we suggest evaluating the most effective dose-ratios after a synergy has successfully been identified and proven.
2. To further evaluate the effectiveness of the detected combination, we recommend utilizing cell lines with different properties (e.g. p53 status) and or in different tumor entities [35].

Limitations

In this work, we focused intensively on synergistic drug interaction in the detection of potential combinatory

approaches. Synergistic effects are desirable, but additive effects or in some cases even compounds with slight antagonisms might be useful as well [18, 59]. For example, if the necessary single dose cannot be reached in vivo for pharmacodynamics reasons or dose limiting toxicity, a combination with a higher cumulative dose might result in a better outcome.

With respect to the genome and metabolism stabilizing anti-tumor approach, we conducted a systematic literature research to identify matching compounds. In contrast, large-scale prediction of drug combinations via different databases [18, 39] is another promising way of narrowing down the field of potential compounds. Generally, we based the calculation of the CI-values on substantial experimental data. If only half of the curve is measured experimentally while the other parts are calculated via curve fitting, changes in slope might be missed which could lead to false low CI-values [45]. Therefore, the amount of experimental data points and EC-range covered must be considered in the interpretation of the resulting CI-values.

Clinical implications

To further evaluate promising combinations, taking already conducted clinical trials of the respective single compounds

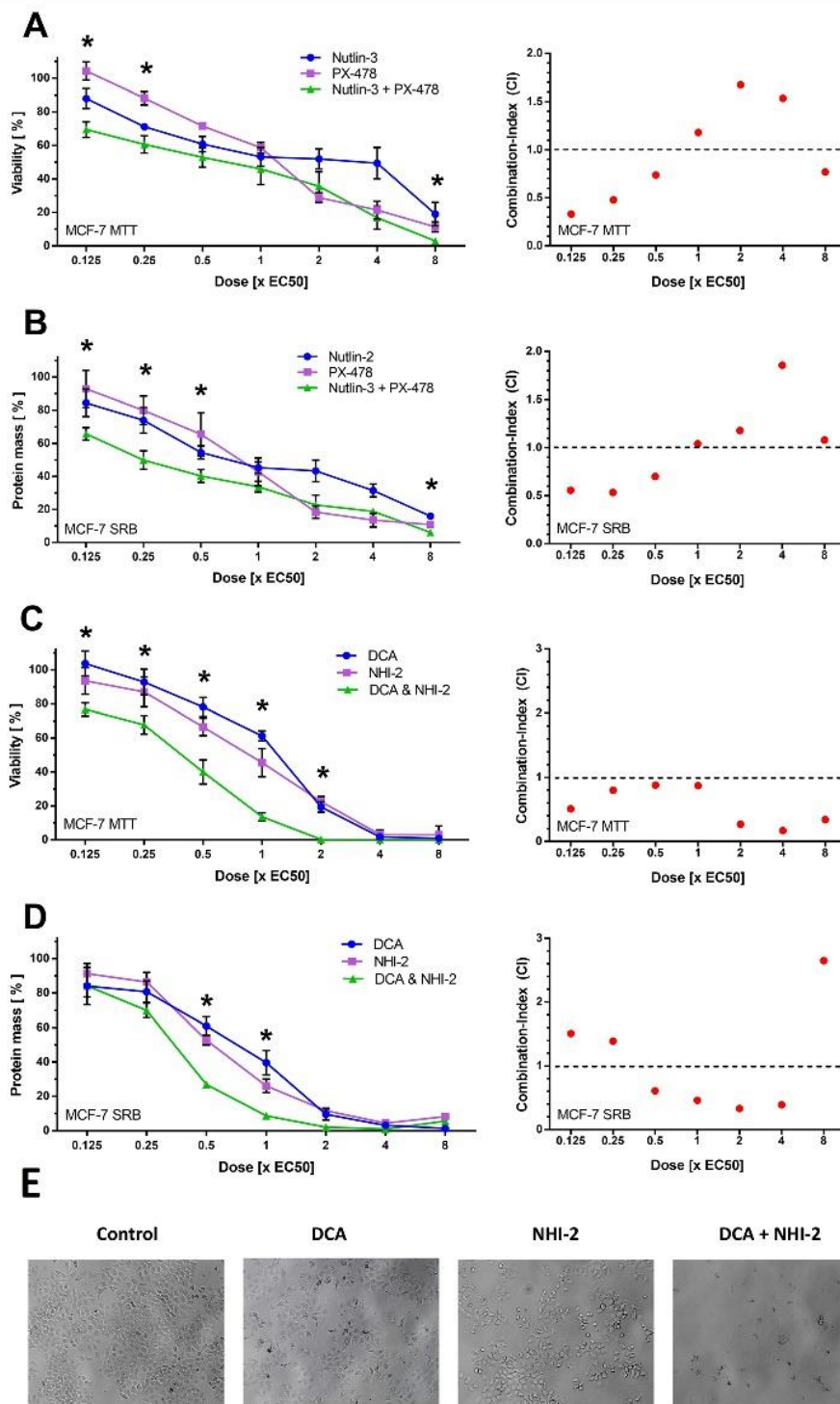


Fig. 6 Nutlin-3 + PX-478 and DCA + NHI-2. MCF-7 cells were seeded into a 96 well plate at a density of 0.5×10^4 /well (MCF-7), incubated 24 h to a confluency of 50%, then incubated with increasing concentrations of Nutlin-3, PX-478 and their combination (**a, b**) as well as DCA, NHI-2 and their combination (**c, d**) and for 48 h. Then, viability was assessed using MTT assay (**a, c**) and protein mass was assessed using SRB assay (**b, d**). CI-Values were calculated by CompuSyn and illustrated with red dots in the diagram on the right. Each dot corresponds to the respective combination shown in the graph to the left. The effects of EC₅₀ of DCA, NHI-2 and DCA + NHI-2 on the cell confluency is illustrated on the bottom (**e**)

into account is important to identify potential obstacles and problems in the translational phase. When looking at DCA, “clinicaltrials.gov” does list 37 studies in the context of cancer and 81 studies in total. In one trial where patients with previously treated metastatic breast or non-small cell lung cancer were treated with DCA, the authors concluded that DCA should be used for patients with longer life expectancy and potentially in combination [60] (ClinicalTrials.gov Identifier: NCT01029925). PX-478 seems to be abandoned since the last clinical trial was conducted in 2010 (ClinicalTrials.gov Identifier: NCT00522652). In this phase 1 clinical trial PX-478 has been well tolerated in low doses with consistent HIF-1 α inhibition in patients with advanced solid tumors [61]. A sufficient effect with well tolerated doses to commence with a phase 2 clinical trial seemed to be missing although a HIF-1 α inhibition was achieved. As a conclusion, it can be stated that these two drugs are tolerated in the respectively needed dose while a convincing effect on cancer was missing. We believe that synergism is an important way to successfully include promising compounds like DCA and or PX-478 in the therapy of cancer. The synergisms with NHI-2 or Nutlin-3 identified in this study may be a solution in this context. For NHI-2 and Nutlin-3 no literature on clinical trials is available. However, it also seems that the effect of NHI-2 and Nutlin-3 on normal non-cancerous cells is tolerable. In vitro treatment with Nutlin-3 induced a significant cytotoxicity on primary CD19(+) B-CLL cells, but not on normal CD19(+) B lymphocytes, peripheral-blood mononuclear cells or bone marrow hematopoietic progenitors [62]. As for the molecular mechanism of NHI-2, Calvaresi et al. stated that LDH-A inhibition is unlikely to harm normal tissues [63].

Conclusion

The here presented three-step concept proved to be cost and time efficient with respect to the resulting data at the example of our combinatory approach. “Likely” and “very likely” synergisms proved to be reliable predictions of MDIS after verification by the method of Chou and Talalay. The combination of Nutlin-3 + PX-478 as well as DCA + NHI-2 could be identified in all three cell lines. In vivo experiments are required to evaluate the potential of these combinations for clinical studies.

Supplementary information

Supplementary information accompanies this paper at <https://doi.org/10.1186/s12885-020-07062-2>.

Additional file 1. Combination experiments, MCF-7 dose-response curves, HT-29 dose response curves, MDA-MB dose response curves and MDIS (minimalistic drug interaction screening). In this file all data concerning the combination experiments, the dose response curves of the three cell lines and the MDIS can be found.

Abbreviations

CSP: Conjectured Synergistical Potency; CI: combination index; DCA: Dichloroacetate; GMSAT: Genome and Metabolism Stabilizing Antitumor Therapy; HIF-1 α : hypoxia inducible factor α ; MDIS: Minimal Drug Interaction Screening; PI3K: phosphatidylinositol 3-kinase; w/v: weight per volume; v/v: volume per volume

Acknowledgements

We gratefully acknowledge the support of Sara Amroune for editing the English version and for critical discussions of this manuscript. We acknowledge support from the German Research Foundation (DFG) and the Open Access Publication Fund of Charité – Universitätsmedizin Berlin. Thanks for the support throughout the project to Dr. Jutta Hinke-Ruhnau, Dr. Karsten Parczyk and Lilith Marie Bechinger.

Authors' contributions

Conceptualization of the project was done by JP, JR and AK. Experiments were performed by JP and JR. AK was responsible for project administration and supervision. Writing and editing was done by JP, JR, AK, BE and KD. All authors read and approved the manuscript.

Funding

Jonas Parczyk received a 6-month scholarship by the Berlin Institute of Health during his doctoral thesis.

Availability of data and materials

All data generated or analysed during this study are included in this published article and its supplementary information file (Additional file 1).

Ethics approval and consent to participate

None of our cell lines required ethics approval.

Consent for publication

Not applicable.

Competing interests

The authors declare that they have no competing interests.

Received: 9 December 2019 Accepted: 11 June 2020

Published online: 02 July 2020

References

1. Society AC. American Cancer Society. Cancer Facts & Figures 2018 (p14-15, p26-27). Atlanta: American Cancer Society; 2018. Available from: <https://www.cancer.org/content/dam/cancer-org/research/cancer-facts-and-statistics/annual-cancer-facts-and-figures/2018/cancer-facts-and-figures-2018.pdf>.
2. Güth U, Magaton I, Jane D, Fisher R, Schöttau A, Vetter M. Primary and secondary distant metastatic breast cancer: two sides of the same coin. *The Breast*. 2014;23(1):26–32. Available from: <https://doi.org/10.1016/j.breast.2013.10.007>.
3. Nowell P. The clonal evolution of tumor cell populations. *Science* (80-). 1976;194(4260):23–8. [cited 2019 Aug 10] Available from: <http://www.ncbi.nlm.nih.gov/pubmed/959840>.
4. Research America. U.S. Investments in Medical and Health Research and Development: 2016 [cited 2019 Jul 22]. Available from: https://www.researchamerica.org/sites/default/files/2016US_Invest_R%26D_report.pdf.
5. Moses H, Matheson DHM, Cairns-Smith S, George BP, Palisch C, Dorsey ER. The Anatomy of Medical Research. *JAMA*. 2015 [cited 2019 Jul 22];313(2):174. Available from: <http://www.ncbi.nlm.nih.gov/pubmed/25585329>.
6. Swanton C, Nicke B, Marani M, Kelly G, Downward J. Initiation of high frequency multi-drug resistance following kinase targeting by siRNAs. *Cell Cycle*. 2007;6(16):2001–4.
7. Chisholm RH, Lorenzi T, Clairambault J. Cell population heterogeneity and evolution towards drug resistance in cancer: biological and mathematical assessment, theoretical treatment optimisation. *Biochim Biophys Acta - Gen Subj*. 2016;1860(11):2627–45. Available from: <https://doi.org/10.1016/j.bbagen.2016.06.009>.
8. Andor N, Maley CC, Ji HP. Genomic Instability in Cancer: Teetering on the Limit of Tolerance. *Cancer Res*. 2017;77(9):2179–85. [cited 2019 Aug 15] Available from: <http://www.ncbi.nlm.nih.gov/pubmed/28432052>.

9. Vander Heiden MG, DeBerardinis RJ. Understanding the Intersections between Metabolism and Cancer Biology. *Cell*. 2017;168(4):657–69. [cited 2019 Aug 15] Available from: <http://www.ncbi.nlm.nih.gov/pubmed/28187287>.
10. Roy D, Sheng GY, Herve S, Carvalho E, Mahanty A, Yuan S, et al. Interplay between cancer cell cycle and metabolism: Challenges, targets and therapeutic opportunities. *Biomed Pharmacother*. 2017;89:288–96. [cited 2019 Aug 15] Available from: <https://www.sciencedirect.com/science/article/abs/pii/S0753332216320923?via%3Dihub>.
11. Evan GI, Vousden KH. Proliferation, cell cycle and apoptosis in cancer. *Nature*. 2001;411(6835):342–8. [cited 2019 Aug 15] Available from: <http://www.nature.com/articles/35077213>.
12. Moore RD, Chaisson RE. Natural history of HIV infection in the era of combination antiretroviral therapy. 1999;(June).
13. Roberts J, Bebenek K, Kunkel T. The accuracy of reverse transcriptase from HIV-1. *Science* (80-). 1988;242(4882):1171–3. [cited 2019 Jul 23] Available from: <http://www.ncbi.nlm.nih.gov/pubmed/2460925>.
14. Memarnejadian A, Nikpoor AR, Davoodian N, Kargar A, Mirzadeh Y, Goukani H. HIV-1 Drug Resistance Mutations among Antiretroviral Drug-Experienced Patients in the South of Iran. *Intervirology*. 2019;1–8. [cited 2019 Jul 23] Available from: <http://www.ncbi.nlm.nih.gov/pubmed/31311021>.
15. Kast RE, Karpel-Massler G, Halatsch M-E. CUSP9* treatment protocol for recurrent glioblastoma: aprepitant, artesunate, auranofin, captopril, celecoxib, disulfiram, itraconazole, ritonavir, sertraline augmenting continuous low dose temozolomide. *Oncotarget*. 2014;5(18):8052–82.
16. Skaga E, Skaga IØ, Grieg Z, Sandberg CJ, Langmoen IA, Vik-Mo EO. The efficacy of a coordinated pharmacological blockade in glioblastoma stem cells with nine repurposed drugs using the CUSP9 strategy. *J Cancer Res Clin Oncol*. 2019;145(6):1495–507. [cited 2019 Aug 23] Available from: <http://www.ncbi.nlm.nih.gov/pubmed/31028540>.
17. Halatsch M, Kast RE, Dwucet A, Hlavac M, Heiland T, Westhoff M, et al. Bcl-2/Bcl-xL inhibition predominantly synergistically enhances the anti-neoplastic activity of a low-dose CUSP9 repurposed drug regime against glioblastoma. *Br J Pharmacol*. 2019;bph.14773. [cited 2019 Aug 23] Available from: <http://www.ncbi.nlm.nih.gov/pubmed/31222722>.
18. Al-Lazikani B, Banerji U, Workman P. Combinatorial drug therapy for cancer in the post-genomic era. *Nat Biotechnol*. 2012;30(7):679–92 Available from: <http://www.ncbi.nlm.nih.gov/pubmed/22781697%5Cnhttp://www.pubmedcentral.nih.gov/articlerender.fcgi?artid=4320499&tool=pmcentrez&rendertype=abstract>.
19. Lane DP. p53, guardian of the genome. *Nature*. 1992;358(6381):15–6. [cited 2019 Aug 2] Available from: <http://www.nature.com/articles/358015a0>.
20. Bykov VJN, Issaeva N, Shilov A, Hultcrantz M, Pugacheva E, Chumakov P, et al. Restoration of the tumor suppressor function to mutant p53 by a low-molecular-weight compound. *Nat Med*. 2002;8(3):282–8. [cited 2019 Jul 23] Available from: <http://www.ncbi.nlm.nih.gov/pubmed/11875500>.
21. Vassilev LT, Vu BT, Graves B, Carvajal D, Podlaski F, Filipovic Z, et al. In vivo activation of the p53 pathway by small-molecule antagonists of MDM2. *Science*. 2004;303(5659):844–8. Available from: <http://www.ncbi.nlm.nih.gov/pubmed/14704432>.
22. Lemos A, Leão M, Soares J, Palmeira A, Pinto M, Saraiva L, et al. Medicinal Chemistry Strategies to Disrupt the p53-MDM2/MDMX Interaction. *Med Res Rev*. 2016;36(5):789–844. [cited 2018 Oct 14] Available from: <http://www.ncbi.nlm.nih.gov/pubmed/27302609>.
23. Chen Z, Lu W, Garcia-Prieto C, Huang P. The Warburg effect and its cancer therapeutic implications. *J Bioenerg Biomembr*. 2007;39(3):267–74. [cited 2019 Jul 23] Available from: <http://link.springer.com/10.1007/s10863-007-9086-x>.
24. Wheaton WW, Weinberg SE, Hamanaka RB, Soberanes S, Sullivan LB, Anso E, et al. Metformin inhibits mitochondrial complex I of cancer cells to reduce tumorigenesis; 2014. p. 1–18.
25. Cluntun AA, Lukey MJ, Cerione RA, Locasale JW. Glutamine Metabolism in Cancer: Understanding the Heterogeneity. *Trends in cancer*. 2017 [cited 2019 Sep 11];3(3):169–80. Available from: <http://www.ncbi.nlm.nih.gov/pubmed/28393116>.
26. Gross MJ, Demo SD, Dennison JB, Chen L, Chernov-Rogan T, Goyal B, et al. Antitumor Activity of the Glutaminase Inhibitor CB-839 in Triple-Negative Breast Cancer. *Mol Cancer Ther*. 2014;13(4):890–901. [cited 2018 Oct 15] Available from: <http://www.ncbi.nlm.nih.gov/pubmed/24523301>.
27. Nakahara T, Takeuchi M, Kinoyama I, Minematsu T, Shirasuna K, Matsuhisa A, et al. YM155, a Novel Small-Molecule Survivin Suppressant, Induces Regression of Established Human Hormone-Refractory Prostate Tumor Xenografts 2007;(17):8014–8021.
28. Vadas O, Burke JE, Zhang X, Berndt A, Williams RL. Structural Basis for Activation and Inhibition of Class I Phosphoinositide 3-Kinases. *Sci Signal*. 2011;4(195):re2–re2. [cited 2019 Jul 24] Available from: <https://stke.sciencemag.org/content/4/195/re2long>.
29. Fischer A, Müller D, Zimmermann-Kordmann M, Kleuser B, Mickleit M, Laabs S, et al. The ether lipid inositol-C2-PAF is a potent inhibitor of cell proliferation in HaCaT cells. *ChemBioChem*. 2006;7(3):441–9.
30. Pelz C, Häckel S, Semini G, et al. Inositol-C2-PAF acts as a biological response modifier and antagonizes cancer-relevant processes in mammary carcinoma cells. *Cell Oncol (Dordr)*. 2018;41(5):505–16. Available from: <https://pubmed.ncbi.nlm.nih.gov/30047091/>.
31. Hung J-Y, Hsu Y-L, Li C-T, Ko Y-C, Ni W-C, Huang M-S, et al. 6-Shogaol, an Active Constituent of Dietary Ginger, Induces Autophagy by Inhibiting the AKT/mTOR Pathway in Human Non-Small Cell Lung Cancer A549 Cells. *J Agric Food Chem*. 2009 28;57(20):9809–16. [cited 2019 Jul 24] Available from: <https://pubs.acs.org/doi/10.1021/jf902315e>.
32. Yin Z, Deng Z, Zhao W, Cao Z. Searching synergistic dose combinations for anticancer drugs. *Front Pharmacol*. 2018;9(MAY):1–7.
33. Sheng Z, Sun Y, Yin Z, Tang K, Cao Z. Advances in computational approaches in identifying synergistic drug combinations. *Brief Bioinform*. 2017;19(6):1172–82. [cited 2019 Jul 26] Available from: <http://www.ncbi.nlm.nih.gov/pubmed/28475767>.
34. Borisy AA, Elliott PJ, Hurst NW, Lee MS, Lehar J, Price ER, et al. Systematic discovery of multicomponent therapeutics. *Proc Natl Acad Sci U S A*. 2003;100(13):7977–82. [cited 2019 Jul 29] Available from: <http://www.ncbi.nlm.nih.gov/pubmed/12799470>.
35. Mayer LD, Janoff AS. Optimizing Combination Chemotherapy by Controlling Drug Ratios. *Mol Interv*. 2007;7(4):216–23. [cited 2019 Jul 29] Available from: <http://www.ncbi.nlm.nih.gov/pubmed/17827442>.
36. Weiss A, Berndsen RH, Ding X, Ho C-M, Dyson PJ, van den Bergh H, et al. A streamlined search technology for identification of synergistic drug combinations. *Sci Rep*. 2015;5:14508. [cited 2019 Jul 26] Available from: <http://www.ncbi.nlm.nih.gov/pubmed/26416286>.
37. Nowak-Sliwinska P, Weiss A, Ding X, Dyson PJ, van den Bergh H, Griffioen AW, et al. Optimization of drug combinations using Feedback System Control. *Nat Protoc*. 2016;11(2):302–15. [cited 2019 Jul 29] Available from: <http://www.ncbi.nlm.nih.gov/pubmed/26766116>.
38. Weiss A, Ding X, van Beijnum JR, Wong I, Wong TJ, Berndsen RH, et al. Rapid optimization of drug combinations for the optimal angiostatic treatment of cancer. *Angiogenesis*. 2015;18(3):233–44. [cited 2019 Aug 21] Available from: <http://www.ncbi.nlm.nih.gov/pubmed/25824484>.
39. Li P, Huang C, Fu Y, Wang J, Wu Z, Ru J, et al. Large-scale exploration and analysis of drug combinations. *Bioinformatics*. 2015;31(12):2007–16.
40. Greco WR, Bravo G, Parsons JC. The Search for Synergy: A Critical Review from a Response Surface Perspective*. 1995 . [cited 2019 Jul 24] Available from: <http://pharmrev.aspetjournals.org/content/pharmrev/47/2/331.full.pdf>.
41. LOEWE S. The problem of synergism and antagonism of combined drugs. *Arzneimittelforschung*. 1953;3(6):285–90. [cited 2019 Aug 27] Available from: <http://www.ncbi.nlm.nih.gov/pubmed/13081480>.
42. Chou T-C. Theoretical basis, experimental design, and computerized simulation of synergism and antagonism in drug combination studies. *Pharmacol Rev*. 2006;58(3):621–81. [cited 2015 Sep 26] Available from: <http://www.ncbi.nlm.nih.gov/pubmed/16968952>.
43. Lines C, Krueger SA, Wilson GD. Cancer Cell culture. *Methods*. 2011;731:359–70 Available from: <http://www.springerlink.com/index/10.1007/978-1-61779-080-5>.
44. Martin N, Trials HIVC, Tumor X, Nude I, Basis T, Design E, et al. CompuSyn by Ting-Chao Chou. 2010;2005(D):3–4.
45. Zhao L, Wientjes MG, Au JL-S. Evaluation of combination chemotherapy: integration of nonlinear regression, curve shift, isobologram, and combination index analyses. *Clin Cancer Res*. 2004;10(23):7994–8004. [cited 2016 Apr 13] Available from: <http://www.ncbi.nlm.nih.gov/pubmed/15585635>.
46. Dai X, Cheng H, Bai Z, Li J. Breast cancer cell line classification and its relevance with breast tumor subtyping. *J Cancer*. 2017;8(16):3131–41.
47. Comşa Ş, Cimpean AM, Raica M. The story of MCF-7 breast Cancer Cell line: 40 years of experience in research. *Anticancer Res*. 2015;35(6):3147–54. Available from: <http://www.ncbi.nlm.nih.gov/pubmed/26026074>.
48. Berglind H, Pawitan Y, Kato S. Analysis of p53 mutation status in human cancer cell lines. *Cancer Biol ...* 2008;(April):701–10. Available from: <http://www.landesbioscience.com/journals/cbt/14BerglindCBT7-5.pdf>.
49. Chou TC, Talalay P. Quantitative analysis of dose-effect relationships: the combined effects of multiple drugs or enzyme inhibitors. *Adv Enzyme*

- Regul. 1984;22:27–55. [cited 2016 mar 8] Available from: <http://www.ncbi.nlm.nih.gov/pubmed/6382953>.
50. Chou T-C. Preclinical versus clinical drug combination studies. *Leuk Lymphoma*. 2008;49(11):2059–80. [cited 2016 Apr 9] Available from: <http://www.ncbi.nlm.nih.gov/pubmed/19021049>.
 51. Chou T. Preclinical versus clinical drug combination studies. 2016;8194(April).
 52. Shimazu K, Tada Y, Morinaga T, Shingyoji M, Sekine I, Shimada H, et al. Metformin produces growth inhibitory effects in combination with nutlin-3a on malignant mesothelioma through a cross-talk between mTOR and p53 pathways. *BMC Cancer*. 2017;17(1):309. [cited 2018 Jun 9] Available from: <http://bmccancer.biomedcentral.com/articles/10.1186/s12885-017-3300-y>.
 53. Koh MY, Spivak-Kroizman T, Venturini S, Welsh S, Williams RR, Kirkpatrick DL, et al. Molecular mechanisms for the activity of PX-478, an antitumor inhibitor of the hypoxia-inducible factor-1. *Mol Cancer Ther*. 2008;7(1):90–100. [cited 2018 Apr 13] Available from: <http://www.ncbi.nlm.nih.gov/pubmed/18202012>.
 54. Lee YM, Lim JH, Chun YS, Moon HE, Lee MK, Huang LE, et al. Nutlin-3, an Hdm2 antagonist, inhibits tumor adaptation to hypoxia by stimulating the FIH-mediated inactivation of HIF-1 α . *Carcinogenesis*. 2009;30(10):1768–75.
 55. Li B, Zhu Y, Sun Q, Yu C, Chen L, Tian Y, et al. Reversal of the Warburg effect with DCA in PDGF-treated human PASM is potentiated by pyruvate dehydrogenase kinase-1 inhibition mediated through blocking Akt/GSK-3 β signalling. *Int J Mol Med*. 2018;42(3):1391–400. [cited 2019 Jul 23] Available from: <http://www.ncbi.nlm.nih.gov/pubmed/29956736>.
 56. Allison SJ, Knight JRP, Granchi C, Rani R, Minutolo F, Milner J, et al. Identification of LDH-A as a therapeutic target for cancer cell killing via (i) p53/NAD(H)-dependent and (ii) p53-independent pathways. *Oncogenesis*. 2014;3(5):e102. Available from: <http://www.pubmedcentral.nih.gov/articlerender.fcgi?artid=4035693&tool=pmcentrez&rendertype=abstract>.
 57. Li B, Li X, Ni Z, Zhang Y, Zeng Y, Yan X, et al. Dichloroacetate and metformin synergistically suppress the growth of ovarian cancer cells. *Oncotarget*. 2016;7(37):1–13. Available from: <http://www.ncbi.nlm.nih.gov/pubmed/27449090>.
 58. Chou T. Preclinical versus clinical drug combination studies. *Leuk Lymphoma*. 2008;49(11):2059–80. [cited 2016 Apr 9] Available from: <http://www.ncbi.nlm.nih.gov/pubmed/19021049>.
 59. Zimmermann GR, Lehar J, Keith CT. Multi-target therapeutics: when the whole is greater than the sum of the parts. *Drug Discov Today*. 2007;12(1–2):34–42.
 60. Garon EB, Christofk HR, Hosmer W, Britten CD, Bahng A, Crabtree MJ, et al. Dichloroacetate should be considered with platinum - based chemotherapy in hypoxic tumors rather than as a single agent in advanced non - small cell lung cancer; 2014. p. 443–52.
 61. Tibes R, Falchook GS, Von Hoff DD, Weiss GJ, Iyengar T, Kurzrock R, et al. Results from a phase I, dose-escalation study of PX-478, an orally available inhibitor of HIF-1 α . *J Clin Oncol*. 2010;28(15_suppl):3076–3076. [cited 2019 Jul 22] Available from: http://ascopubs.org/doi/10.1200/jco.2010.28.15_suppl.3076.
 62. Secchiero P, Barbarotto E, Tiribelli M, Zerbinati C, Di Iasio MG, Gonelli A, et al. Functional integrity of the p53-mediated apoptotic pathway induced by the nongenotoxic agent nutlin-3 in B-cell chronic lymphocytic leukemia (B-CLL). *Blood*. 2006;107(10):4122–9.
 63. Calvaresi EC, Granchi C, Tuccinardi T, et al. Dual targeting of the Warburg effect with a glucose-conjugated lactate dehydrogenase inhibitor. *Chembiochem*. 2013;14(17):2263–7. Available from: <https://pubmed.ncbi.nlm.nih.gov/24174263/>.

Publisher's Note

Springer Nature remains neutral with regard to jurisdictional claims in published maps and institutional affiliations.

Ready to submit your research? Choose BMC and benefit from:

- fast, convenient online submission
- thorough peer review by experienced researchers in your field
- rapid publication on acceptance
- support for research data, including large and complex data types
- gold Open Access which fosters wider collaboration and increased citations
- maximum visibility for your research: over 100M website views per year

At BMC, research is always in progress.

Learn more biomedcentral.com/submissions



11.3 Publication 3

Dichloroacetate and PX-478 Exhibit Strong Synergistic Effects in a Various Number of Cancer Cell Lines.

Jonas Parczyk*, Jérôme Ruhnau*, Carsten Pelz, Max Schilling, Hao Wu, Nicole Nadine Piaskowski, Britta Eickholt, Hartmut Kühn, Kerstin Danker, Andreas Klein

*geteilte Erstautorenschaft

BMC Cancer. 2021

doi: 10.21203/rs.3.rs-88933/v1

Impact factor: 3.15 - 2-year Impact Factor 3.432 - 5-year Impact Factor

RESEARCH ARTICLE

Open Access

Dichloroacetate and PX-478 exhibit strong synergistic effects in a various number of cancer cell lines



Jonas Parczyk^{*†} , Jérôme Ruhnau^{*†}, Carsten Pelz, Max Schilling, Hao Wu, Nicole Nadine Piaskowski, Britta Eickholt, Hartmut Kühn, Kerstin Danker and Andreas Klein

Abstract

Background: One key approach for anticancer therapy is drug combination. Drug combinations can help reduce doses and thereby decrease side effects. Furthermore, the likelihood of drug resistance is reduced. Distinct alterations in tumor metabolism have been described in past decades, but metabolism has yet to be targeted in clinical cancer therapy. Recently, we found evidence for synergism between dichloroacetate (DCA), a pyruvate dehydrogenase kinase inhibitor, and the HIF-1 α inhibitor PX-478. In this study, we aimed to analyse this synergism in cell lines of different cancer types and to identify the underlying biochemical mechanisms.

Methods: The dose-dependent antiproliferative effects of the single drugs and their combination were assessed using SRB assays. FACS, Western blot and HPLC analyses were performed to investigate changes in reactive oxygen species levels, apoptosis and the cell cycle. Additionally, real-time metabolic analyses (Seahorse) were performed with DCA-treated MCF-7 cells.

Results: The combination of DCA and PX-478 produced synergistic effects in all eight cancer cell lines tested, including colorectal, lung, breast, cervical, liver and brain cancer. Reactive oxygen species generation and apoptosis played important roles in this synergism. Furthermore, cell proliferation was inhibited by the combination treatment.

Conclusions: Here, we found that these tumor metabolism-targeting compounds exhibited a potent synergism across all tested cancer cell lines. Thus, we highly recommend the combination of these two compounds for progression to in vivo translational and clinical trials.

Keywords: PX-478, HIF-1 α inhibition, Dichloroacetate, Synergism, Cancer therapy, Drug combination, Cancer cell lines, Metabolism

* Correspondence: jonasparczyk@outlook.com; jerome.ruhnau@gmail.com
†Jonas Parczyk and Jérôme Ruhnau contributed equally to this work.

Charité – Universitätsmedizin Berlin, Corporate Member of Freie Universität Berlin, Humboldt-Universität zu Berlin, and Berlin Institute of Health, Charitéplatz 1, 10117 Berlin, Germany



© The Author(s). 2021 **Open Access** This article is licensed under a Creative Commons Attribution 4.0 International License, which permits use, sharing, adaptation, distribution and reproduction in any medium or format, as long as you give appropriate credit to the original author(s) and the source, provide a link to the Creative Commons licence, and indicate if changes were made. The images or other third party material in this article are included in the article's Creative Commons licence, unless indicated otherwise in a credit line to the material. If material is not included in the article's Creative Commons licence and your intended use is not permitted by statutory regulation or exceeds the permitted use, you will need to obtain permission directly from the copyright holder. To view a copy of this licence, visit <http://creativecommons.org/licenses/by/4.0/>. The Creative Commons Public Domain Dedication waiver (<http://creativecommons.org/publicdomain/zero/1.0/>) applies to the data made available in this article, unless otherwise stated in a credit line to the data.

Introduction

In the last decade, combinatorial approaches for cancer therapy have become increasingly popular [1]. Drugs designed to act against individual molecular targets can hardly combat a multigenic disease such as cancer [2]. However, synergistic drug combinations can lead to reduced drug doses with less pronounced side effects, increased response rates and attenuated likelihoods of drug resistance [1–3].

In a previous work [4], we screened 14 selected compounds, including dichloroacetate (DCA) and PX-478, for synergistic interactions in cancer cell lines. The combination of DCA and PX-478 displayed significantly stronger effects on cell viability than either single compound. Therefore, we aimed to further investigate this combination using a widely accepted method of quantifying synergism over the whole dose-response curve introduced by Chou and Talalay [5].

Compounds

DCA, a chlorinated carboxylic acid that was originally administered in the treatment of hereditary lactate acidosis [6], is an inhibitor of pyruvate dehydrogenase kinase (PDK). Thus, it leads to increased pyruvate dehydrogenase activity and therefore to an increase in pyruvate decarboxylation to acetyl-CoA, partially reversing the Warburg effect [7]. The Warburg effect describes alterations in tumor metabolism that lead to enhanced aerobic glycolysis and a reduction in oxidative phosphorylation. These alterations, while being less energy efficient, provide the necessary building blocks the tumor needs for proliferation [8, 9]. Furthermore, the reduction in cell respiration results in suppression of the mitochondrial-K⁺ channel axis and thus hyperpolarisation of the mitochondrial membrane. Consequently, the release of cytochrome c and AIF is impaired, leading to apoptosis resistance [10]. DCA was found to normalise this axis and thereby induce the apoptosis of cancer cells [11, 12]. In addition to its effects on the mitochondrial membrane potential, DCA is believed to lead to a significant increase in reactive oxygen species (ROS) generation, which plays an important role in the induction of apoptosis [13–17]. In contrast, other authors reported that DCA may function as a sensitiser for ROS-induced alterations but did not significantly increase ROS production per se [16, 18]. In addition, DCA has been shown to positively regulate p53 as well as to downregulate autophagy, thereby leading to enhanced tumor cell apoptosis and attenuated cell proliferation [19, 20].

PX-478 is a small molecule that interferes with the transcription and translation of hypoxia-inducible factor-1 α (HIF-1 α) and leads to diminished ubiquitination of HIF-1 α [21]. HIF-1 α is physiologically activated by hypoxia and mediates multiple cellular alterations via transactivation of various target genes,

such as GLUT1, LDHA and VEGF, and hence increases aerobic glycolysis in order for the cell to sustain hypoxic conditions [22]. Hence, PX-478-mediated inhibition of HIF-1 α was found to induce apoptosis and cell cycle arrest in cancer cells [23, 24]. In oesophageal squamous cell cancer, PX-478 induces apoptosis, reduces cell proliferation and inhibits epithelial-mesenchymal transition [25]. Welsh et al. identified that the antitumor effect of PX-478 is positively correlated with HIF-1 α levels in human xenografts [26]. In a study by Lang et al., PX-478 acted synergistically with an ROS inducer, ATO, leading to more efficient ROS-induced apoptosis via blocking ROS clearance by the HIF-1/FOXO1/SESN3 pathway [24].

HIF-1 α -mediated inhibition of mitochondrial ROS production (as a reaction to ROS accumulation, hypoxia and cytokine stimulation) is achieved partially through a decrease in the production of acetyl-CoA via upregulation of PDK-1 and -3, the direct targets of DCA [27, 28]. Additionally, DCA-mediated inhibition of PDK leads to HIF-1 α inhibition and, thereby suppresses angiogenesis [14].

Apart from preliminary results indicating a likely synergism [4], the anticipated interplay of DCA and PX-478 regarding ROS generation, apoptosis and proliferation makes this combination especially interesting for further investigations.

In this study, we examined the effects of the combination of DCA and PX-478 on eight cancer cell lines and the non-cancerous cell line HEK-293. In addition, we studied the impact of the combination on ROS generation, apoptosis induction and cell cycle arrest.

Methods

Cell culture

The breast cancer cell lines MCF-7 and MDA MB-231 were a kind gift from Göran Landberg (Sahlgrenska Cancer Center, University of Gothenburg, Gothenburg, Sweden). The colon cancer cell line HT-29, the hepatocellular cancer cell line HEPG2, the cervical cancer cell line HeLa and the adenocarcinoma lung cancer cell lines A549 and H441, as well as the non-cancerous cell line HEK-293, were purchased from the American Type Culture Collection (ATCC). The glioblastoma cell line U251 was a kind gift from Kai Murk (Charité Berlin, Germany). A549, HEK-293, HeLa, HEPG2, HT-29, MCF-7 and U251 cells were cultured in DMEM, and H441 and MDA-MB-231 cells were cultured in DMEM/F12. All media contained penicillin/streptomycin (100 U ml⁻¹), L-glutamine (DMEM: 584 mg l⁻¹, DMEM/F12: 365.1 mg l⁻¹) and 10% heat-inactivated foetal calf serum (PAN Biotech, Germany). The humidified incubator was set at 37 °C with 5% CO₂. Cells were harvested using 0.05% trypsin/0.02% ethylenediaminetetraacetic acid (EDTA) in PBS.

Compounds

PX-478 (Hözel Diagnostika Handels GmbH, Cologne, Germany) and DCA (Sigma-Aldrich, Munich, Germany) were dissolved in distilled water.

Cell viability and cell proliferation assays

A total of 0.75×10^4 A549, 1×10^4 HEK-293, 0.3×10^4 HeLa, 0.6×10^4 HEPG2, 1.5×10^4 HT-29, 0.5×10^4 MCF-7, 1.5×10^4 MDA-MB-231, 1×10^4 H441 and 0.3×10^4 U251 cells per well were seeded in flat bottom 96-well plates. After 24 h, when the cells were approximately 50% confluent, DCA, PX-478 or the combination was added. After 48 h of further incubation, a sulforhodamine B (SRB) assay was performed. For the SRB assay, cells were fixed with 10% trichloroacetic acid (w/v) and stained with 0.06% SRB in 1% acetic acid for 30 min. Cells were then repeatedly washed with 1% acetic acid (v/v) and dissolved in 10 mM Tris (pH 10.5). The protein mass was measured by determining the optical density at a wavelength of 492 nm in a microplate reader. Additionally, in HT-29 cell MTT assays were performed according to the manufacturer's instructions (data are shown in additional file 1). All experiments were performed independently three times with at least 2 technical triplicates (mostly with 3).

Dose-response curves were generated using GraphPad Prism 7.05 statistical analysis software. The half-maximal effective concentration (EC_{50}) of each compound was determined via nonlinear regression.

Confirmation of synergism

Synergism was evaluated with four to seven different concentrations (mostly with 6), as suggested by Chou and Talalay [5].

Cells were treated with the combination of DCA and PX-478 at a constant $EC_{50}:EC_{50}$ ratio as well as with the single compounds alone. Significant differences between each single compound and the combination were assessed by an unpaired t-test. Only concentrations with *p*-values of ≤ 0.05 for both single compounds compared to the combination were considered to exhibit significant differences and are marked with an asterisk (*) in the figures.

Combination indices (CIs) were calculated using CompuSyn software [29]. The CI is a quantitative value indicating the synergism of a drug combination at specific concentrations. A value of less than 0.9 indicates synergism (the lower the CI, the stronger the synergism). Values from 0.9 to 1 indicate a nearly additive effect, and a CI value of greater than 1.1 indicates antagonism [30]. CI values were calculated as follows:

$$CI = \frac{(D)_1}{(Dx)_1} + \frac{(D)_2}{(Dx)_2}$$

In the numerators, $(D)_1$ and $(D)_2$ are the concentrations of drug 1 and drug 2, respectively, in the drug

combination that have a certain effect on cell viability (*x* %). In the denominators, $(Dx)_1$ and $(Dx)_2$ are the concentrations of each drug alone (drug 1 or drug 2, respectively) that are necessary to obtain the same effect (*x* %) as the drug combination (both drug 1 and drug 2). The concentrations $(Dx)_1$ and $(Dx)_2$ were calculated by CompuSyn with reference to the cell viability data for the respective compounds. To enhance analytical robustness, most concentrations of the compounds were doubled. Therefore, potential calculation errors were minimised, as suggested by Zhao et al. [31]. To generate the median-effect plots, the following equation was used:

$$D_x = D_m \left[\frac{fa}{1-fa} \right]^{1/m}$$

where D_m is the median effective dose, *m* is the slope of the median-effect curve, and *fa* is the fraction affected. Since calculation of a CI value is appropriate only when neither single compound has an effect close to 100%, the respective CI values are not shown in the Results section [31]. All data collected in this study can be found in additional file 1 (additional file 1).

Membrane lipid oxidation rate

HT-29 cells were seeded in 10 cm diameter Petri dishes and treated with the EC_{50} dose of DCA, the EC_{50} dose of PX-478 or the combination after 24 h when the cells were approximately 80% confluent. After incubation for an additional 48 h, cells were harvested with trypsin, pelleted and resuspended in 500 μ l of PBS. For lipid extraction, cells were homogenised in a mixture of methanol:chloroform:water (2:1:1 by volume) using a modified Bligh/Dyer method. The extracted lipid suspension was bubbled with argon to prevent artificial oxidation. Then, alkaline hydrolysis was carried out, and the resulting free fatty acids were analysed by reversed-phase HPLC (RP-HPLC). Arachidonic acid and its oxygenated derivative 10-/15-hydroxyeicosatetraenoic acid (HETE) were identified by their specific retention times and UV spectra and were quantified via integration [32].

Flow cytometric analysis

Samples were analysed with BD FACS Calibur and Cell Quest.

Detection of intracellular ROS

Intracellular ROS were detected via an oxidation-sensitive fluorescent probe (2',7'-dichlorodihydrofluorescein diacetate [H2DCFDA], Bio-Techne GmbH, Germany). HeLa and MCF-7 cells were seeded in 6 cm diameter Petri dishes and treated after 24 h at a confluence of 50%. Cells were treated with the EC_{50} dose of DCA, PX-478 or the combination for 48 h. Then, cells were harvested and

washed twice with PBS. Next, the cells were incubated with 50 μ M H2DCFDA at 37 °C for 20 min in the dark and were then placed on ice. Cells were washed 2 more times before being analysed by flow cytometry.

Evaluation of apoptosis by Annexin-V-FITC and propidium iodide staining

HeLa and MCF-7 cells were seeded in 6 cm diameter Petri dishes and incubated for 24 h to a confluence of approximately 60%. After 24 h, cells were treated with PX-478, DCA or the combination and harvested 48 h later. The following concentrations were used: HeLa cells— EC_{50} DCA and 0.5 x EC_{50} PX-478; MCF-7 cells— EC_{50} DCA and EC_{50} PX-478. Cells were washed twice with PBS, placed on ice immediately, transferred to binding buffer (10 mM Hepes, 140 mM NaCl, 2.5 mM $CaCl_2$; pH 7.4) and stained with Annexin-V-FITC (Hözel Diagnostika Handels GmbH, Germany) in the dark according to the manufacturer's instructions. After 15 min, propidium iodide (50 μ g/ml) was added, and the cells were analysed by flow cytometry.

Western blot analysis

For Western blotting, cells were seeded in 6 cm diameter Petri dishes, grown to approximately 80% confluence and treated with the noted compounds. 24 h later, the cells were washed with PBS and lysed with lysis buffer (50 mM β -glycerophosphate pH 7.6, 1.5 mM EGTA, 1.0 mM EDTA, 1% (v/v) Triton X-100, 0.2% (v/v) protease inhibitor cocktail, 0.4% (v/v) PMSF, 100 mM sodium vanadate, 500 mM NaF). The samples were separated under reducing conditions by 10% SDS-PAGE and transferred to nitrocellulose membranes (Thermo Fisher, Rockford, USA). The primary antibodies and the corresponding working concentrations are listed in Table 1. Proteins were detected using SuperSignal West Pico Chemiluminescent Substrate (Pierce, Thermo Fisher Scientific, Bonn, Germany). Signals were visualised using a VersaDoc™ 4000 MP and QuantityOne® 4.6.5 software (BioRad Laboratories, Munich, Germany) and quantified using ImageJ 1.52a software (National Institute of Health, USA; version 1.8.0_112).

Metabolic assays

MCF-7 cells were seeded in an XF 96-well culture microplate (Agilent, Santa Clara, USA) at 3×10^4 cells

per well in 180 μ l of prewarmed assay medium. After 24 h, a mitochondrial respiration assay or glycolytic rate assay was performed with a Seahorse XFe96 Analyzer (Agilent Technologies). For the mitochondrial respiration assay, the oxygen consumption rate (OCR) was measured using the mitochondrial stress test procedure in XF media (nonbuffered DMEM containing 10 mM glucose, 2 mM L-glutamine and 1 mM sodium pyruvate). The glycolytic rate was measured in accordance with the Agilent Seahorse XFp Glycolytic Stress Test Kit instructions. After four measurements of either the baseline OCR or baseline extracellular acidification rate (ECAR), DCA solution was injected into the appropriate wells to the desired working concentration. Before each measurement, the assay medium was gently mixed to restore normal oxygen tension and pH in the microenvironment surrounding the cells. Two hours after treatment with DCA (6 measurements), the actual mitochondrial respiration assay or glycolytic stress test was performed. When metabolic analysis was complete, the cells were immediately fixed, and an SRB assay was performed as described above for data normalisation. Graphs were produced using GraphPad Prism 7.05 statistical analysis software. Glycolytic capacity and maximal respiration (Fig. 5) were calculated as follows:

- maximal respiration (OCR) = (maximum rate measured after injection of carbonyl cyanide-4-(trifluoromethoxy)phenylhydrazone [FCCP]) – (non-mitochondrial respiration rate)
- non-mitochondrial respiration (OCR) = minimum rate measured after injection of rotenone & antimycin A)
- Glycolytic capacity (ECAR) = (maximum rate measured after injection of oligomycin) – (non-glycolytic acidification rate)
- non-glycolytic acidification (ECAR) = minimum rate measured after injection of 2-deoxy-D-glucose (2DG).

Statistical analysis

Statistical analysis was performed using unpaired T-tests in GraphPad Prism 7.05 statistical analysis software. Differences with a *p*-value of ≤ 0.05 were considered significant: significant differences compared to the control are marked with an asterisk (*), while significant differences

Table 1 List of antibodies

Antibody raised against	Purchased from	Source	Dilution
β -actin	Cell Signaling (Danvers, USA)	Mouse	1:4000
PARP/cleaved PARP (9542)	Cell Signaling (Danvers, USA)	Rabbit	1:1000
Retinoblastoma p795 (9301)	Cell Signaling (Danvers, USA)	Rabbit	1:1000
Cyclin D1 (DCS-6)	Thermo Scientific (Waltham, USA)	Mouse	1:200

between the combination and both the control and each single compound are marked with two asterisks (**). All experiments were performed with at least 2 technical and 3 biological replicates.

Results

The combination of DCA and PX-478 produces synergistic effects in eight cancer cell lines and shows only minimal effects on the non-cancerous cell line HEK-293

In this study, we evaluated the effects of DCA and PX-478 on eight cancer cell lines, including lung (A549 and H441), breast (MCF-7 and MDA-MB-231), cervical (HeLa), hepatocellular (HepG2), colon cancer (HT-29) and glioblastoma (U251) cell lines (Fig. 1). The EC₅₀ values used for treatment in the combinatorial experiments were determined for all cell lines in preceding experiments and are henceforth referred to as the approximated half-maximal effective concentration (EC_{50a})

values [4] (see additional file 1). The actual EC₅₀ values for the experiments conducted herein were calculated afterwards (see Table 2).

While the combination showed synergistic effects in six investigated tumor entities, the combination exhibited synergistic effects over the complete dose-response curve in A549 (lung adenocarcinoma) and HEPG2 (hepatocellular carcinoma) cells with CI values ranging from 0.61 to 0.87 and 0.56 to 0.79, respectively.

EC₅₀ data and best CI values are listed in Table 2. As illustrated, the synergism between DCA and PX-478 was observed in all analysed cell lines, with the lowest CI value in MCF-7 at 0.125 x EC₅₀ (CI = 0.4). To minimise extrapolation errors, we calculated CI values relying on experimental data and eliminated CI values for concentrations where the effect of either single compound was too close to 100%, as suggested by Zhao et al. [31]. Interestingly, the combination of DCA and PX-478 strongly

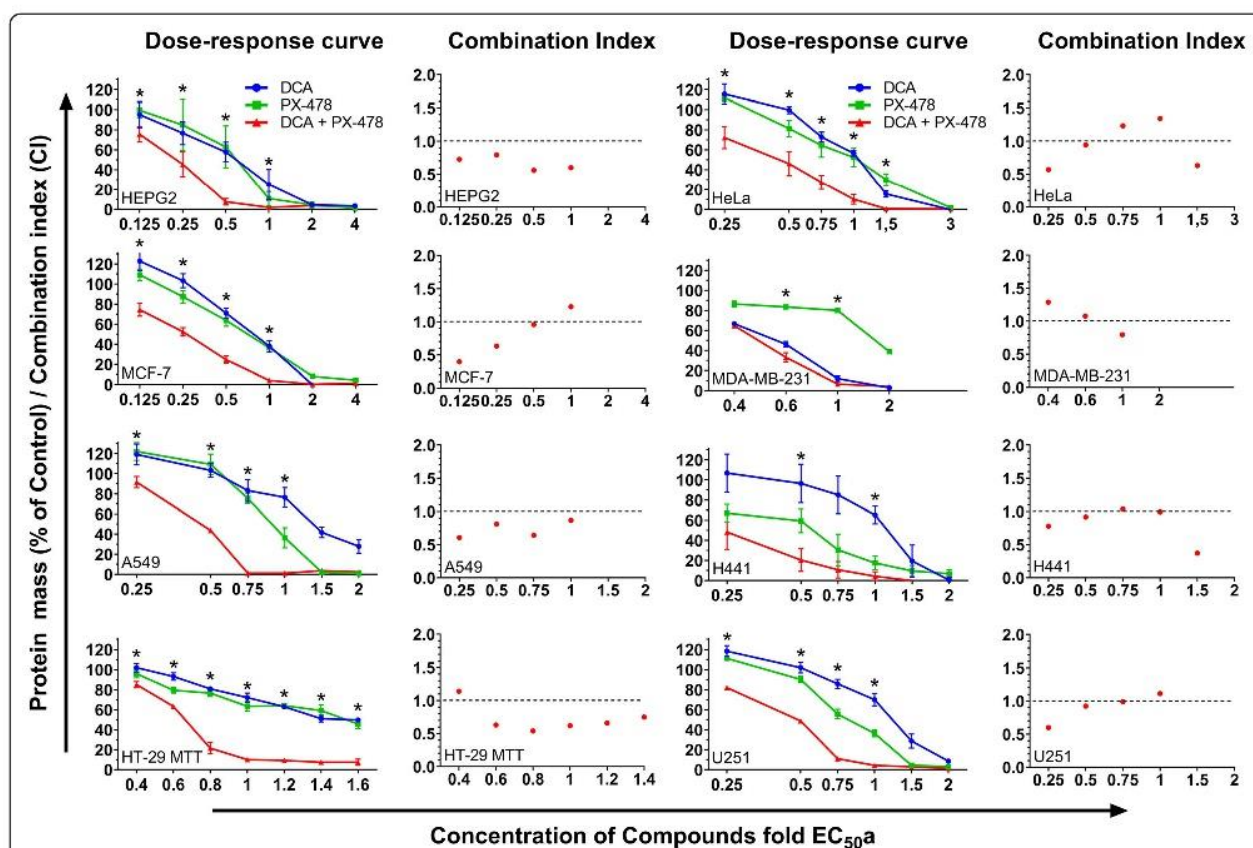


Fig. 1 Synergistic interactions between DCA and PX-478 in eight cancer cell lines. Figure 1 shows the dose-response curves for DCA, PX-478 and their combination in eight different cell lines as well as the respective CIs (shown to the right of each dose-response curve). Cells were seeded in 96-well plates and treated at a confluence of approximately 50%. Forty-eight hours later, an SRB (protein mass) assay was performed. If applicable, a CI was calculated with CompuSyn for each concentration. A CI of less than 0.9 indicates synergism, a CI between 0.9 and 1.1 indicates a nearly additive effect, and a CI of greater than 1.1 indicates antagonism. Approximated EC₅₀ values were used (EC_{50a}) at a constant EC_{50a}:EC_{50a} ratio. Concentrations for which the effect of combination was significantly different from that of both single compounds and the control ($p \leq 0.05$, unpaired T-Test) are marked with an asterisk (*). Synergistic interactions were confirmed for all cancer cell lines, as indicated by the CI values and predominant left shifts of the curves. Without exception, the effects of the drug combination surpassed the effects of each single compound

Table 2 EC₅₀ values for the single compounds and the combination

Cell line	EC ₅₀ DCA (mM)	EC ₅₀ PX-478 (μM)	EC ₅₀ Combination DCA (mM)/PX-478 (μM)	Best CI
A549 (lung)	41.9	30	14.2/15.8	0.61
H441 (lung)	38.6	23.5	8.3/11.9	0.78
HeLa (cervical)	21.2	13.4	8.9/5.8	0.57
HEPG2 (hepatocellular)	21.4	17.7	8.4/6.3	0.56
HT-29 (colon)	26.5	75.6	18.1/28.2	0.65
MCF-7 (breast)	31.5	11.2	10.2/4	0.4
MDA-MB-231 (breast)	26.1	276	23.4/79	0.8
U251 (glioblastoma)	25	30.5	9.5/16.8	0.6

affected cell viability or the protein mass in all cell lines, leading to a left shift in the dose-response curves. The combination treatment allowed the concentration of each single drug to be noticeably reduced (Table 2). For example, in MCF-7 cells, the EC₅₀ values of DCA and PX-478 were reduced by 68 and 64%, respectively. Collectively considering all cell lines, the EC₅₀ values of the compounds were profoundly reduced by an average of 60.7% when used in combination relative to when used as single agents.

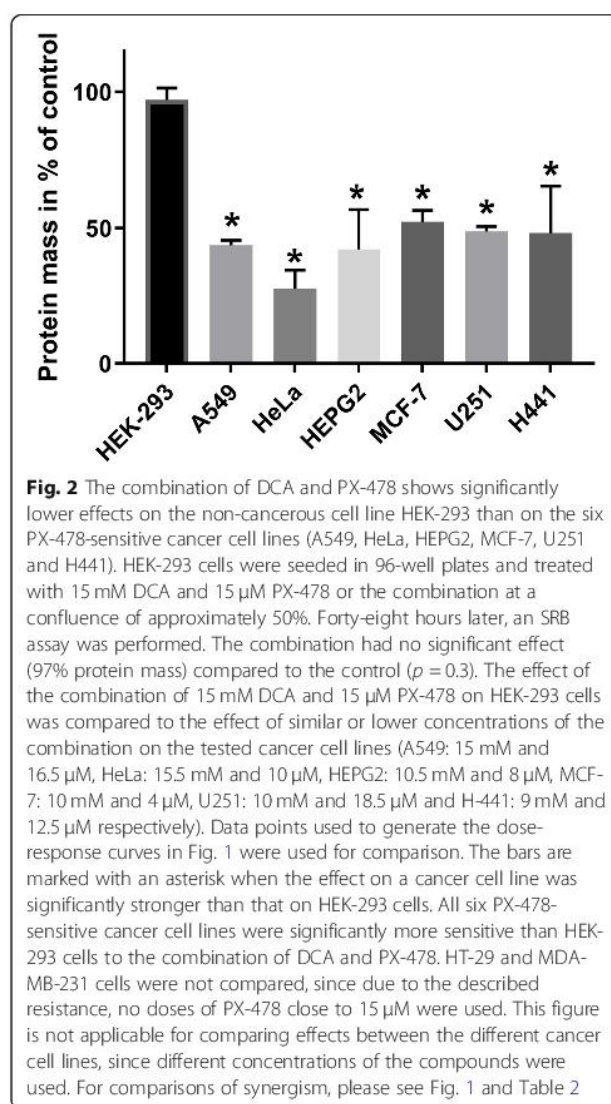
Comparison of the EC₅₀ values of PX-478 in HT-29 and MDA-MB-231 cells indicates that noticeably higher doses were needed in these cell lines than in the other cell lines, indicating resistance to PX-478. For MDA-MB-231 cells, the resistance to PX-478 resulted in the highest CI value compared to the other cell lines. Interestingly, the dose-response curve for DCA was close to that for the combination (Table 2 and Fig. 1). However, a stronger synergism was shown for HT-29 cells even though a higher dose of PX-478 was required (CI = 0.65).

The six cell lines that were sensitive to PX-478 were significantly more sensitive to the combination of DCA and PX-478 than the immortalised non-cancerous cell line HEK-293 at a comparable concentration (Fig. 2). For example, in MCF-7 cells, 10 mM DCA and 4 μM PX-478 led to a reduction of 48% in the protein mass, while 15 mM DCA and 15 μM PX-478 led to a reduction of only 3% in HEK-293 cells (*p* = 0.000007). Since we detected a PX-478 resistance in MDA MB-231 and HT-29 cells, we did not use concentrations of PX-478 in comparable dosages for the combination.

Table 2 lists the EC₅₀ values for DCA, PX-478 and the combination of both in all tested cell lines. The EC₅₀ values were calculated via curve fitting with the program GraphPad Prism. In the last column, the lowest CI value indicating synergism (CI < 0.9) is listed.

The combination of DCA and PX-478 increases ROS levels and leads to apoptosis and cell cycle arrest

The existing data for PX-478 and DCA suggest some theories concerning the mechanisms underlying their



synergism. In the following experiments, the effects of this combination on increasing reactive oxygen species generation, arresting the cell cycle and inducing apoptosis were investigated.

The combination of DCA and PX-478 increases ROS levels in HT-29, MCF-7 and HeLa cell lines

To investigate the relevance of the combination to ROS production, we performed HPLC measurements with HT-29 cells to analyse the oxidation of arachidonic acid

derivatives (Fig. 3a). DCA-treated cells showed a non-significant (21%, $p = 0.21$) increase in the 5- and 10-HETE levels compared to those in control cells. In cells treated with PX-478, the oxidation ratio was significantly increased by 58% compared to that in control cells ($p = 0.04$). The combination treatment led to a 109% increase in the oxidation ratio, which was significantly higher than that observed for the control treatment ($p = 0.02$) but did not differ significantly from that observed for PX-478 alone ($p = 0.22$).

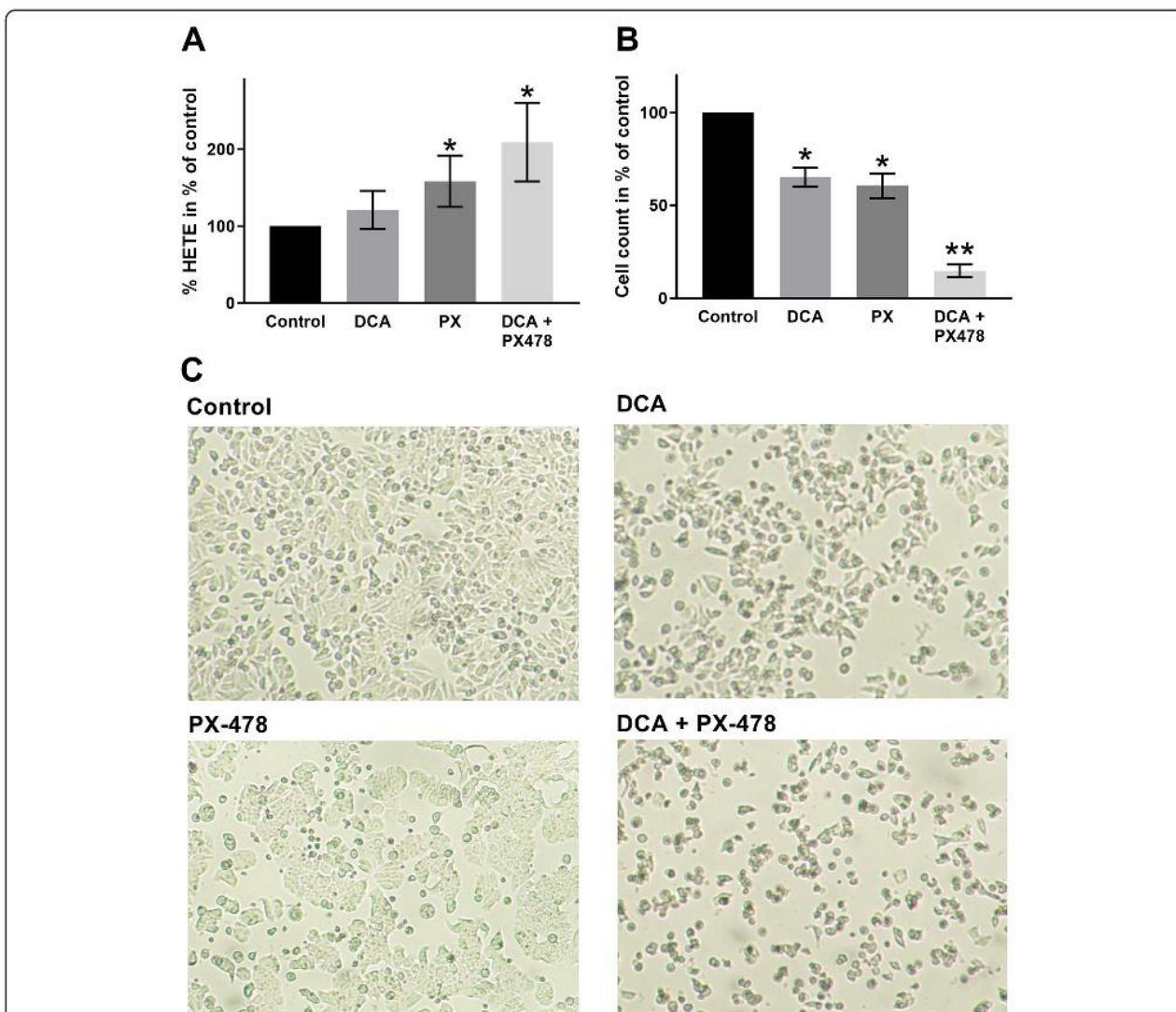


Fig. 3 The combination of DCA and PX-478 leads to increased ROS activity in HT-29 cells. Figure 3 shows HPLC analysis results and cell counts for HT-29 cells. **a:** HPLC results for the proportion of arachidonic acid to its oxygenated derivatives 10-/15-HETE for drug treatment compared to the control treatment are presented. Cells were treated with either the EC₅₀ dose of DCA, the EC₅₀ dose of PX-478 or the combination. Cells treated with PX-478 alone and with the combination of DCA and PX-478 showed a significant increase in the oxidation ratio compared to that in control cells, although the difference between the combination and PX-478 was noticeable but not significant. **b:** The cell count as a percentage of the control cell count is presented. Treatment with the single compounds DCA and PX-478 led to significant reductions of 65 and 61%, respectively. Only 15% of the control cells remained after the combination treatment. Significant differences from the control are marked with an asterisk (*), while significant differences from both the control and each single compound are marked with two asterisks (**). **c:** The profound effects of DCA, PX-478 and DCA + PX-478 on cell confluency are shown. All cells were imaged at 40x magnification with a Nikon D90

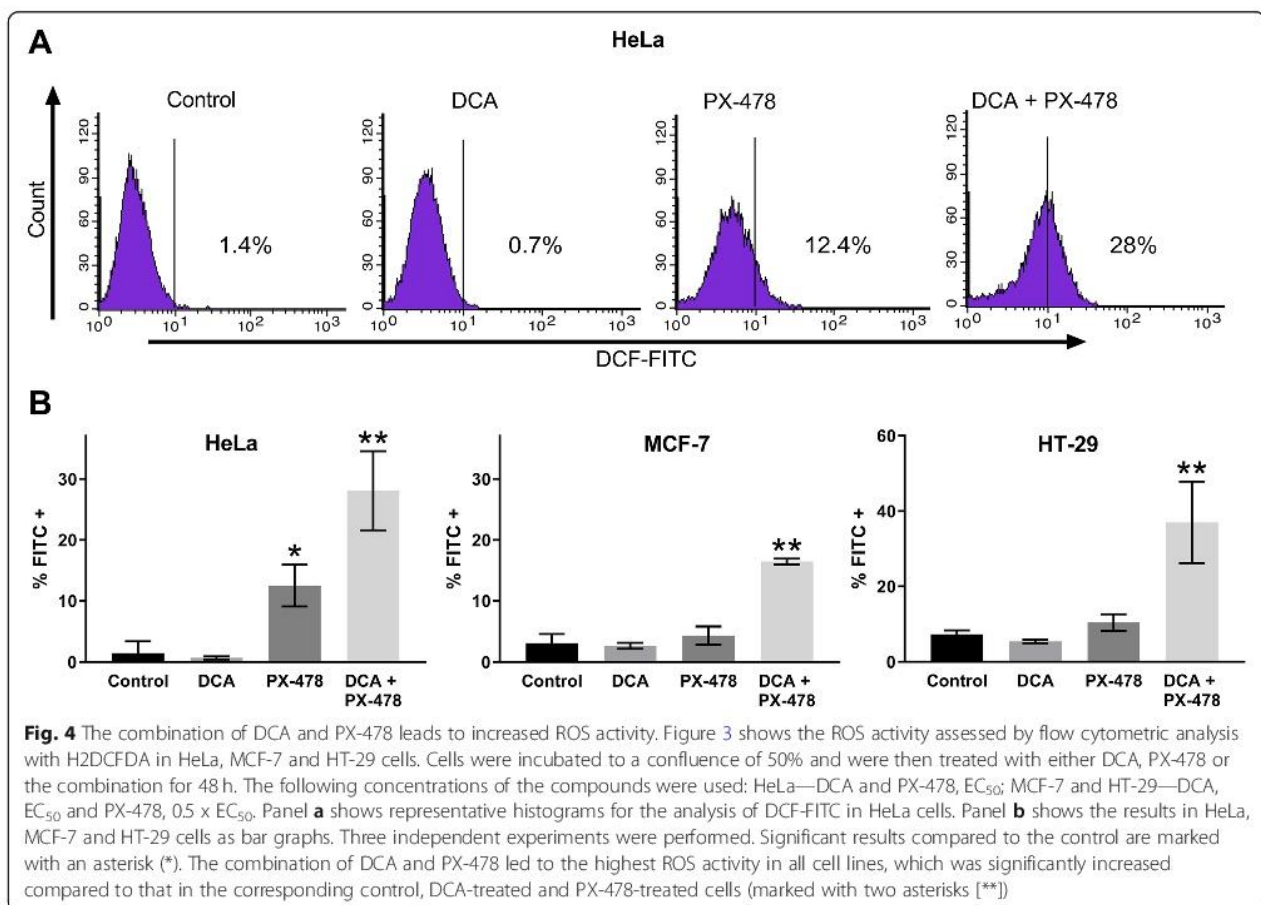
Furthermore, we evaluated the relevance of this combination to ROS via FACS analysis with H2DCFDA in HeLa, MCF-7 and HT-29 cells (Fig. 4). H2DCFDA reacts with ROS, and fluorescent dichlorofluorescein (DCF) can be measured in the FL1 channel. The results shown in Fig. 4b confirmed our HPLC results in HT-29 cells. FACS analysis showed that compared to the control treatment, DCA did not affect ROS activity in any cell line. ROS production was significantly increased in HeLa cells (2 to 12%, $p = 0.008$) but not in MCF-7 cells (3 to 4%, $p = 0.37$) or HT-29 cells (7 to 10%, $p = 0.089$) treated with PX-478 alone compared to control cells. Compared to the single compounds, the combination led to significant increases of 28% ($p = 0.021$), 16% ($p = 0.0002$) and 37% ($p = 0.014$) in HeLa, MCF-7 and HT-29 cells, respectively. Thus, as our results in HeLa, MCF-7 and HT-29 cells suggest, increased ROS is likely to play an important role in the synergism of DCA + PX-478 combination treatment.

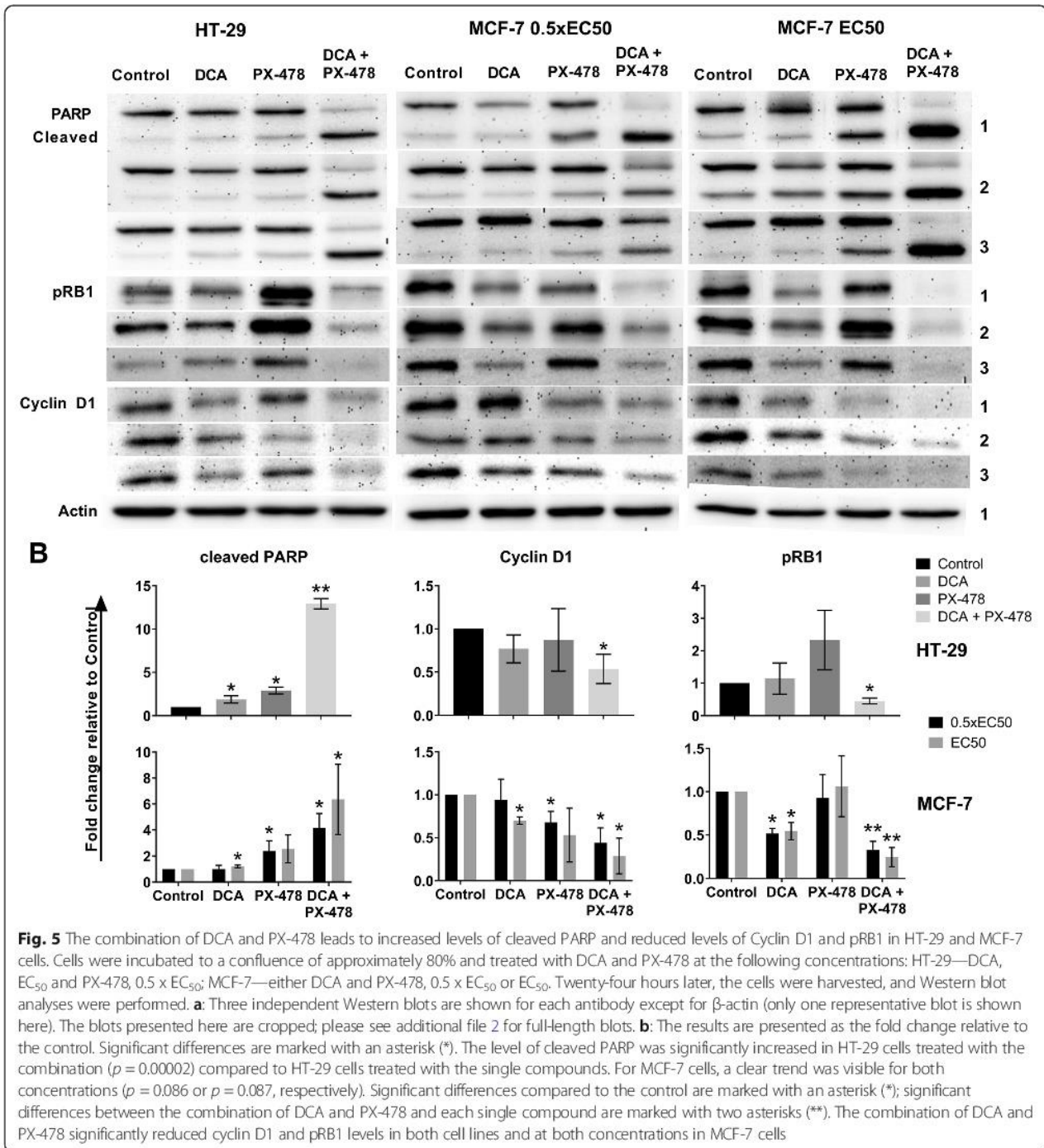
The combination of DCA and PX-478 leads to apoptosis and a reduction in proliferation

Western blot analyses of PARP/cleaved PARP, Ser795-phosphorylated Retinoblastoma protein (pRB1) and Cyclin

D1 were performed in HT-29 and MCF-7 cells (Fig. 5). In MCF-7 cells, two concentrations of DCA and PX-478 (EC_{50} and $0.5 \times EC_{50}$) and the respective combinations were analysed. In HT-29 cells ($DCA EC_{50}$ and $PX-478 0.5 \times EC_{50}$), the level of cleaved PARP was significantly higher in cells treated with the combination than in cells treated with the single compounds ($p = 0.002$). In MCF-7 cells, the combination led to the highest levels of cleaved PARP at both doses, with significant differences compared to control and DCA-treated cells but non-significant differences compared to PX-478-treated cells ($p = 0.086$ and $p = 0.087$). However, via FACS analysis with Annexin-V-FITC staining, we identified significantly increased levels of programmed cell death for the combination of DCA and PX-478 in MCF-7 cells compared to PX-478-treated cells (Fig. 6). While 12% of PX-478-treated cells were Annexin-V-FITC-positive, the percentage increased to 20% after combination treatment ($p = 0.004$). Thus, we concluded that apoptosis is a relevant factor for this synergism in HT-29 and MCF-7 cells.

For both cell lines, pRB1 levels were significantly lower in combination-treated cells than in single compound-treated cells and control cells (Fig. 5). Furthermore, we observed an interesting effect of the combination in

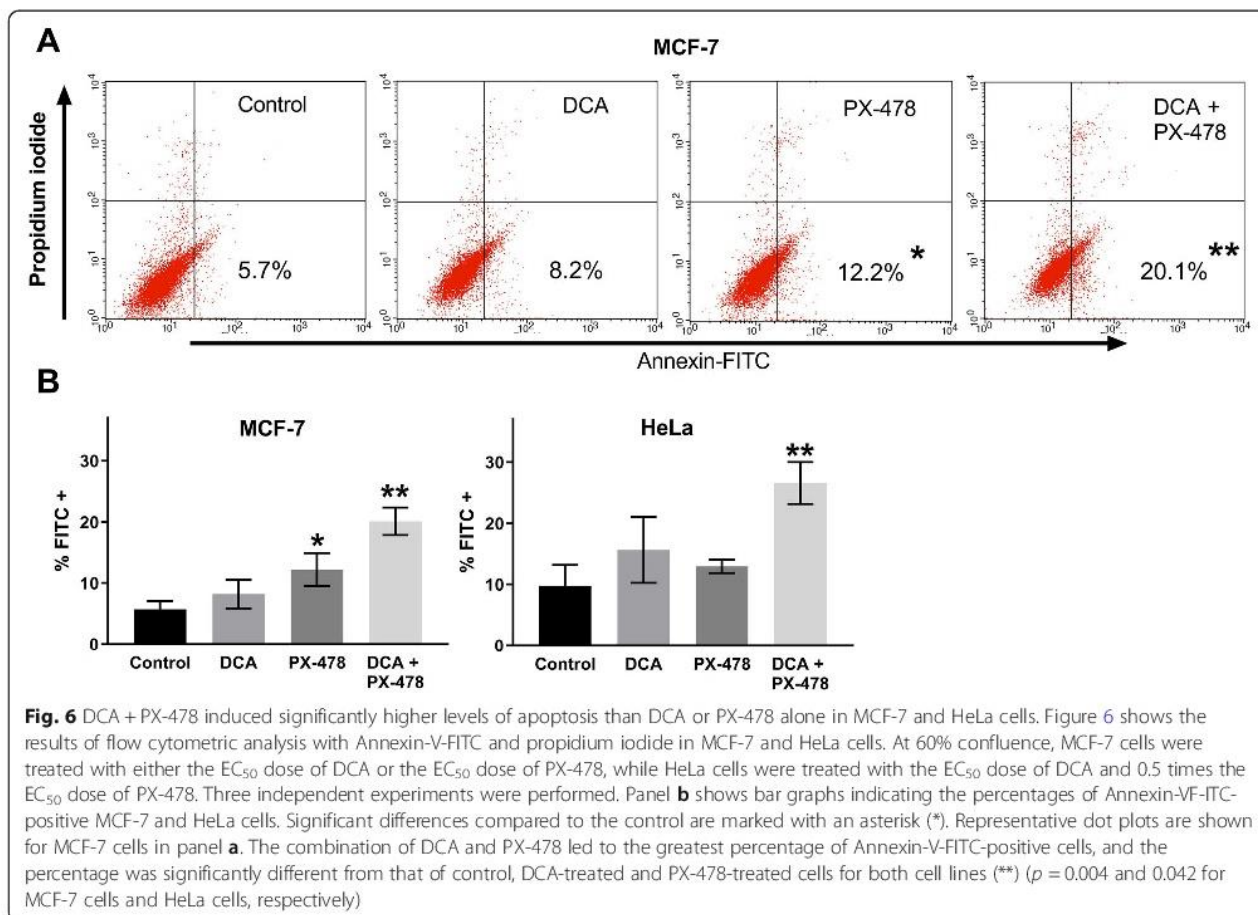




MCF-7 cells: while PX-478 alone did not affect the level of pRB1 at 0.5 x EC₅₀ and EC₅₀, DCA led to decreased levels of pRB1 (52 and 54%, respectively). For the combination, pRB1 levels were reduced to 33% compared to control at the lower concentration and 25% at the higher concentration ($p = 0.027$ and 0.046 compared to the single compounds, respectively). These data suggest that DCA alone has limited effects on pRB1 levels in MCF-7

cells while the combination affects RB1 phosphorylation more strongly.

Furthermore, we used Western blotting to evaluate the impact of the compounds on Cyclin D1 levels. In HT-29 and MCF-7 cells, the level of Cyclin D1 exhibited the greatest reduction for the combination treatment ($p = 0.009$ and $p = 0.005$, respectively, compared to control treatment). However, the differences with respect to



each single compound were non-significant (Fig. 5). Collectively, these data suggest that the combination of DCA and PX-478 synergistically reduces cell proliferation.

The effect of DCA was verified via real-time measurement of metabolism (seahorse XFe96)

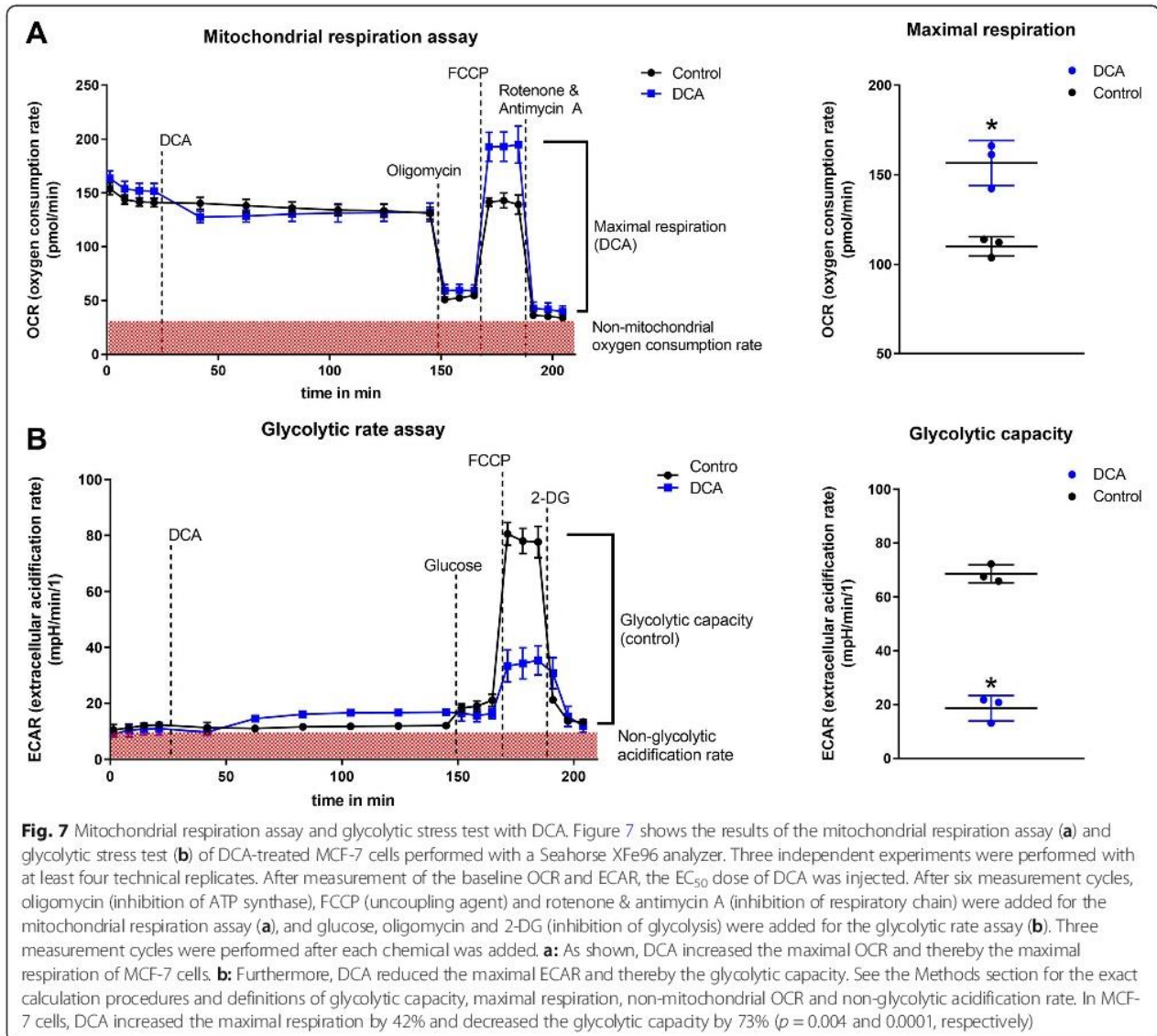
To verify the effects of DCA on glycolysis, studies with the Seahorse XFe96 Analyzer were performed (Fig. 7). We measured real-time changes in the oxygen consumption rate (OCR) and the extracellular acidification rate (ECAR). Two hours after treatment with DCA, the protocols for the mitochondrial respiration assay and the glycolytic rate assay were performed. The results supported the hypothesis that DCA increases the influx of pyruvate into mitochondria, which led to a 42% increase in maximal respiration ($p = 0.004$). In addition, we observed a 73% reduction in glycolytic capacity when DCA was added ($p = 0.0001$).

Discussion

In this study, we demonstrate that DCA and PX-478 are a potent combination that exerts synergistic effects in all

tested cancer cell lines and proved thereby to be effective in various tumor entities in vitro including colorectal, lung, breast, cervical, liver and brain cancer while having limited effects on the non-cancerous cell line HEK-293 (Figs. 1 and 2). We found the combination to induce cell cycle arrest and apoptosis as well as increasing the generation of ROS in a colorectal and a breast cancer cell line (HT-29 and MCF-7).

The EC₅₀ of PX-478 ranged from 11.2 to 276 μM, indicating a drug resistance for MDA MB-231 cells (276 μM). Interestingly, this resistance does not inhibit synergism, with a CI value of 0.8. However, best CI values were lower in all other cell lines. Via its effect on HIF-1α, PX-478 has already shown synergistic potential with different compounds. In combination with arsenic trioxide (ATO), PX-478 increases ROS and, likely, ROS-induced apoptosis [24]. As our data suggest, this mechanism might also apply to the combination of DCA + PX-478. Interestingly, both DCA and PX-478 mediate antitumoral effects through inhibition of PDKs, which can partially explain the synergism observed here. While DCA suppresses PDK-1, HIF-1α increases PDK-1 expression [27, 28]. Thus, PX-478 reinforces the primary



effect of DCA indirectly, thereby synergistically increasing ROS production when combined with DCA, as our data suggest (Figs. 3 and 4). These results are in line with the findings of Lang et al. and support the hypothesis that PX-478, as a HIF-1 α inhibitor, may be beneficial for different therapeutic approaches.

The EC₅₀ of DCA ranged from 21.2 mM to 41.9 mM (Fig. 2). A heterogeneity of the DCA-mediated effects in different cancer cell lines can be seen when our real-time metabolic assay results are compared with those of Tataranni et al. and Lucido et al. [17, 33]. DCA strongly increased maximal respiration and decreased glycolytic capacity in MCF-7 cells (Fig. 7), while in pancreatic carcinoma as well as head and neck squamous cell cancer, both glycolytic capacity and maximal respiration were decreased. Consistent with our findings however, Ma

et al. found increased maximal respiration in non-small cell lung cancer cells treated with DCA [34].

Hence, literature as well as our data suggest that DCA mediates heterogenic metabolic modulation depending on the metabolic status of a cancer cell. Interestingly, cells primarily undergoing oxidative phosphorylation as well as cells relying primarily on aerobic glycolysis can both be sensitive to DCA [35–39].

As DCA has attracted considerable attention in recent years, many examples of synergism have been detected. 5-Fluorouracil, a platinum-based chemotherapy, a SIRT2 inhibitor, metformin, omeprazole + tamoxifen, sorafenib, erlotinib and gefitinib have shown synergistic effects in combination with DCA in vivo and in vitro [15, 34, 40–48].

Clinical trials with DCA in cancer therapy, congenital lactic acidosis and pulmonary arterial hypertension have

been performed in recent decades and are ongoing [49–51]. Although DCA has not yet been implemented in clinical cancer treatment regimens, interest in DCA has not decreased. Authors of clinical trials with DCA suggest DCA in combination with chemotherapy in previously treated metastatic breast cancer and non-small cell lung cancer (ClinicalTrials.gov Identifier: NCT01029925) [45] and as an apoptosis sensitiser for recurrent solid tumors (ClinicalTrials.gov Identifier: NCT00566410) in less advanced disease stage [52].

Although a phase 1 clinical trial of PX-478 conducted in 2010 in patients with advanced solid tumors showed that PX-478 was well tolerated at low doses, with consistent HIF-1 α inhibition and prolonged duration of stable disease [53], it seems to have been abandoned as an anticancer drug, as no further clinical trials with PX-478 have been registered. If PX-478 is used in combination with DCA, obstacles such as its dose-limiting toxicity could be eliminated. We believe that synergism is an important strategy for successfully including promising compounds such as DCA and/or PX-478 in cancer therapy. Our data indicates that the concentrations of DCA and PX-478 could be reduced by an average of approximately 60.7%. Considering the concentrations of DCA achieved in clinical studies and our EC₅₀ values in the different cell lines tested, we conclude that combination of DCA and PX-478 can help attain the concentrations needed for a therapeutic effect.

Limitations

In this study, we focused on the effect of the specific compounds and their combination rather than identifying whether a certain effect can be directly linked to a specific mode of action of a single compound. These conclusions must be drawn considering the existing data for single compounds.

While DCA exerts an immediate effect via PDH activation (see the results of the real-time metabolic assays, Fig. 7), PX-478-mediated inhibition of the transcription factor HIF-1 α consequently shows relatively delayed effects. HIF-1 α , having a short half-life of eight to 20 min itself [54], regulates more than 100 proteins, exemplarily GLUT1 and VEGFA, with half-lives of approximately 7–8 h [55, 56].

We performed Western blot analysis after 24 or 48 h of incubation to partially address this issue, but we did not consistently quantify the individual effects of DCA and PX-478 at the respective time points. Consequently, we did not analyse the dynamics of this combination.

Conclusion

In summary, we found synergistic effects of the combination DCA and PX-478 in all analysed cancer cell lines,

including colorectal, lung, breast, cervical, liver and brain cancer. Induction of apoptosis, generation of ROS and inhibition of proliferation played important roles in this synergism. Considering the promising synergism between the two compounds presented here and the evidence generated by various research groups about the effects of DCA and PX-478, commencement of in vivo trials (e.g. xenografts) is recommended.

Abbreviations

CI: Combination index; DCA: Dichloroacetate; FACS: Fluorescence-activated cell sorting; HPLC: High performance liquid chromatography; HIF-1 α : Hypoxia inducible factor α ; ROS: Reactive oxygen species; w/v: Weight per volume; v/v: Volume per volume

Supplementary Information

The online version contains supplementary material available at <https://doi.org/10.1186/s12885-021-08186-9>.

Additional file 1. Includes data of: Combination experiments with DCA and PX-478, flow cytometric analysis, HPLC analysis, Western blot analysis and Seahorse analysis.

Additional file 2. Includes all Western Blots.

Acknowledgements

We acknowledge support from the German Research Foundation (DFG) and the Open Access Publication Fund of Charité – Universitätsmedizin Berlin. Thanks for the support throughout the project to Gudrun Mrawietz, Klaus-Dieter Irrgang, Kai Murk, Juliane Schiweck, Marjann Schäfer, Gustav Steinemann, Laura Michalick, Lothar Ludka, Kim Stolte, Marlon Tilgner and Michael Föhling. This work is dedicated to Ralf Redemund and Jutta Hinke-Ruhnau.

Authors' contributions

Conceptualisation of the project was done by JP, JR and AK. Experiments were performed by JP, JR, CP, MS, HW, NN, HK and AK. AK and JP were responsible for project administration and supervision. Writing and editing was done by JP, JR, AK, BE and KD. All authors read and approved the manuscript.

Funding

Jonas Parczyk received a stipend by the Berlin Institute of Health. Open Access funding enabled and organized by Projekt DEAL.

Availability of data and materials

All data generated or analysed during this study are included in this published article and its supplementary files (additional file 1 and additional file 2).

Declarations

Ethics approval and consent to participate

Not applicable.

Consent for publication

Not applicable.

Competing interests

The authors declare that they have no competing interests.

Received: 30 September 2020 Accepted: 14 April 2021

Published online: 30 April 2021

References

- Schweim JK, Schweim HG. Status quo and future developments of combinations of medicinal products. *Synergy* 2014;1(1):70–75. Available from: <http://dx.doi.org/https://doi.org/10.1016/j.synres.2014.07.007>

2. Zimmermann GR, Lehár J, Keith CT. Multi-target therapeutics: when the whole is greater than the sum of the parts. *Drug Discov Today*. 2007;12(1–2):34–42. <https://doi.org/10.1016/j.drudis.2006.11.008>.
3. Al-Lazikani B, Banerji U, Workman P. Combinatorial drug therapy for cancer in the post-genomic era. *Nat Biotechnol*. 2012;30(7):679–92. Available from: <http://www.ncbi.nlm.nih.gov/pubmed/227816979%5Cnhttp://www.pubmedcentral.nih.gov/articlerender.fcgi?artid=4320499&tool=pmcentrez&rendertype=abstract>. <https://doi.org/10.1038/nbt.2284>.
4. Ruhnau J, Parczyk J, Danker K, Eickholt B, Klein A. Synergisms of genome and metabolism stabilizing antitumor therapy (GMSAT) in human breast and colon cancer cell lines: a novel approach to screen for synergism. *BMC Cancer*. 2020;20(1):617. Available from: <http://pmc/articles/PMC7331156/?report=abstract>. [cited 2020 Sep 13].
5. Chou TC, Talalay P. Quantitative analysis of dose-effect relationships: the combined effects of multiple drugs or enzyme inhibitors. *Adv Enzyme Regul*. 1984;22:27–55 [cited 2016 Mar 8] Available from: <http://www.ncbi.nlm.nih.gov/pubmed/6382953>.
6. Abdelmalak M, Lew A, Ramezani R, Shroads AL, Coats BS, Langaee T, et al. Long-term safety of dichloroacetate in congenital lactic acidosis. *Mol Genet Metab*. 2013;109(2):139–43 [cited 2016 Mar 22] Available from: <http://www.pubmedcentral.nih.gov/articlerender.fcgi?artid=3751427&tool=pmcentrez&rendertype=abstract>.
7. Stacpoole PW. The pharmacology of dichloroacetate. *Metabolism*. 1989;38:1124–44.
8. Chen Z, Lu W, Garcia-Prieto C, Huang P. The Warburg effect and its cancer therapeutic implications. *J Bioenerg Biomembr*. 2007;39(3):267–274. [cited 2019 Jul 23] Available from: <http://link.springer.com/https://doi.org/10.1007/s10863-007-9086-x>
9. Warburg O, Wind F, Negelein E. The metabolism of tumors in the body. *J Gen Physiol*. 1927;8(6):519–30. <https://doi.org/10.1085/jgp.8.6.519>.
10. Bonnet S, Archer SL, Allalunis-Turner J, Haromy A, Beaulieu C, Thompson R, et al. A mitochondria-K⁺ channel Axis is suppressed in Cancer and its normalization promotes apoptosis and inhibits Cancer growth. *Cancer Cell*. 2007;11(1):37–51. <https://doi.org/10.1016/j.ccr.2006.10.020>.
11. Bonnet S, Archer SL, Allalunis-Turner J, Haromy A, Beaulieu C, Thompson R, et al. A mitochondria-K⁺ channel axis is suppressed in cancer and its normalization promotes apoptosis and inhibits cancer growth. *Cancer Cell*. 2007;11(1):37–51 [cited 2018 Jun 13] Available from: <https://www.sciencedirect.com/science/article/pii/S1535610806003722?via%3Dihub>.
12. Wong JYY, Huggins GS, Debidda M, Munshi NC, De Vivo I. Dichloroacetate induces apoptosis in endometrial cancer cells. *Gynecol Oncol*. 2008;109(3):394–402. <https://doi.org/10.1016/j.ygyno.2008.01.038>.
13. Saed GM, Fletcher NM, Jiang ZL, Abu-Soud HM, Diamond MP. Dichloroacetate induces apoptosis of epithelial ovarian cancer cells through a mechanism involving modulation of oxidative stress. *Reprod Sci*. 2011;18(12):1253–61 [cited 2020 Jan 20] Available from: <http://www.ncbi.nlm.nih.gov/pubmed/21701041>.
14. Sutendra G, Dromparis P, Kinnaird A, Stenson TH, Haromy A, Parker JMR, McMurtry MS, Michelakis ED Mitochondrial activation by inhibition of PDKII suppresses HIF1a signaling and angiogenesis in cancer. *Oncogene* 2013; 32(13):1638–1650. Available from: <http://dx.doi.org/https://doi.org/10.1038/onc.2012.198>
15. Ward NP, Poff AM, Koutnik AP, D'Agostino DP. Complex I inhibition augments dichloroacetate cytotoxicity through enhancing oxidative stress in VM-M3 glioblastoma cells. *PLoS One*. 2017;12(6):1–18.
16. Lu H, Lu Y, Xie Y, Qiu S, Li X, Fan Z. Rational combination with PDK1 inhibition overcomes cetuximab resistance in head and neck squamous cell carcinoma. *JCI Insight*. 2019;4(19):1–16.
17. Tataranni T, Agriesti F, Pacelli C, Ruggieri V, Laurenzana I, Mazzoccoli C, et al. Dichloroacetate affects mitochondrial function and Stemness-associated properties in pancreatic Cancer cell lines. *Cells*. 2019;8(5):478. <https://doi.org/10.3390/cells8050478>.
18. Alkarakooly Z, Al-Anbaky QA, Kannan K, Ali N. Metabolic reprogramming by Dichloroacetic acid potentiates photodynamic therapy of human breast adenocarcinoma MCF-7 cells. *PLoS One*. 2018;13(10):e0206182.
19. Lu X, Zhou D, Hou B, Liu QX, Chen Q, Deng XF, et al. Dichloroacetate enhances the antitumor efficacy of chemotherapeutic agents via inhibiting autophagy in non-small-cell lung cancer. *Cancer Manag Res*. 2018;10:1231–41. <https://doi.org/10.2147/CMAR.S156530>.
20. Agnoletto C, Melloni E, Casciano F, Rigolin GM, Rimondi E, Celeghini C, et al. Sodium dichloroacetate exhibits anti-leukemic activity in B-chronic lymphocytic leukemia (B-CLL) and synergizes with the p53 activator Nutlin-3. *Oncotarget*. 2014;5(12):4347–60 Available from: <http://www.pubmedcentral.nih.gov/articlerender.fcgi?artid=4147328&tool=pmcentrez&rendertype=abstract>.
21. Koh MY, Spivak-Kroizman T, Venturini S, Welsh S, Williams RR, Kirkpatrick DL, et al. Molecular mechanisms for the activity of PX-478, an antitumor inhibitor of the hypoxia-inducible factor-1alpha. *Mol Cancer Ther*. 2008;7(1):90–100 [cited 2019 Dec 22] Available from: <http://www.ncbi.nlm.nih.gov/pubmed/18202012>.
22. Semenza GL. Targeting HIF-1 for cancer therapy. *Nat Rev Cancer*. 2003;3(10):721–32. <https://doi.org/10.1038/nrc1187>.
23. Palayoor ST, Mitchell JB, Cerna D, Degraff W, John-Aryankalayil M, Coleman CN. PX-478, an inhibitor of hypoxia-inducible factor-1alpha, enhances radiosensitivity of prostate carcinoma cells. *Int J Cancer*. 2008;123(10):2430–7 [cited 2018 Apr 13] Available from: <http://www.ncbi.nlm.nih.gov/pubmed/18729192>.
24. Lang M, Wang X, Wang H, Dong J, Lan C, Hao J, et al. Arsenic trioxide plus PX-478 achieves effective treatment in pancreatic ductal adenocarcinoma. *Cancer Lett*. 2016;378(2):87–96 [cited 2018 Apr 13] Available from: <http://www.ncbi.nlm.nih.gov/pubmed/27212442>.
25. Zhu Y, Zang Y, Zhao F, Li Z, Zhang J, Fang L, et al. Inhibition of HIF-1 α by PX-478 suppresses tumor growth of esophageal squamous cell cancer in vitro and in vivo. *Am J Cancer Res*. 2017;7(5):1198–212 [cited 2020 Jan 19] Available from: <http://www.ncbi.nlm.nih.gov/pubmed/28560067>.
26. Welsh S, Williams R, Kirkpatrick L, Paine-Murrieta G, Powis G. Antitumor activity and pharmacodynamic properties of PX-478, an inhibitor of hypoxia-inducible factor-1alpha. *Mol Cancer Ther*. 2004;3(3):233–44.
27. Kim JW, Tchernyshyov I, Semenza GL, Dang CV. HIF-1-mediated expression of pyruvate dehydrogenase kinase: a metabolic switch required for cellular adaptation to hypoxia. *Cell Metab*. 2006;3(3):177–85. <https://doi.org/10.1016/j.cmet.2006.02.002>.
28. Kirito K, Hu Y, Komatsu N. HIF-1 prevents the overproduction of mitochondrial ROS after cytokine stimulation through induction of PDK-1. *Cell Cycle*. 2009;8(17):2844–9. <https://doi.org/10.4161/cc.8.17.9544>.
29. Chou TC, Martin N. CompuSyn for Drug Combinations: PC Software and User's Guide: A Computer Program for Quantitation of Synergism and Antagonism in Drug Combinations, and the Determination of IC50 and ED50 and LD50 Values. Paramus: ComboSyn Inc; 2005.
30. Chou T-C. Preclinical versus clinical drug combination studies. *Leuk Lymphoma*. 2008;49(11):2059–80 [cited 2016 Apr 9] Available from: <http://www.ncbi.nlm.nih.gov/pubmed/19021049>.
31. Zhao L, Wientjes MG, Au JL-S. Evaluation of combination chemotherapy: integration of nonlinear regression, curve shift, isobologram, and combination index analyses. *Clin Cancer Res*. 2004;10(23):7994–8004 [cited 2016 Apr 13] Available from: <http://www.ncbi.nlm.nih.gov/pubmed/15585635>.
32. Kuhn H, Belkner J, Wiesner R, Brash AR. Oxygenation of biological membranes by the pure reticulocyte lipoxygenase. *J Biol Chem*. 1990; 265(30):18351–61. [https://doi.org/10.1016/S0021-9258\(17\)44759-4](https://doi.org/10.1016/S0021-9258(17)44759-4).
33. Lucido CT, Miskimins WK, Vermeer PD. Propranolol promotes glucose dependence and synergizes with dichloroacetate for anti-cancer activity in HNSCC. *Basel: Cancers*. 2018;10(12):476.
34. Ma W, Zhao X, Wang K, Liu J, Huang G. Dichloroacetic acid (DCA) synergizes with the SIRT2 inhibitor Sirtinol and AGK2 to enhance anti-tumor efficacy in non-small cell lung cancer. *Cancer Biol Ther*. 2018 Sep 2;19(9):835–46. <https://doi.org/10.1080/15384047.2018.1480281>.
35. Schoonjans CA, Joudiou N, Brusa D, Corbet C, Feron O, Gallez B. Acidosis-induced metabolic reprogramming in tumor cells enhances the anti-proliferative activity of the PDK inhibitor dichloroacetate. *Cancer Lett*. 2020 Feb 1;470:18–28. <https://doi.org/10.1016/j.canlet.2019.12.003>.
36. Zhou L, Liu L, Chai W, Zhao T, Jin X, Guo X, et al. Dichloroacetic acid upregulates apoptosis of ovarian cancer cells by regulating mitochondrial function. *Onco Targets Ther*. 2019;12:1729–39. <https://doi.org/10.2147/OTT.S194329>.
37. Chaudhary AK, Bhat TA, Kumar S, Kumar A, Kumar R, Underwood W, et al. Mitochondrial dysfunction-mediated apoptosis resistance associates with defective heat shock protein response in African-American men with prostate cancer. *Br J Cancer*. 2016;114(10):1090–100. <https://doi.org/10.1038/bjc.2016.88>.
38. Roh J-L, Park JY, Kim EH, Jang HJ, Kwon M. Activation of mitochondrial oxidation by PDK2 inhibition reverses cisplatin resistance in head and neck

- cancer. *Cancer Lett.* 2016;371(1):20–9 [cited 2020 Jan 24] Available from: <http://www.ncbi.nlm.nih.gov/pubmed/26607904>.
39. Ruggieri V, Agriesti F, Scrima R, Laurenzana I, Perrone D, Tataranni T, et al. Dichloroacetate, a selective mitochondria-targeting drug for oral squamous cell carcinoma: a metabolic perspective of treatment. *Oncotarget.* 2015;6(2): 1217–30. <https://doi.org/10.18632/oncotarget.2721>.
 40. Xuan Y, Hur H, Ham I-H, Yun J, Lee J-Y, Shim W, et al. Dichloroacetate attenuates hypoxia-induced resistance to 5-fluorouracil in gastric cancer through the regulation of glucose metabolism. *Exp Cell Res.* 2014;321(2): 219–30 [cited 2018 May 28] Available from: <https://www.sciencedirect.com/science/article/pii/S0014482713005260?via%3Dihub>.
 41. Fang J, Xie J, Wang B-S, Wang B-S, Yu D-H, Yu D-H, et al. Dichloroacetate shifts the metabolism from glycolysis to glucose oxidation and exhibits synergistic growth inhibition with cisplatin in HeLa cells. *Int J Oncol.* 2011; 38(2):409–17 [cited 2018 May 28] Available from: <http://www.spandidos-publications.com/ijco/38/2/409>.
 42. Yang Z, Tam KY. Anti-cancer synergy of dichloroacetate and EGFR tyrosine kinase inhibitors in NSCLC cell lines. *Eur J Pharmacol.* 2016;789:458–67 Available from: <https://www.sciencedirect.com/science/article/pii/S001429991630509X?via%3Dihub>.
 43. Haugrud AB, Zhuang Y, Coppock JD, Miskimins WK. Dichloroacetate enhances apoptotic cell death via oxidative damage and attenuates lactate production in metformin-treated breast cancer cells. *Breast Cancer Res Treat.* 2014;147(3):539–50. <https://doi.org/10.1007/s10549-014-3128-y>.
 44. Choi YW, Lim IK. Sensitization of metformin-cytotoxicity by dichloroacetate via reprogramming glucose metabolism in cancer cells. *Cancer Lett.* 2014; 346(2):300–8 [cited 2018 may 18] Available from: <http://www.ncbi.nlm.nih.gov/pubmed/24480191>.
 45. Garon EB, Christofk HR, Hosmer W, Britten CD, Bahng A, Crabtree MJ, et al. Dichloroacetate should be considered with platinum-based chemotherapy in hypoxic tumors rather than as a single agent in advanced non-small cell lung cancer. *J Cancer Res Clin Oncol.* 2014;140(3):443–52. <https://doi.org/10.1007/s00432-014-1583-9>.
 46. Ishiguro T, Ishiguro R, Ishiguro M, Iwai S. Co-treatment of dichloroacetate, omeprazole and tamoxifen exhibited synergistically antiproliferative effect on malignant tumors: in vivo experiments and a case report. *Hepatogastroenterology.* 2012;59(116):994–6 [cited 2016 Apr 12] Available from: <http://www.ncbi.nlm.nih.gov/pubmed/22580646>.
 47. Shen YC, Ou DL, Hsu C, Lin KL, Chang CY, Lin CY, et al. Activating oxidative phosphorylation by a pyruvate dehydrogenase kinase inhibitor overcomes sorafenib resistance of hepatocellular carcinoma. *Br J Cancer.* 2013;108(1): 72–81. <https://doi.org/10.1038/bjc.2012.559>.
 48. Liang Y, Hou L, Li L, Li L, Zhu L, Wang Y, et al. Dichloroacetate restores colorectal cancer chemosensitivity through the p53/miR-149-3p/PDK2-mediated glucose metabolic pathway. *Oncogene.* 2020;39(2):469–85 [cited 2020 Sep 25] Available from: <http://www.nature.com/articles/s41388-019-1035-8>.
 49. Michelakis ED, Gurtu V, Webster L, Barnes G, Watson G, Howard L, et al. Inhibition of pyruvate dehydrogenase kinase improves pulmonary arterial hypertension in genetically susceptible patients. *Sci Transl Med.* 2017;9(413): eaa04583.
 50. Shroads AL, Coats BS, McDonough CW, Langaee T, Stacpoule PW. Haplotype variations in glutathione transferase zeta 1 influence the kinetics and dynamics of chronic dichloroacetate in children. *J Clin Pharmacol.* 2015; 55(1):50–55. [cited 2018 Jun 14] Available from: <http://doi.wiley.com/https://doi.org/10.1002/jcph.371>
 51. Dunbar EM, Coats BS, Shroads AL, Langaee T, Lew A, Forder JR, et al. Phase 1 trial of dichloroacetate (DCA) in adults with recurrent malignant brain tumors. *Invest New Drugs.* 2014;32(3):452–64 [cited 2018 Jun 14] Available from: <http://www.ncbi.nlm.nih.gov/pubmed/24297161>.
 52. Chu QS, Sangha R, Sprattlin J, Vos LJ, Mackey JR, Mcewan AJB, et al. A phase I open-labeled, single-arm, dose-escalation, study of dichloroacetate (DCA) in patients with advanced solid tumors. *Invest New Drugs.* 2015;1:603–10.
 53. Tibes R, Falchook GS, Von Hoff DD, Weiss GJ, Iyengar T, Kurzrock R, et al. Results from a phase I, dose-escalation study of PX-478, an orally available inhibitor of HIF-1 α . *J Clin Oncol.* 2010;28(15_suppl):3076–3076. [cited 2019 Jul 22] Available from: http://ascopubs.org/doi/https://doi.org/10.1200/jco.2010.28.15_suppl.3076.
 54. Jewell UR, Kvietkova I, Scheid A, Bauer C, Wenger RH, Gassmann M. Induction of HIF-1 α in response to hypoxia is instantaneous. *FASEB J.* 2001; 15(7):1312–4. <https://doi.org/10.1096/fj.00-0732fje>.
 55. Abir R, Fisch B, Jessel S, Felz C, Ben-Haroush A, Orvieto R. Improving posttransplantation survival of human ovarian tissue by treating the host and graft. *Fertil Steril.* 2011;95(4):1205–1210. Available from: <http://dx.doi.org/https://doi.org/10.1016/j.fertnstert.2010.07.1082>
 56. Fernandes R, Hosoya K, Ichi, Pereira P. reactive oxygen species downregulate glucose transport system in retinal endothelial cells. *Am J Physiol Cell Physiol.* 2011;300(4):927–36.

Publisher's Note

Springer Nature remains neutral with regard to jurisdictional claims in published maps and institutional affiliations.

Ready to submit your research? Choose BMC and benefit from:

- fast, convenient online submission
- thorough peer review by experienced researchers in your field
- rapid publication on acceptance
- support for research data, including large and complex data types
- gold Open Access which fosters wider collaboration and increased citations
- maximum visibility for your research: over 100M website views per year

At BMC, research is always in progress.

Learn more biomedcentral.com/submissions



12. Lebenslauf / Curriculum vitae

Mein Lebenslauf wird aus datenschutzrechtlichen Gründen in der elektronischen Version meiner Arbeit nicht veröffentlicht.

13. Publikationsliste / List of Publications

Genome reorganization in different cancer types: detection of cancer specific breakpoint regions

Christoph Standfuß, Jonas Parczyk, Jérôme Ruhnau and Andreas Klein

Mol Cytogenet 12, 25 (2019). Molecular Cytogenetics volume 12, Article number: 25 (2019)

doi:10.1186/s13039-019-0435-3

Impact factor: 1.233 - 2-year Impact Factor 1.408 - 5-year Impact Factor

Synergisms of genome and metabolism stabilizing antitumor therapy (GMSAT) in human breast and colon cancer cell lines: a novel approach to screen for synergism

Jérôme Ruhnau*, Jonas Parczyk*, Kerstin Danker, Britta Eickholt, and Andreas Klein

*geteilte Erstautorenschaft

BMC Cancer. 2020; 20: 617. Published online 2020 Jul 2.

doi: 10.1186/s12885-020-07062-2

PMCID: PMC7331156

PMID:

32615946

Impact factor: 3.15 - 2-year Impact Factor 3.432 - 5-year Impact Factor

Dichloroacetate and PX-478 Exhibit Strong Synergistic Effects in a Various Number of Cancer Cell Lines.

Jonas Parczyk*, Jérôme Ruhnau*, Carsten Pelz, Max Schilling, Hao Wu, Nicole Nadine Piaskowski, Britta Eickholt, Hartmut Kühn, Kerstin Danker, Andreas Klein

*geteilte Erstautorenschaft

BMC Cancer. 2021

doi: 10.21203/rs.3.rs-88933/v1

Impact factor: 3.15 - 2-year Impact Factor 3.432 - 5-year Impact Factor

14. Danksagung / Acknowledgements

Es gibt einige liebevolle Menschen, die ich hier nennen möchte. Manche sind mir im Verlauf dieses langjährigen Projektes sehr ans Herz gewachsen, andere hatte ich schon vorher in meinem Herzen.

Ganz besonders danke ich Andreas Joseph Klein, der mich als Freund und Betreuer immer wieder tatkräftig und mit bestem Willen unterstützt hat.

Ebenfalls möchte ich mich bei Jérôme Ruhнау dafür bedanken, dass er mir stets ein guter Freund war und das Projekt und mich, trotz eigener privater Schwierigkeiten, immer unterstützt hat.

Carsten Pelz hat mich in meiner praktischen Arbeit im Labor liebevoll unterstützt und hatte für methodische Rückfragen, insbesondere zu den Western Blots, immer ein Ohr. Er ist als "Bench-Nachbar" in mein Herz gewachsen.

Der nächste Karsten, mein Vater, war immer ein guter wissenschaftlicher Diskussionspartner und stand stets komplett und selbstlos hinter mir.

Olaf, meinem Bruder, danke ich besonders für seinen mathematischen Beitrag zum Screening-Versuch. Leonard und Angelika waren mir emotional immer eine große Stütze.

Hao Wu hat in mir die Freude am Seahorse XF Analyzer entflammt und trotz eigener Aufgaben immer Zeit gehabt, mir zu helfen. Meike Kespohl hat uns engagiert bei den FACS Analysen unterstützt. Es war mir eine große Freude, meine Erfahrungen an Max Schilling und Nicole Piaskowski weiterzugeben und mit ihnen im Labor zu arbeiten.

Kerstin Danker hat mit ihrer wissenschaftlichen Expertise und Energie zur Förderung der Qualität meiner Arbeit beigetragen. Britta Eickholt hat unser Projekt unterstützt und uns immer in unserer Forschung bestärkt.

Ebenfalls danken möchte ich Pia Djermeister für ihre sehr dynamische und effektive Hilfe in administrativen Prozessen.

Besonderer Dank gilt Christoph Standfuß, Vivien Roth, Iryna Trotsyuk, Gudrun Mrawietz, Lothar Lucka und Hartmut Kühn für ihre Unterstützung.